The $[FHCl]^-$ molecular anion: Structural aspects, global surface, and vibrational eigenspectrum

Neil E. Klepeis, Allan L. L. East, Attila G. Császár, and Wesley D. Allen
Department of Chemistry, Stanford University, Stanford, California 94305

Timothy J. Lee and David W. Schwenke
NASA Ames Research Center, MS 230-3, Moffett Field, California 94035

(Received 24 March 1993; accepted 18 May 1993)

The $[FHCl]^-$ molecular anion has been investigated in detail by means of state-of-the-art *ab initio* electronic structure methods, including restricted Hartree–Fock (RHF), Møller–Plesset perturbation theory (MP2–MP4), and coupled-cluster and Brueckner methods incorporating various degrees of excitation [CCSD, CCSD(T), BD, BD(T), and BD(TQ)]. The one-particle Gaussian basis sets ranged in quality from F[6*s*4*p*2*d*], Cl[10*s*7*p*2*d*], and H[4*s*2*p*] to F[18*s*13*p*6*d*4*f*], Cl[20*s*14*p*7*d*5*f*], and H[8*s*3*p*2*d*1*f*]. The first phase of the investigation focused on the prediction of thermochemical, spectroscopic, and bonding properties of $[FHCl]^-$ and the chemical interpretation thereof. The final proposals for the geometric structure and binding energy of the complex are $r_e(H–F)=0.963\pm0.003$ Å, $R_e(H–Cl)=1.925\pm0.015$ Å, and $D_0(HF+Cl^-)=21.8\pm0.4$ kcal mol^{-1}. A Morokuma decomposition of the ion-molecule bonding gave the following electrostatic (ES), polarization (PL), exchange repulsion (EX), dispersion (DISP), and charge-transfer plus higher-order mixing (CT+MIX) components of the vibrationless complexation energy: −27.3 (ES), −5.2 (PL), +18.3 (EX), −4.5 (DISP), and −5.0 (CT+MIX) kcal mol^{-1}. The second phase of the work involved the construction of a CCSD global surface from 208 and 228 energy points for linear and bent conformations, respectively, these being fit to rms errors of only 3.9 and 9.3 cm^{-1}, respectively, below 8000 cm^{-1}. The surface was represented by a flexible analytic form which reproduces the quartic force field at equilibrium, exhibits the proper asymptotic properties, and is generally applicable to ion-molecule systems. The final phase of the study entailed the determination of converged $J=0$ and $J=1$ variational eigenstates of the $[FHCl]^-$ surface to near the $HF+Cl^-$ dissociation threshold by employing Jacobi coordinates and vibrational configuration interaction expansions in terms of natural modals. The fundamental vibrational frequencies given by the analysis were $\nu_1=247$, $\nu_2=876$, and $\nu_3=2884$ cm^{-1}. The complete vibrational eigenspectrum was then analyzed in terms of several contemporary dynamical issues, including vibrational adiabaticity, anharmonic resonances, densities of high-lying states, and signatures of quantum ergodicity.

I. INTRODUCTION

A. Transition state spectroscopy via photodetachment of hydrogen bihalide anions

The elucidation of transition state regions of reactive potential energy surfaces is a *sine qua non* of chemical reaction dynamics. In traditional approaches, features of transition states are deduced via the determination of asymptotic properties of reactions, including thermal and microscopic rate coefficients and state-specific product energy and angular distributions. In recent years, however, the direct spectroscopic characterization of transition states for simple chemical reactions has become a viable technique.[1–5] The most successful applications of transition state spectroscopy have involved half-collision experiments, in which the transition state is accessed by photoexcitation of a stable precursor rather than in a scattering event. In this way the extensive averaging over initial conditions which attends full collision studies is averted because severe restrictions are placed on the starting geometry. Two effective techniques for imposing such geometric constraints are the photodetachment of stable negative ions and the photoexcitation of van der Waals precursors.[1]

The scattering wave functions of long-lived, quasibound vibrational manifolds in transition state regions effectuate abrupt resonances in reaction cross sections as a function of total energy for fixed angular momentum.[6] Myriad efforts to characterize and quantify resonances for reactive scattering have focused on the $H+H_2$ (Refs. 7–26) and $F+H_2$ (Refs. 27–44) systems, often spawning considerable debate over data interpretation. In a recent series of half-collision experiments involving photodetachment of hydrogen bihalide anions $[XHY]^-$, Neumark and co-workers[1,2,45–49] have observed sharp spectral features which provide compelling evidence for quasibound states and reactive resonances on the X+HY neutral surfaces for hydrogen transfer. In such heavy–light–heavy systems, the skew angle between the entrance and exit valleys is very acute in conventional mass-scaled coordinate representations of the surface; in particular, the subtended angles range from 7° for IHI to 18° for FHF. Consequently, the mode involving hydrogen transfer in the transition state can to a large extent become dynamically uncoupled from the dissociation channels of the system, providing

auspicious circumstances for the occurrence of quasibound vibrational states.

The photoelectron spectrum of $[IHI]^-$ is characteristic of the symmetric hydrogen bihalide anions.[1,2,46] Photodetachment at 266 nm (4.66 eV) produces electron kinetic energy peaks (widths) at 0.734 (0.074), 0.560 (0.023), and 0.369 (0.050) eV, all of which correspond to levels above the I+HI dissociation threshold. These three features, which are spaced 1400–1550 cm^{-1} apart, are attributable to a $v_3' = (0,2,4)$ progression in the antisymmetric hydrogen stretching mode of IHI, whose counterpart in the antecedent anion exhibits a fundamental frequency near 673 cm^{-1} in matrix-isolation spectra.[50] Another intense band due to an excited electronic state of IHI appears in the photoelectron spectrum when higher-energy photons (213 nm, 5.82 eV) are used for electron detachment.[2] Enhanced resolution of the three principal v_3' peaks is achieved via threshold photodetachment spectroscopy, revealing additional progressions within each band.[47] The characteristic spacing of the features of the $v_3' = (2,4)$ bands is approximately 100 cm^{-1}, implicating upper-state manifolds of quasibound *symmetric* stretching levels in the IHI transition state region.[51] In contrast, the structure within the $v_3' = 0$ peak appears to signal a progression in internal rotor states of the IHI complex.[2]

Mixed bihalide anions which are strongly asymmetric yield photoelectron spectra whose structure is markedly different from that observed for $[IHI]^-$. In the $[FHI]^-$ case, well-resolved peaks appear in the 213 nm spectrum at electron kinetic energies of 2.143, 1.992, and 1.098 eV,[48] but these features are due to $\Delta v_3 = 0$ transitions which access three different low-lying electronic states of the neutral species, as shown by the absence of isotopic shifts upon deuterium substitution. Presumably, progressions in the antisymmetric hydrogen stretching mode are not observed because the associated potential energy cross sections are very similar on the initial and final surfaces, a circumstance anticipated for an anion of pronounced $FH \cdot I^-$ character. The photoelectron spectrum of $[ClHI]^-$ constitutes an unambiguous intermediate case between $[IHI]^-$ and $[FHI]^-$ in that vibrational progressions within two low-lying electronic states of the neutral are observed whose intensity profiles fall off rapidly as v_3' increases.[48] The level spacings within these progressions are strikingly similar to the fundamental frequency of free HCl.

The rich structure in the experimental photoelectron spectra of $[XHY]^-$ species has prompted several theoretical simulations of the photodetachment process in hydrogen bihalide anions. All of these theoretical studies have been based on the Condon approximation, whereby the photodetachment cross section $\sigma(E)$ is proportional to the square modulus of the overlap integral $\langle \psi^{(0)}(E) | \psi_v^{(-)} \rangle$ between bound vibrational wave functions of the anion, $\psi_v^{(-)}$, and continuum wave functions, $\psi^{(0)}(E)$, for reactive scattering on the neutral surface. In constructing effective collinear surfaces to reproduce their photodetachment experiments, Neumark and co-workers[2,49] have employed the adiabatic bend and diagonal-corrected vibrational adiabatic hyperspherical (DIVAH) models in simple one- and two-dimensional quantum mechanical analyses of the observed Franck–Condon profiles. Schatz[52–56] has simulated the photoelectron spectra of $[ClHCl]^-$ and $[IHI]^-$ by computing neutral scattering wave functions on model London–Eyring–Polanyi–Sato (LEPS) surfaces using a three-dimensional coupled-channel method and hyperspherical coordinates. The $[ClHCl]^-$ and $[IHI]^-$ spectra have also been analyzed by Gazdy and Bowman[57] by means of a three-dimensional L^2 simulation. Complementary time-dependent analyses of the $[XHY]^-$ photoelectron spectra have given additional insights into the nature of the quasibound states in the XHY transition state regions. In the usual quantum mechanical approach,[2,48,58–62] the initial wave packet derived from the ground vibrational state of the anion is propagated on a model neutral surface, and the time autocorrelation function, whose Fourier transform yields $\sigma(E)$, is concurrently evaluated. In the classical mechanical method of analysis (CMMA), which has been applied to the FH_2^- and $[ClHCl]^-$ systems by Hahn *et al.*,[63,64] the "assignment" of quantal resonances is achieved by the identification and characterization of associated periodic orbits in classical trajectory simulations.

A major impediment to quantitative theoretical treatments of the photodetachment process in hydrogen bihalide systems is the lack of reliable *ab initio* surfaces for both the initial and final states. Heretofore harmonic oscillator wave functions have been assumed for the vibrational states of most anions, an approximation which is known to be particularly severe for symmetric bihalide species.[65–69] Moreover, neutral scattering wave functions have generally been computed on LEPS surfaces of dubious quality. A step toward the elimination of this dearth of potential surface information has been accomplished in the *ab initio* investigation reported here on the mixed bihalide species $[FHCl]^-$, in which the chemical and physical characteristics of the complex are thoroughly analyzed (Sec. III), a global potential energy surface is constructed (Sec. IV), and the vibrational eigenspectrum is determined to near the $HF+Cl^-$ dissociation threshold (Sec. V).

B. Spectroscopic and thermochemical issues for hydrogen bihalide anions

The intrigues of transition state spectroscopy notwithstanding, the present study of $[FHCl]^-$ was motivated primarily by an inherent interest in the vibrational dynamics and thermochemistry of the hydrogen bihalide anions. These species are prototypes of the extremes of hydrogen bonding, as actualized by a competition between halide anions of widely varying proton affinities. The vibrational motion of the central proton occurs on surfaces ranging in character from the particle-in-a-box paradigm for the centrosymmetric ions[69] to perturbed anharmonic oscillators of free hydrogen halides for the strongly asymmetric species. In the former case, the principal hydrogen stretching frequency is downshifted by as much as 2600 cm^{-1} upon complexation, and the structure of the vibrational spectrum is dominated by electron correlation and higher-order anharmonicity effects.[65] Microscopic probes of reaction dynamics on $[XHY]^-$ surfaces provide a view complemen-

TABLE I. Selected structural and spectroscopic data for hydrogen bihalide anions.[a,b]

EXPERIMENT			
$[FHF]^-$ **38.6 kcal mol^{-1}** **G(1.1389, 1.1389) Å** **G[583, 1286, 1331] cm^{-1}** (75;90; 90; 89,85,92, 72)	**$[FHCl]^-$** **21.8 kcal mol^{-1}** **S[275, 843, 2710] cm^{-1}** **M[na, 829, 2491] cm^{-1}** (77; 81; 85; 73)	**$[FHBr]^-$** ***17* kcal mol^{-1}** **S[220, 740, *2900*] cm^{-1}** **M[na, 749, 2803] cm^{-1}** (76; 81; 85; 73)	**$[FHI]^-$** ***15* kcal mol^{-1}** **S[180, 635, 3145] cm^{-1}** **M[na, na, 2950] cm^{-1}** (76; 81; 85; 73)
$[FHF]^-$ **45.0 kcal mol^{-1}** **(1.144, 1.144) Å** **ν[570, 1302, 1316] cm^{-1}** (97; 66; 67; 65, 98, 99)	**$[ClHCl]^-$** **23.1 kcal mol^{-1}** **G(1.5733, 1.5733) Å** **G[*318*, *795*, 723] cm^{-1}** (76-78; 91; 91; 82, 87, 73)	**$[ClHBr]^-$** **19.6 kcal mol^{-1}** **S[170, 1100, 1650][c] cm^{-1}** **M[na, 1365, 1115][c] cm^{-1}** (79; 83; 86; 73)	**$[ClHI]^-$** **14.4 kcal mol^{-1}** **M[na, 1065, 1560][c] cm^{-1}** (79; 50; 73; 93)
$[FHCl]^-$ **20 ± 2 kcal mol^{-1}** **(0.963, 1.924) Å** **ν[250, 863, 2814] cm^{-1}** (103;100; 100)	**$[ClHCl]^-$** **22.4 kcal mol^{-1}** **(1.563, 1.563) Å** **ν[300, 789, 694] cm^{-1}** (69; 67; 67; 68, 99)	**$[BrHBr]^-$** **20.9 kcal mol^{-1}** **S(1.675, 1.675) Å** **M[177, na, 727] cm^{-1}** (79;94; 86; 73, 80,95,96)	**$[BrHI]^-$** **16.1 kcal mol^{-1}** **M[na, na, 920] cm^{-1}** (79; 88; 73)
$[FHBr]^-$ **17.6 kcal mol^{-1}** **(0.947, 2.149) Å** (104)	**$[ClHBr]^-$** **14 ± 1 kcal mol^{-1}** **(1.357, 2.065) Å** (105)	**$[BrHBr]^-$** **19.7 kcal mol^{-1}** **(1.680, 1.680) Å** **ν[200, *765*, 837] cm^{-1}** (101; 101; 101; 102)	**$[IHI]^-$** **17.0 kcal mol^{-1}** **M[*130*, na, *673*] cm^{-1}** (79; 88; 73, 50, 96)
$[FHI]^-$ **18.8 kcal mol^{-1}** **(0.947, 2.23) Å** **ω[220, na, 3380] cm^{-1}** (106)	**$[ClHI]^-$** **na**	**$[BrHI]^-$** **na**	**$[IHI]^-$** **(1.911, 1.911) Å** **ν[135, 503, 571] cm^{-1}** (56)
THEORY			

[a]The binding energy relevant to the preferred dissociation channel $[XHY]^- \rightarrow HX + Y^-$ is listed first in kcal mol^{-1}. Most of the experimental values are actually enthalpies of complexation at ambient temperature, while the theoretical results are 0 K predictions. If available, the H–X and H–Y bond distances for each $[XHY]^-$ anion are sequentially given next in Å. The experimental data include zero-point vibrational effects. Sets of fundamental vibrational frequencies (ν_1,ν_2,ν_3) then appear in cm^{-1}, where ν_1 corresponds to the interhalogen (symmetric) stretch, ν_2 to the degenerate bend, and ν_3 to the principal (antisymmetric) hydrogen stretch. The selected condensed-phase experimental frequencies are those most closely correspondent with the character of the anion in the gas phase. Finally, selected references are provided in the order of the listed data entries, semicolons being used to partition the list accordingly. Those references in the last partition are supplementary to the listed data.

[b]Abbreviations: G=gas phase, S=solid phase, M=matrix isolation, na=not available. The data in italics are estimates; underlined frequencies are average positions of split bands. In the theoretical section, ω and ν indicate whether the frequency predictions are harmonic or anharmonic results, respectively.

[c]The bending frequencies in these cases may actually be overtones.

tary to bound-state spectroscopy experiments, as exemplified by the studies of Leone and co-workers[70,71] in which the nascent vibrational product distributions for the thermal proton abstraction reactions $X^- + HY \rightarrow HX(\nu) + Y^-$ (X=F, Cl; Y=Cl, Br, I) were measured via infrared chemiluminescence detection in a flowing afterglow apparatus.

In Table I, a grid of relevant structural and spectroscopic data is presented for the hydrogen bihalide ions in the form of an array partitioned into experimental (upper) and theoretical (lower) triangles. The references listed therein[50,56,65–69,72–106] are current and apposite but by no means exhaustive in each case. Review articles by Emsley,[72] Ault,[73] and Andrews[74] can be perused for additional details. For most ions the binding energy (14–39 kcal mol^{-1}) associated with the preferred dissociation channel, $[XHY]^- \rightarrow HX + Y^-$, has been determined in ion-cyclotron resonance experiments involving halide exchange equilibria by Larson and McMahon[75–78] and Caldwell and Kebarle.[79] The early condensed-phase

investigations by Evans and Lo[80–84] and the matrix-isolation studies of Ault and co-workers[50,73,85–88] account for most of the infrared data for these systems. Two distinct structural types are consistently revealed in the vibrational spectra: (type I) asymmetric ions with localized potential wells and high hydrogen-stretching frequencies, and (type II) centrosymmetric ions with broad surfaces and low hydrogen-stretching frequencies. Both type I and type II absorptions are typically observed for each anion, indicating strong interactions with various trapping-site environments and the necessity of gas-phase IR data for unambiguous characterizations. The first recording of a high-resolution infrared spectrum of any polyatomic molecular anion in the gas phase occurred in a 1986 investigation of $[FHF]^-$ by Kawaguchi and Hirota[89] in which velocity-modulation infrared diode laser spectroscopy was employed. Subsequent work[90,91] by these researchers using this technique on the $[FHF]^-$ and $[ClHCl]^-$ systems has provided the only gas-phase geometric structures and fundamental frequencies currently available for hydrogen bihalide anions.

Reliable *ab initio* predictions for the $[XHY]^-$ anions require immense one-particle basis sets and rigorous electron correlation techniques, as well as careful treatments of vibrational anharmonicity. These criteria are vividly demonstrated in the bichloride and bibromide cases, for which restricted Hartree–Fock theory with flexible basis sets erroneously predicts $C_{\infty v}$ rather than $D_{\infty h}$ optimum geometric structures.[69,101] To date the most systematic theoretical effort to characterize the $[XHY]^-$ anions has been undertaken by Sannigrahi and co-workers, who have reported MRD-CI studies of $[FHF]^-$,[99] $[ClHCl]^-$,[99] $[BrHBr]^-$,[102] $[FHCl]^-$,[103] $[FHBr]^-$,[104] $[ClHBr]^-$,[105] and $[FHI]^-$ [106] using moderately sized basis sets. The predicted bond distances of the last three species, in which the HF and HCl units are essentially preserved, constitute the only available structural data for these ions. The associated binding-energy predictions suffer from basis set superposition errors, size consistency problems, and uncertainties in zero-point vibrational energies but are broadly consistent with experimental estimates of the corresponding quantities. The data listed in Table I for the other two heavy-halide systems, $[BrHBr]^-$ and $[IHI]^-$, are from the Br[14*s*11*p*3*d*], H[3*s*2*p*1*d*] MP2 results of Ikuta *et al.*[101] and the very recent I[RECP+3*s*3*p*2*d*1*f*], H[5*s*4*p*1*d*] ANO-type CCSD(T) predictions of Schatz and co-workers,[56] respectively, the agreement with experiment being reasonably good where such comparisons are apt.

The previous theoretical work[65–69,97–100,103,107–109] of greatest significance to the current study is that which has focused on the thermochemistry and vibrational dynamics of $[FHF]^-$, $[ClHCl]^-$, and $[FHCl]^-$. A controversial assignment by Kawaguchi and Hirota[89] of the antisymmetric stretching fundamental (ν_3) of $[FHF]^-$ in their initial gas-phase infrared study heightened theoretical interest in this system. In 1986, Janssen *et al.*[65] reported unprecedented variation in *ab initio* predictions of the harmonic and anharmonic components of ν_3 as the level of theory was systematically improved, but their final results, as well as concurrent predictions by Botschwina[98] and Yamashita and Morokuma,[109] led to the reassignment of ν_3 to a band subsequently detected at 1331 cm^{-1}.[90] More recently, Špirko and co-workers[66,67] have constructed a mixed MP4 and CCSDT-1a surface for $[FHF]^-$ using a F[5*s*3*p*2*d*], H[3*s*2*p*] basis set. A three-dimensional variational vibrational analysis[67] on this surface subsequently predicted the fundamental frequencies $(\nu_1,\nu_2,\nu_3)=(570,1302,1316)$ cm^{-1}, all of which lie within 20 cm^{-1} of experiment. A Cl[7*s*5*p*2*d*], H[3*s*2*p*] MP4 surface for $[ClHCl]^-$ was simultaneously reported by Špirko *et al.*[67] which gave $(\nu_1,\nu_2,\nu_3)=(300,789,694)$ cm^{-1} by the same vibrational method, as compared to values of (318, 795, 723) cm^{-1} deduced from the observed spectrum by Kawaguchi.[91] Other *ab initio* vibrational analyses of $[ClHCl]^-$ include the two-dimensional variational treatments of Botschwina and co-workers[68] (Cl[10*s*10*p*3*d*], H[5*s*2*p*] CEPA-1) and Ikuta *et al.*[69] [DZ+(*d*,*p*) MP4] based on local representations of the potential energy surface.

Only two notable theoretical investigations have focused on the $[FHCl]^-$ system. The MRD-CI study of Sannigrahi and Peyerimhoff,[103] in which a F[7*s*4*p*1*d*], Cl[9*s*6*p*2*d*], and H[3*s*2*p*] basis set was employed, predicted a binding energy of 20 ± 2 kcal mol^{-1} and a geometric structure with an H–Cl separation near 1.93 Å and an H–F bond elongated by *ca.* 0.04 Å relative to free hydrogen fluoride. The proposed binding energy is ostensibly in excellent agreement with the empirically derived chloride affinity (21.8 kcal mol^{-1}) of Larson and McMahon.[76,77] Nonetheless, the striking disparity apparent in Table I which remains between the analogous experimental binding energy (38.6 kcal mol^{-1})[75] of $[FHF]^-$ and the high-level *ab initio* results of Frisch *et al.* (45.0 kcal mol^{-1})[97] warrants a more extensive theoretical analysis of the corresponding energetics of the $[FHCl]^-$ system. Recently, Botschwina[100] has published a brief summary of a vibrational analysis of $[FHCl]^-$ performed with the same techniques utilized previously for $[ClHCl]^-$.[68] The report was restricted to bond distances and fundamental vibrational frequencies, as given in Table I.

II. THEORETICAL METHODS

A. Basis sets

The atomic Gaussian-orbital basis sets employed in this study are denoted as TZ(1+)(2*d*,2*p*), TZ(2+)(2*d*,2*p*), TZ(1+)(3*d*,3*p*), TZ(1+)(2*d*1*f*,2*p*1*d*), QZ(1+)(2*d*1*f*,2*p*1*d*), and *n*HF(*extpol*). In the first five cases, whose designations are of the form $A(k+)(x,y)$, A is broadly descriptive of the underlying *sp* basis, $(k+)$ symbolizes the addition of k sets of diffuse orbitals to each center, and x and y indicate the sets of polarization functions appended to the heavy atoms and the hydrogen atom, respectively. The *n*HF(*extpol*) basis is comprised of a large, uncontracted *sp* set of near Hartree–Fock quality (*n*HF) augmented by an extended set of *d*- and *f*-type polarization functions (*extpol*). The basis sets used here range in number of contracted Gaussian func-

TABLE II. Total energies (hartree) at various levels of theory.[a]

	F^-	HF	Cl^-	HCl	$[FHCl]^-$
Set A[b]					
TZ(1+)(2*d*,2*p*) (91)	[Cl(13*s*10*p*2*d*/10*s*7*p*2*d*), F(11*s*7*p*2*d*/6*s*4*p*2*d*), H(6*s*2*p*/4*s*2*p*)]				
RHF	−99.455 170	−100.064 714	−459.569 831	−460.102 466	−559.665 859
CCSD	−99.710 250	−100.314 724	−459.753 453	−460.294 828	−560.104 825
TZ(2+)(2*d*,2*p*) (100)	[Cl(14*s*11*p*2*d*/11*s*8*p*2*d*), F(12*s*8*p*2*d*/7*s*5*p*2*d*), H(7*s*2*p*/5*s*2*p*)]				
RHF	−99.455 233	−100.064 721	−459.569 868	−460.102 485	−559.665 902
CCSD	−99.710 542	−100.314 809	−459.753 535	−460.294 883	−560.105 008
TZ(1+)(3*d*,3*p*) (98)	[Cl(13*s*10*p*3*d*/10*s*7*p*3*d*), F(11*s*7*p*3*d*/6*s*4*p*3*d*), H(6*s*3*p*/4*s*3*p*)]				
RHF	−99.455 178	−100.065 137	−459.569 859	−460.103 306	−559.666 213
CCSD	−99.716 121	−100.319 240	−459.758 045	−460.298 140	−560.113 638
TZ(1+)(2*d*1*f*,2*p*1*d*) (105)	[Cl(13*s*10*p*2*d*1*f*/10*s*7*p*2*d*1*f*), F(11*s*7*p*2*d*1*f*/6*s*4*p*2*d*1*f*), H(6*s*2*p*1*d*/4*s*2*p*1*d*)]				
RHF	−99.455 179	−100.066 222	−459.569 908	−460.104 148	−559.667 292
CCSD	−99.736 578	−100.343 351	−459.786 100	−460.329 137	−560.166 673
Set B[c]					
QZ(1+)(2*d*1*f*,2*p*1*d*) (116)	[Cl(13*s*10*p*2*d*1*f*/11*s*8*p*2*d*1*f*), F(11*s*7*p*2*d*1*f*/7*s*5*p*2*d*1*f*), H(6*s*2*p*1*d*/4*s*2*p*1*d*)]				
RHF	−99.455 205	−100.065 875	−459.570 005	−460.104 230	−559.666 454
MP2	−99.745 194	−100.345 318	−459.770 741	−460.309 333	−560.154 224
MP3	−99.733 780	−100.344 438	−459.787 438	−460.329 600	−560.168 698
MP4	−99.753 684	−100.355 364	−459.793 960	−460.336 643	−560.187 348
CCSD	−99.739 271	−100.346 807	−459.786 180	−460.329 198	−560.169 554
BD	−99.738 278	−100.346 394	−459.786 124	−460.329 121	−560.169 029
CCSD(T)	−99.748 020	−100.353 765	−459.793 961	−460.337 001	−560.185 460
BD(T)	−99.747 832	−100.353 639	−459.793 986	−460.337 004	−560.185 370
BD(TQ)	−99.746 575	−100.353 488	−459.794 305	−460.337 516	–
*n*HF(+)(*extpol*) (281)	[Cl(20*s*14*p*7*d*5*f*), F(18*s*13*p*6*d*4*f*), H(8*s*3*p*2*d*1*f*)]				
RHF	−99.459 445	−100.070 732	−459.576 858	−460.112 661	−559.678 078
MP2	−99.762 826	−100.361 887	−459.789 157	−460.327 362	−560.188 494
MP2(FULL)[d]	−99.829 683	−100.428 862	−460.190 670	−460.729 139	−560.657 157
EXPT[e]	−99.929 2	−100.528 7	–	–	–

[a]For each basis set, the total number of contracted Gaussian functions is given in parentheses followed by the contraction designation.
[b]Determined at the respective RHF and CCSD optimum structures.
[c]Determined at the TZ(1+)(3*d*,3*p*) CCSD optimum geometry.
[d]All core and virtual orbitals active in the correlation procedure.
[e]Exact correlated, relativistic energies derived from the empirical total energy (−99.8043 a.u.) (Ref. 110) and electron affinity (3.399 eV) (Ref. 111) of the fluorine atom and $D_e(H\text{–}F)=141.00$ kcal mol^{-1} (Ref. 112).

tions (CGFs) from 91 in the TZ(+)(2*d*,2*p*) case to 281 in the *n*HF(*extpol*) set. For each basis set the size and contraction designation appear in Table II.

The TZ (triple-ζ) *sp* basis for fluorine consists of the (10*s*6*p*) Gaussian primitives of Huzinaga[113] and the (5*s*3*p*) contractions of Dunning.[114] The analogous hydrogen basis is a Huzinaga–Dunning[113,114] (5*s*/3*s*) set in which the exponents are scaled for molecular calculations by the standard factor of 1.49[2]. For chlorine, the TZ basis involves the (12*s*9*p*) neutral-atom primitives of McLean and Chandler[115] contracted to (9*s*6*p*) according to (4,1,1,1,1,1,1,1,1) and (4,1,1,1,1,1) schemes for the *s* and *p* functions, respectively. The Gaussian exponents of the diffuse functions in the TZ(1+) basis sets are $\alpha_s(F)=0.1164$, $\alpha_p(F)=0.071\,61$, $\alpha_s(H)=0.066\,96$, $\alpha_s(Cl)=0.051\,77$, and $\alpha_p(Cl)=0.045\,25$. The exponents of the additional *s* and *p* primitives employed in the TZ(2+) case are $\alpha_s(F)=0.039\,51$, $\alpha_p(F)=0.024\,32$, $\alpha_s(H)=0.020\,51$, $\alpha_s(Cl)=0.015\,89$, and $\alpha_p(Cl)=0.016\,08$. All of these diffuse-function exponents were derived from average even-tempering ratios computed from the last three valence primitives in the underlying TZ *sp* sets. The QZ (quadruple-ζ) *sp* functions consist merely of looser contractions of the primitives in the TZ basis sets for each atom. Specifically, for fluorine a Huzinaga–Dunning[113,114] (10*s*6*p*/5*s*4*p*) contraction is utilized, whereas for chlorine (3,1,1,1,1,1,1,1,1,1) and (3,1,1,1,1,1,1) contraction schemes of the McLean–Chandler[115] *s* and *p* primitives are used to arrive at (12*s*9*p*/10*s*7*p*) sets. The hydrogen (5*s*/3*s*) contraction in the QZ set is the same as that selected in the TZ case. Likewise, the diffuse functions appended to all atoms in the QZ and TZ basis sets are identical.

The polarization-function exponents employed for fluorine and hydrogen in both the TZ and QZ basis sets are the correlation-optimized values of Dunning.[116] In particular, the exponents for the $2d$, $3d$, and $1f$ sets for fluorine are, in order, (0.855, 3.107), (0.586, 1.725, 5.014), and 1.917, while those of the $2p$, $3p$, and $1d$ sets for hydrogen are (0.388, 1.407), (0.292, 0.838, 2.292), and 1.057. The corresponding d polarization sets for chlorine are based on a reference exponent of 0.619 for correlated wave functions, as given by a formula proposed by Ahlrichs and Taylor.[117] Successive splitting of this value by multiplicative factors of $3^{1/2}$ and $3^{-1/2}$ gives $2d$ and $3d$ sets with the exponents (0.357, 1.072) and (1.857, 0.619, 0.206), respectively. The chlorine $1f$ set involves the exponent $\alpha_f=0.70$, as recommended by Frisch, Pople, and Binkley.[118] The supernumerary s and p orbitals of the Cartesian polarization manifolds are *not* excluded in the TZ and QZ basis sets, i.e., six and ten components are used in the d and f sets, respectively.

The uncontracted nHF(*extpol*) basis is comprised of F($18s13p6d4f$), Cl($20s14p7d5f$), and H($8s3p2d1f$) primitive sets, whose exponents are explicitly given in a footnote.[119] For fluorine and chlorine these sets are built up from the F($17s12p$) and Cl^-($19s14p$) primitives of Partridge,[120–123] the former being augmented by a set of diffuse s and p orbitals and the latter by a single diffuse s function in order to fully span the range of exponents present in the TZ(1+) and QZ(1+) basis sets. For hydrogen the $7s$ primitive set of van Duijneveldt[124] is employed after the addition of a diffuse s function. The nHF(*extpol*) polarization manifolds for fluorine are constructed from the $3d$ and $2f$ correlation-optimized sets of Dunning,[116] which are expanded to $6d$ and $4f$ sets by even-tempered extension into the core region. In a similar fashion, the $3d$ set for chlorine appearing in the TZ(1+)($3d$,$3p$) basis is enlarged to yield a $7d$ set capable of describing core correlation effects. The associated $5f$ set for chlorine is obtained by first splitting the $\alpha_f=0.70$ exponent multiplicatively with factors of $3^{\pm 1/2}$ prior to even-tempered expansion into the core region using a geometric ratio of 3. For hydrogen, polarization is effected in the nHF(*extpol*) basis with the $3p$ set described above, to which the $2d$ and $1f$ manifolds of Dunning[116] are appended. In the nHF(*extpol*) basis, only real combinations of the true $l=2$ and 3 spherical harmonics are included in the d and f sets.

B. Electronic wave functions

All reference electronic wave functions in this study were determined by the single-configuration, self-consistent-field, restricted Hartree–Fock method (RHF).[125–128] Dynamical electron correlation was accounted for primarily by the coupled-cluster singles and doubles method (CCSD),[129–134] but in some cases additional predictions were obtained using Møller–Plesset perturbation theory through fourth order [MP2, MP3, and MP4(SDTQ)],[135–138] CCSD theory augmented by a perturbative contribution from connected triple excitations [CCSD(T)],[139,140] and the Brueckner doubles (BD) method with analogous corrections for both triple and quadruple excitations [BD(T) and BD(TQ)].[141,142] The electronic structure computations used to construct the global potential energy surface of $[FHCl]^-$ were performed with the program package TITAN,[143] whereas PSI[144] and GAUSSIAN 92[145] were employed for auxiliary predictions. Unless otherwise stated, the fluorine $1s$ and the chlorine $1s$, $2s$, and $2p$ core orbitals were excluded from the active space in the correlation treatments. Several high-lying virtual orbitals with energies greater than 21 hartree were also frozen in the correlation procedures. The number of such virtual orbitals attributable to the (F,Cl) core regions were (2, 7) and (2, 11) in the TZ and QZ basis sets, respectively. In the nHF(*extpol*) case, the number of frozen virtual orbitals localized on fluorine and chlorine were 58 and 62, respectively, while two extra frozen virtuals arose from the tight hydrogen primitives.

C. Vibrational analyses

Optimum geometric structures and harmonic vibrational frequencies for $[FHCl]^-$ and its diatomic fragments were determined with each of the four TZ basis sets at both the RHF and CCSD levels of theory. Analytic first- and second-derivative techniques[146–152] were employed to facilitate the RHF predictions, whereas energy points alone were used in the CCSD cases. Nonetheless, the CCSD optimum bond distances were located to 10^{-4} Å by a cyclic interpolation scheme, and the corresponding harmonic frequencies were determined to *ca.* 0.1 cm^{-1} via double-finite difference procedures with displacement sizes of 0.01 Å and 0.02 rad for the simple internal coordinates. As described in Sec. IV, the global potential energy surface for $[FHCl]^-$ was generated at the TZ(1+)($3d$,$3p$) CCSD level of theory, and ancillary RHF and MP2 data were obtained in the process. In order to guide the rigorous construction and vibrational analysis of the final surface, the complete TZ(1+)($3d$,$3p$) CCSD quartic force field for $[FHCl]^-$ was explicitly evaluated by numerical differentiation. A total of 10 single, 12 double, and 2 triple displacements of the simple internal coordinates sufficed to determine all constants in the quartic field from energy points computed to high precision (10^{-10} a.u. or better). The step sizes employed to generate the grid of energy data were 0.01 Å and 0.02 rad, as before. After transformation of the TZ(1+)($3d$,$3p$) CCSD internal-coordinate quartic force field to a reduced normal-coordinate representation, vibrational anharmonic constants (χ_{ij}) and vibration-rotation interaction constants (α_i^B) were determined using formulas derived from second-order perturbation theory as applied to the standard vibration–rotation Hamiltonian[153–157] for semirigid linear molecules. This procedure has been investigated extensively in the systematic studies of vibrational anharmonicity in linear and asymmetric top molecules by Allen and co-workers.[158,159] A description of the variational techniques[160–165] employed in the rigorous vibrational analysis of the TZ(1+)($3d$,$3p$) CCSD global surface is reserved for Sec. V.

TABLE III. Calibration data—spectroscopic constants of HF and HCl.[a,b]

	r_e	ω_e	$\omega_e x_e$	f_{rr}	f_{rrr}	f_{rrrr}
HF						
TZ(1+)(2*d*,2*p*) CCSD	0.9160 (+0.0176)	4176 (–287)	89.71	9.8344	–72.277	484.57
TZ(2+)(2*d*,2*p*) CCSD	0.9159 (+0.0175)	4176 (–287)	90.21	9.8355	–72.315	483.12
TZ(1+)(3*d*,3*p*) CCSD	0.9152 (+0.0177)	4159 (–302)	88.90	9.7540	–71.883	489.06
TZ(1+)(2*d*1*f*,2*p*1*d*) CCSD	0.9154 (+0.0177)	4202 (–273)	89.21	9.9555	–72.913	486.66
EXPT[c]	0.9168	4138.3	89.88	9.6568	–71.20	480.7
HCl						
TZ(1+)(2*d*,2*p*) CCSD	1.2723 (+0.0064)	3027 (–116)	61.76	5.2878	–30.599	143.31
TZ(2+)(2*d*,2*p*) CCSD	1.2723 (+0.0064)	3027 (–115)	61.72	5.2874	–30.598	143.44
TZ(1+)(3*d*,3*p*) CCSD	1.2725 (+0.0072)	3010 (–123)	53.87	5.2280	–29.260	142.05
TZ(1+)(2*d*1*f*,2*p*1*d*) CCSD	1.2749 (+0.0079)	3028 (–112)	52.77	5.2924	–29.370	141.80
EXPT[c]	1.2746	2990.9	52.82	5.1631	–28.74	139.9

[a]Equilibrium distances (r_e) in Å, harmonic frequencies (ω_e) and anharmonic constants ($\omega_e x_e$) in cm^{-1}, force constants (f_{rr},f_{rrr},f_{rrrr}) of order n in aJ $Å^{-n}$.
[b]For each basis set the CCSD–RHF correlation shifts for r_e and ω_e are given in parentheses.
[c]Reference 166. The listed cubic and quartic constants were derived from the observed r_e, α_e, ω_e, and $\omega_e x_e$ constants via standard expressions from second-order perturbation theory (Ref. 167).

III. STRUCTURAL ASPECTS OF THE $[FHCl]^-$ COMPLEX

A. Calibrations

Investigation of the $[FHCl]^-$ molecular anion was initiated with calibrations of various theoretical methods for the HF, HCl, F^-, and Cl^- fragments. In Table III theoretical equilibrium bond distances, harmonic vibrational frequencies, vibrational anharmonic constants, and force constants through fourth order for HF and HCl are compared with experimental counterparts. The CCSD–RHF correlation shifts for the bond distances of HF and HCl are modest, *ca.* +0.018 and +0.007 Å, respectively, and relatively insensitive to the basis sets listed in the table. The CCSD equilibrium bond lengths which result for HF and HCl are all within 0.0016 and 0.0023 Å, respectively, of the accepted r_e values, displaying a tendency toward the underestimation of these quantities. The high accuracy of the CCSD structural predictions indicates a balance of residual errors due to limitations of the correlation treatment and incompleteness of the basis set, although for these simple hydrides such errors are substantially mitigated relative to those of multiply bonded species.

The CCSD harmonic frequencies for HF and HCl are uniformly higher than experiment, but the ranges of error are only 21–64 and 19–37 cm^{-1}, respectively. The TZ(1+)(3*d*,3*p*) CCSD method happens to provide the best predictions, in large part because the correlation shifts of −302 and −123 cm^{-1} predicted for ω_e(HF) and ω_e(HCl), respectively, are largest for this level of theory. The CCSD predictions for $\omega_e x_e$ of HF all lie within 1 cm^{-1} of the empirical value (89.88 cm^{-1}) as a consequence of excellent individual reproduction of the underlying f_{rrr} and f_{rrrr} constants. For HCl only the TZ(1+)(3*d*,3*p*) and TZ(1+)(2*d*1*f*,2*p*1*d*) CCSD anharmonic constants compare as favorably with the observed value, $\omega_e x_e$(HCl) =52.82 cm^{-1}. In the TZ(1+)(2*d*,2*p*) and TZ(2+)(2*d*,2*p*) CCSD cases, the $\omega_e x_e$ values are *ca.* 9 cm^{-1} too large, a disparity which can be traced entirely to the overestimation of f_{rrr}^2 relative to f_{rr}.

The principal conclusion of these calibrations is that the TZ(1+)(3*d*,3*p*) CCSD method is a particularly advantageous level of theory in reproducing the harmonic and fundamental vibrational frequencies of HF and HCl, while also maintaining high accuracy in corresponding predictions of bond lengths and relative energies (*vide infra*). Accordingly, in this study the full potential surface for $[FHCl]^-$ was generated at the TZ(1+)(3*d*,3*p*) CCSD level, which for the HF and HCl asymptotes yields r_e distances to approximately 0.002 Å, ω_e values to 20 cm^{-1}, anharmonicities to 2 cm^{-1}, and f_{rr}, f_{rrr}, and f_{rrrr} force constants to 1%–2%. In addition, the TZ(1+)(3*d*,3*p*) CCSD method predicts the dipole moments μ_e(HF)

$=1.828$ and $\mu_e(HCl)=1.114$ D, which are in excellent agreement with the experimentally deduced μ_e values of 1.796 and 1.093 D, respectively.[168] Therefore, the asymptotic ion-dipole character of the $HF+Cl^-$ and $HCl+F^-$ dissociation channels is accurately represented by the TZ(1+)(3*d*,3*p*) CCSD potential surface.

Total energies at several levels of theory are listed for F^-, HF, Cl^-, HCl, and $[FHCl]^-$ in Table II along with the aforementioned basis set designations. Set A therein involves RHF and CCSD values obtained with the TZ(1+)(2*d*,2*p*), TZ(2+)(2*d*,2*p*), TZ(1+)(3*d*,3*p*), and TZ(1+)(2*d*1*f*,2*p*1*d*) basis sets at the optimum geometry for each level of theory. Within this data set the various CCSD energy lowerings in millihartrees (mH) which arise from augmentation of the TZ(1+)(2*d*,2*p*) basis lie in the following ranges: (1+)→(2+), [0.05(HCl), 0.29(F^-)]; (2*d*,2*p*)→(3*d*,3*p*), [3.31(HCl), 8.81($[FHCl]^-$)]; and (2*d*,2*p*)→(2*d*1*f*,2*p*1*d*), [26.3(F^-), 61.8($[FHCl]^-$)]. Because the upper limit of the first range amounts to less than 0.2 kcal mol^{-1}, the sufficiency of the (1+) diffuse *sp* basis is demonstrated, in accord with the observation of nearly identical spectroscopic constants at the TZ(1+)(2*d*,2*p*) and TZ(2+)(2*d*,2*p*) CCSD levels in Table III. The considerable magnitude of the (2*d*,2*p*)→(2*d*1*f*,2*p*1*d*) energy reductions relative to the (2*d*,2*p*)→(3*d*,3*p*) values is entirely consistent with the results of Dunning[116] and numerous others, demonstrating that the preference of the (2*d*,2*p*)→(3*d*,3*p*) augmentation in predicting the vibrational frequencies of HF and HCl arises from a more precise balance of residual errors rather than a more robust set of wave functions.

The total energy values listed in set B of Table II, which are based on TZ(1+)(3*d*,3*p*) CCSD reference geometries, consist of high-level correlation results for the QZ(1+)(2*d*1*f*,2*p*1*d*) basis and MP2 predictions for the *n*HF(+)(*extpol*) set. For HCl and Cl^-, the general trend is a lowering of the QZ(1+)(2*d*1*f*,2*p*1*d*) total energy as the correlation treatment is systematically improved,

$$E(HCl,Cl^-):\quad RHF>MP2>BD>CCSD>MP3$$
$$>MP4>CCSD(T)>BD(T)>BD(TQ),$$

whereas oscillatory patterns are seen in the analogous series for HF and F^-,

$$E(HF,F^-):\quad RHF>MP3>(MP2)>BD>CCSD$$
$$>(MP2)>BD(TQ)>BD(T)>CCSD(T)>MP4,$$

the MP2 entry occurring after MP3 for HF but following CCSD for F^-. This behavior is consonant with the QZ(1+)(2*d*1*f*,2*p*1*d*) values of the $\mathcal{T}_1$ diagnostic derived from the Euclidean norm of the t_1(CCSD) amplitudes,[169] *viz.*, F^-(0.0197), HF(0.0093), Cl^-(0.0055), and HCl(0.0058). To wit, the $\mathcal{T}_1$ value for F^- lies near the onset of substantial multireference character in electronic wave functions according to the 0.02 cutoff proposed by Lee and Taylor,[169] and thus, for example, sizeable oscillations in the MP*n* energies are not unexpected. In contrast, the chloride ion exhibits a very small $\mathcal{T}_1$ diagnostic and is strongly dominated by the Hartree–Fock reference. This occurrence is manifested in a monotonic MP*n* series and remarkable agreement (within 0.035 kcal mol^{-1}) between the BD and BD(T) values and their coupled-cluster counterparts. The QZ(1+)(2*d*1*f*,2*p*1*d*) value of $\mathcal{T}_1$ for the $[FHCl]^-$ complex is 0.0086, which is shifted slightly downward from that of HF. Single-reference correlation treatments, at least in the bound regions of the surface, are thus entirely sufficient for this complex.

A comparison of analogous QZ(1+)(2*d*1*f*,2*p*1*d*) and *n*HF(+)(*extpol*) total energies in Table II reveals energy lowerings from this final basis set enlargement of 4.2–11.6 and 16.6–34.3 mH at the RHF and MP2 levels, respectively. The addition to the *n*HF(+)(*extpol*) basis of *g*-type functions and higher-order spherical harmonics would likely engender a further reduction of comparable magnitude in the MP2 energy. The correlation of the core electrons of the composite $[FHCl]^-$ system leads to a 469 mH lowering of the total energy at the *n*HF(+)(*extpol*) MP2 level with all core and virtual orbitals active [MP2(FULL)]. However, comparison of the corresponding F^- and HF results to the exact total energies of these species, which include only limited relativistic contributions, shows that only about 40% of the core correlation energy is recovered in these cases by the *n*HF(+)(*extpol*) MP2(FULL) procedure.

B. Geometric structure and spectroscopic constants

Theoretical predictions for the geometric structure and harmonic vibrational frequencies of $[FHCl]^-$ appear in Table IV. At the equilibrium geometry of $[FHCl]^-$, the hydrogen fluoride moiety remains intact, even though the H–F distance is elongated by 0.045 Å due to chloride complexation. By comparison, the hydrogen halide distances in the centrosymmetric $[FHF]^-$ and $[ClHCl]^-$ ions are elongated by 0.22 and 0.30 Å relative to the corresponding monomers.[90,91] The H–Cl distance in $[FHCl]^-$ is approximately 0.66 Å longer than in free hydrogen chloride and 0.36 Å longer than in $[ClHCl]^-$;[91] however, the experimental chloride binding energies of $[FHCl]^-$ and $[ClHCl]^-$ differ by only 1.3 kcal mol^{-1}.[77] The CCSD–RHF correlation shifts for r_e(H–F) of $[FHCl]^-$ are consistently near +0.031 Å, while those for the H–Cl separation range from −0.120 to −0.128 Å. These shifts are considerably greater than in the monomers, and the latter indicate a substantial tightening and strengthening of the hydrogen bond as dispersion forces are included in the theoretical treatment. The RHF and MRD-CI structures of $[FHCl]^-$ obtained by Sannigrahi and Peyerimhoff[103] with a F[7*s*4*p*1*d*], Cl[9*s*6*p*2*d*], and H[3*s*2*p*] basis set display similar characteristics; specifically, the predicted correlated distances are r_e(H–F)=0.952 and R_e(H–Cl)=1.933 Å with respective correlation shifts of +0.024 and −0.132 Å. The interhalogen distances (cf. Table I) in $[FHF]^-$, $[FHCl]^-$, and $[ClHCl]^-$ are 2.28, 2.90, and 3.15 Å, respectively, which are, in order, 0.52, 0.25, and 0.35 Å shorter than the sums of the van der Waals radii of the halide atoms in these complexes.[170] According to the criterion of Emsley,[72] the symmetric bihalide species can be unambiguously catego-

TABLE IV. Theoretical predictions for the ion-molecule complex $[FHCl]^-$.[a,b]

	$D_e(1)$[c]	$D_e(2)$[c]	ΔE_e[c]	r_e(H-F)	R_e(H-Cl)	$\omega_1(\sigma)$	$\omega_2(\pi)$	$\omega_3(\sigma)$
TZ(1+)(2*d*,2*p*)	23.00	62.59	39.59	0.9617	1.9303	253	899	3232
CCSD	(+3.35)	(−5.32)	(−8.67)	(+0.0312)	(−0.1277)	(+39)	(+61)	(−500)
TZ(2+)(2*d*,2*p*)	23.01	62.49	39.48	0.9617	1.9300	253	880	3233
CCSD	(+3.36)	(−5.40)	(−8.76)	(+0.0312)	(−0.1280)	(+38)	(+43)	(−500)
TZ(1+)(3*d*,3*p*)	22.80	62.36	39.56	0.9600	1.9427	250	883	3240
CCSD	(+3.21)	(−5.24)	(−8.45)	(+0.0307)	(−0.1197)	(+37)	(+47)	(−495)
TZ(1+)(2*d*1*f*,2*p*1*d*)	23.36	63.35	39.99	0.9606	1.9330	248	869	3256
CCSD	(+3.81)	(−4.40)	(−8.21)	(+0.0310)	(−0.1268)			

[a]Dissociation energies (D_e) in kcal mol^{-1}, equilibrium distances (r_e,R_e) in Å, harmonic frequencies (ω_i) in cm^{-1}, and force constants (f_{rr},f_{rrr},f_{rrrr}) of order n in aJ Å^{-n}.
[b]The CCSD–RHF correlation shifts for the various quantities are given in parentheses.
[c](1) $[FHCl]^- \rightarrow HF + Cl^-$; (2) $[FHCl]^- \rightarrow HCl + F^-$. ΔE_e refers to the proton-transfer reaction $HF + Cl^- \rightarrow HCl + F^-$.

rized as systems with "strong" ion-molecule hydrogen bonds while $[FHCl]^-$ is marginal is this regard.

The general trend in the CCSD structural predictions for $[FHCl]^-$ is that augmentation of the TZ(1+)(2*d*,2*p*) basis slightly contracts the H–F distance and concomitantly increases the H–Cl separation. Higher-order correlation terms should produce the opposite effect. In view of the data in Tables III and IV, the following final structure is thus proposed: $r_e(\text{H–F}) = 0.963 \pm 0.003$ and $R_e(\text{H–Cl}) = 1.925 \pm 0.015$ Å. These proposals encompass the CEPA-1 bond distances, $r_e(\text{H–F}) = 0.9627$ and $R_e(\text{H–Cl}) = 1.9240$ Å, given in the brief report of Botschwina.[100] From the final structure it becomes evident that in photodetachment experiments involving $[FHCl]^-$, the Franck–Condon accessible region of the neutral surface is displaced well into the HF+Cl product valley, in similarity with the $[FHI]^-$ and $[ClHI]^-$ systems investigated by Bradforth *et al.*[48]

The CCSD predictions for the harmonic stretching frequencies of $[FHCl]^-$ lie in the narrow ranges $\omega_1 \in [248,253]$ and $\omega_3 \in [3232,3256]$ cm^{-1}. The correlation shifts reduce ω_3 by approximately 500 cm^{-1}, an immense change which is almost twice that observed for hydrogen fluoride itself. In contrast, the H–Cl stretching frequency is increased 37–39 cm^{-1} by electron correlation, in accord with the previously observed tightening of the hydrogen bond due to dispersion forces. Such effects also shift the degenerate bending frequency upward by 43–61 cm^{-1} to the range $\omega_2 \in [869,899]$ cm^{-1}.

The TZ(1+)(3*d*,3*p*) CCSD quartic force field for $[FHCl]^-$ and resulting anharmonic constants and fundamental frequencies are presented in Table V. Because the fundamental frequencies derived in Sec. V by variational methods applied to the global surface are well reproduced by second-order perturbation theory applied to the quartic force field, it is of merit to point out certain chemical characteristics of the latter predictions here. The H–F stretching fundamental ($\nu_3 = 2913$ cm^{-1}) exhibits a large negative anharmonicity (-327 cm^{-1}) and is downshifted 1068 cm^{-1}, or 27%, from ν_0 of free hydrogen fluoride. The rigorous variational result, $\nu_3 = 2884$ cm^{-1}, gives an even larger anharmonicity (-357 cm^{-1}) and complexation shift (-1097 cm^{-1}). According to Emsley,[72] the sizeable ν_3 downshift in $[FHCl]^-$ places the hydrogen bond in this species at the lower limit of the class of "strong" ion-molecule hydrogen bonds. In the prototype of extreme hydrogen bonding, $[FHF]^-$, the antisymmetric stretching fundamental (1331 cm^{-1})[90] is downshifted 66% from ν_0(HF) and displays a positive anharmonicity[65] due to the dominance of quartic terms in the potential energy expansion. The ν_1 fundamental (246 cm^{-1}) of $[FHCl]^-$ shows limited anharmonicity (-4 cm^{-1}) and lies roughly 70 cm^{-1} lower than the symmetric stretching fundamental of the more strongly bonded bichloride ion.[91] The bending fundamental ($\nu_2 = 878$ cm^{-1}) is also predominantly harmonic in nature and lies between $\nu_2([FHF]^-) = 1286$ and $\nu_2([ClHCl]^-) = 773$ cm^{-1}.[90,91]

Experimental data for the fundamental frequencies of $[FHCl]^-$ were first obtained in a 1966 study by Evans and Lo,[81] who treated crystalline tetraalkylammonium halides with HF gas and recorded the infrared spectra of the products in the solid phase and in methylene chloride and acetonitrile solutions. The salt $(C_2H_5)_4N^+[ClHF]^-$ gave rise to absorptions at 2710, 1588, 863, 823, and 275 cm^{-1} in the solid phase and 2850, 1570, and 835 cm^{-1} in solution. Apart from the bands near 1580 cm^{-1}, which are attributable to the bending overtone $2\nu_2$, the condensed-phase spectral features are in direct correspondence with predicted fundamental frequencies of gas-phase $[FHCl]^-$. The very strong, solution-phase absorption at 2850 cm^{-1} is in particularly good agreement with the final variational result ($\nu_3 = 2884$ cm^{-1}) of Sec. V. The matrix-isolation spectra of the hydrogen bihalide ions are characteristic of two distinct structural types, which in the case of $[FHCl]^-$ give rise to intense hydrogen stretching absorptions at both 2491 and 933 cm^{-1}.[73] The large deviation of these frequencies from the predicted gas-phase value of ν_3 indicates that in each of the two matrix trapping sites, the counterion has a considerable influence on the electronic structure of the $[FHCl]^-$ species.

C. Proton-transfer energy and chloride affinity

In Table IV and Fig. 1 theoretical data are presented for the proton-transfer energy (ΔE_e) of the reaction $HF + Cl^- \rightarrow HCl + F^-$, the chloride affinity of hydrogen fluoride, $D_e(1)$, as evaluated from $[FHCl]^- \rightarrow HF + Cl^-$, and the energy, $D_e(2)$, of the complementary dissociation

TABLE V. Characteristics of the TZ(1+)(3*d*,3*p*) CCSD global surface of $[FHCl]^-$.[a]

	Actual	Fitted
E_0	−560.113638	−560.113639
ΔE_e	39.56	39.56
$D_e(HF+Cl^-)$	22.80	22.80
r_e(H-F)	0.9600	0.9600
R_e(H-Cl)	1.9427	1.9427
ρ_e(F-H-Cl)[b]	0.0	0.0
$\omega_1(\sigma)$	249.8	249.8
$\omega_2(\pi)$	883.2	883.2
$\omega_3(\sigma)$	3240.4	3240.8
$\nu_1(\sigma)$[c]	246.1	246.0 (247)
$\nu_2(\pi)$	877.7	886.7 (876)
$\nu_3(\sigma)$	2913.3	2914.4 (2884)
f_{rr}	6.8214	6.8231
f_{Rr}	0.7017	0.7018
f_{RR}	0.4784	0.4784
$f_{\rho\rho}$	0.1862	0.1862
f_{rrr}	−52.164	−52.288
f_{Rrr}	−0.027	−0.043
f_{RRr}	−1.707	−1.711
f_{RRR}	−2.081	−2.082
$f_{\rho\rho r}$	−0.0392	−0.0393
$f_{\rho\rho R}$	−0.2394	−0.2395
f_{rrrr}	356.71	359.21
f_{Rrrr}	−1.614	−1.987
f_{RRrr}	1.689	1.575
f_{RRRr}	4.699	4.679
f_{RRRR}	7.232	7.242
$f_{\rho\rho rr}$	−0.050	−0.051
$f_{\rho\rho Rr}$	0.377	0.377
$f_{\rho\rho RR}$	0.470	0.470
$f_{\rho\rho\rho\rho}$	0.272	0.394
χ_{11}	−2.89	−2.89
χ_{21}	−9.34	−9.35
χ_{22}	−16.36	−12.96
χ_{31}	22.73	22.60
χ_{32}	65.80	65.74
χ_{33}	−202.13	−201.70
$\chi_{\ell_2\ell_2}$	15.34	14.21
$10^3\,\alpha_1$	2.052	2.052
$10^3\,\alpha_2$	0.096	0.097
$10^3\,\alpha_3$	−4.633	−4.626

[a]Units: E_0(hartree), ΔE_e and D_e(kcal mol^{-1}), r_e and R_e(Å), ω_i, ν_i, χ_{ij} and $10^3\alpha_i$ (cm^{-1}), and force constants relative to simple internal coordinates consistent with energy in aJ, distances in Å, and angles in rad.
[b]The bending displacement variable $\rho=\pi-\theta$(F–H–Cl) is a true angle and not a linear bending coordinate.
[c]Fundamental frequencies obtained via second-order perturbation theory (no anharmonic resonances observed). The rigorous values given by variational techniques appear in parentheses.

$[FHCl]^- \rightarrow HCl+F^-$. The CCSD results in Table IV place ΔE_e in the range 39.48–39.99 kcal mol^{-1} and incorporate negative correlation contributions of 8.21–8.76 kcal mol^{-1} magnitude. The source of this correlation effect is readily identified. At the TZ(1+)(2*d*1*f*,2*p*1*d*) CCSD level, for example, a comparison of the valence-shell correlation energies reveals that $\epsilon_{corr}(F^-)$ is greater than ϵ_{corr}(HF) by 2.7 kcal mol^{-1}, but $\epsilon_{corr}(Cl^-)$ is in fact less than ϵ_{corr}(HCl) by 5.5 kcal mol^{-1}. Thus, the correlation contributions for the $HF \rightarrow H^+ + F^-$ and $Cl^- + H^+ \rightarrow HCl$ half reactions are actually cumulative rather than compensatory, as anticipated from the $\mathcal{T}_1$ diagnostics reported above. In Fig. 1, a plot appears of the ΔE_e values derived from the QZ(1+)(2*d*1*f*,2*p*1*d*) entries of set B in Table II. The oscillatory pattern of the MP*n* predictions is prominent, and even the MP4 result is removed by 3 kcal mol^{-1} from the apparent *n*-particle limit. However, the BD and CCSD reaction energies, 40.85 and 40.49 kcal mol^{-1}, respectively, are quite similar, and the addition of the perturbative correction for connected triple excitations essentially brings these two values into coincidence at 39.4 kcal mol^{-1}. Even though the proton-transfer process is isogyric, the (Q) contribution arising from connected quadruple excitations is not negligible; in particular, ΔE_e is increased to 39.97 kcal mol^{-1} at the BD(TQ) level. It is reasonable to approximate the effect of basis set incompleteness on the QZ(1+)(2*d*1*f*,2*p*1*d*) BD(TQ) prediction as the QZ(1+)(2*d*1*f*,2*p*1*d*)$\rightarrow n$HF(+)(*extpol*) MP2 shift in ΔE_e, which amounts to −0.42 kcal mol^{-1}. Correlating the core electrons in the nHF(+)(*extpol*) MP2 procedure gives an additional change of −0.09 kcal mol^{-1}; hence, a final value of 39.45 is engendered for ΔE_e. Zero-point vibrational corrections including anharmonicity result in ΔE_0=37.83 kcal mol^{-1}. The accepted heats of formation at 0 K (in kcal mol^{-1})[171] for the species involved in the proton-transfer reaction are HF(−65.13 ±0.19), HCl(−22.02±0.05), F^-(−59.91±0.14), and Cl^-(−54.82±0.10), which yield ΔE_0=38.02±0.26 kcal mol^{-1}. Thus, the *ab initio* methods employed here predict a proton-transfer energy well within the error bars of the accepted value.

The vibrationless chloride affinity of HF is close to 23 kcal mol^{-1}, according to the CCSD values of $D_e(\mathbf{1})$ in Table IV. As seen therein, the dispersion forces which contract R_e(H–Cl) and increase ω_1 in the $[FHCl]^-$ complex also lead to associated enhancements of 3–4 kcal mol^{-1} in the chloride affinity. The pattern of the QZ(1+)(2*d*1*f*,2*p*1*d*) predictions for $D_e(\mathbf{1})$, as depicted in Fig. 1, is inverted relative to the proton-transfer profile. The span of the MP*n* oscillations is less than 1 kcal mol^{-1}, however, and the (T) contribution to the BD and CCSD values is significantly smaller. The BD(T) result leads to a prediction of 23.6 kcal mol^{-1} for the *n*-particle limit with the QZ(1+)(2*d*1*f*,2*p*1*d*) basis. As in the ΔE_e case, the nHF(+)(*extpol*) frozen- and unfrozen-core MP2 results provide further corrections to this prediction, viz., −0.45 and +0.11 kcal mol^{-1}, respectively. The unknown error due to relaxation of the TZ(1+)(3*d*,3*p*) CCSD structure of $[FHCl]^-$ should be quite limited, because the f_{RR} constant in Table V indicates that the 0.01 Å uncertainty in R_e(H–Cl) corresponds to energy changes less than 0.004 kcal mol^{-1}. The final theoretical value for the vibrationless chloride affinity is thus $D_e(\mathbf{1})$=23.3±0.4 kcal mol^{-1}. The zero-point vibrational energy (ZPVE) of $[FHCl]^-$ includ-

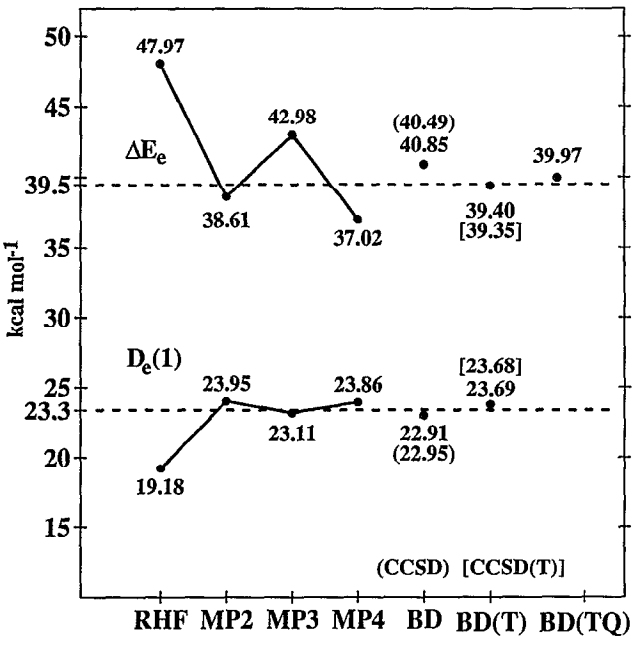

FIG. 1. Values (in kcal mol^{-1}) for the $[FHCl]^-$ binding energy, $D_e(1)$, and the (HF,Cl^-) proton-transfer energy, ΔE_e, as predicted with the QZ(1+)(2d1f,2p1d) basis set. The depicted asymptotes, $D_e(1)=23.3$ and $\Delta E_e=39.5$ kcal mol^{-1}, mark the final predictions derived in the text after additional corrections for basis set incompleteness and core electron correlation.

ing anharmonicity is 2576 cm^{-1}, according to the rigorous variational analysis of Sec. V; the analogous value for ZPVE(HF) is 2058 cm^{-1}. The vibrationally adiabatic binding energy $D_0(1)=21.8\pm0.4$ kcal mol^{-1} is thus ascertained. It is worth noting that the TZ(1+)(3d,3p) CCSD level of theory used to generate the global surface of $[FHCl]^-$ predicts a vibrationless binding energy (22.80) within 0.5 kcal mol^{-1} of the final $D_e(1)$ result. The best previous *ab initio* prediction[103] gave $D_e(1)=20\pm2$ kcal mol^{-1}.

In the ion–cyclotron resonance experiments of Larson and McMahon,[76,77] the chloride-exchange reaction $ClSO_2^- + HF \rightleftharpoons ClHF^- + SO_2$ was found to have a gas-phase equilibrium constant of 2.1 at ambient temperature. By invoking statistical thermodynamic approximations for the entropy change of this reaction and employing a chloride affinity of 20.9 for the SO_2 reference species, the enthalpy of complexation at 298 K for $[FHCl]^-$ was ascertained to be 21.8 kcal mol^{-1}. By comparison, the chloride affinities of HCl, HCN, and H_2O were found to be, in order, 23.1, 21.0, and 14.4 kcal mol^{-1},[77] and the fluoride affinities of HF, HCN, and H_2O were placed at 38.5, 21.1, and 23.3 kcal mol^{-1},[75] respectively. Based on the molecular parameters reported here, the thermal correction for the enthalpy of $[FHCl]^-$ complexation gives the empirical result $D_0(1)=20.7$ kcal mol^{-1}, in agreement with the proposed theoretical value within experimental uncertainty.

The chloride affinity of hydrogen fluoride was used by Larson and McMahon[76] to estimate the bromide and iodide affinities of HF as 17 and 15 kcal mol^{-1}, respectively, on the basis of an assumed linear correlation between the halide affinity (ΔH_{XA}) and the change ($\Delta\nu$) in the H–F stretching frequency upon complexation. While these estimates are quite reasonable, the current predictions show that the origin of the gas-phase ΔH_{XA} vs $\Delta\nu$ plot and the associated $[FHF]^-$ and $[FHCl]^-$ points do not lie on a straight line, as claimed previously.[76] In particular, from the $\Delta\nu$ shifts for $[FHCl]^-$ and $[FHF]^-$ of 1097 (*vide supra*) and 2627 cm^{-1},[90] respectively, as well as $\Delta H_{XA}(Cl)=21.8$ kcal mol^{-1} for HF, a hydrogen bond energy for $[FHF]^-$ of 52 kcal mol^{-1} is estimated using a linear extrapolation, as compared to the direct empirical value[75] of 38.5 and the best *ab initio* prediction[97] of 45 kcal mol^{-1}.

D. Bonding analysis

The $[FHCl]^-$ species is one of the chloride-ion adducts of Brønsted acids whose hydrogen bonds have been analyzed previously by Larson and McMahon[77] by means of a simple electrostatic model consisting of ion–permanent dipole, ion–induced dipole, and electronic repulsion terms. Good agreement between the observed chloride affinities and those predicted by the electrostatic model was found for numerous first-period hydrides, including HF, HCN, H_2O, and NH_3. The hydrogen bonding was thus characterized as "appreciably electrostatic" in these instances. Indeed, plots of halide binding energies vs gas-phase acidities for a series of chloride and fluoride adducts suggested that Cl^- binding to Brønsted acids exhibits significantly more electrostatic character than F^- binding. However, for the strong acids HCl, HCO_2H, and CH_3CO_2H, deficiencies in the predictions of the electrostatic model evidenced considerable charge transfer in the corresponding chloride-ion adducts.

The hydrogen bond in $[FHCl]^-$ was subjected to a rigorous analysis in the current investigation according to the energy decomposition scheme of Morokuma.[172–175] The implementation of the Morokuma procedure employed the QZ(1+)(2d1f,2p1d) basis set and assumed the TZ(1+)(3d,3p) CCSD optimum structures for hydrogen fluoride and the hydrogen-bonded complex. The method was programmed independently at Stanford and checked using the $[FHF]^-$ system as a benchmark.[176] The bonding analysis entailed the following steps: (a) The RHF energy and molecular orbitals (ϕ°) were determined for each of the Cl^- and HF fragments, giving the individual Hartree–Fock wave functions $\Psi^\circ(Cl^-)$ and $\Psi^\circ(HF)$ and the composite energy E_1. (b) The nascent hydrogen bond was formed by placing the chloride ion at the optimum interhalogen distance of 2.9027 Å while maintaining the asymptotic H–F separation of 0.9151 Å. (c) The energy (E_2) of the unrelaxed, composite Hartree-product wave function $\Psi^\circ(Cl^-)\Psi^\circ(HF)$ was evaluated to give the electrostatic binding energy, $\epsilon_{ES}=E_2-E_1$. (d) Orbital relaxation within each fragment was allowed in the presence of mutual electrostatic interactions, providing the optimum Hartree-product wave function $\Psi(Cl^-)\Psi(HF)$ and hence the polarization component of the binding energy, $\epsilon_{PL}=E_3-E_2$. (e) A properly antisymmetrized composite Hartree–Fock wave function was constructed from the unrelaxed, overlapping molecular orbitals $\phi^\circ(Cl^-)$ and $\phi^\circ(HF)$.

From the resulting energy (E_4), the magnitude of the interfragment exchange repulsion was computed as $\epsilon_{EX}=E_4-E_2$. (f) The geometry of the hydrogen-bonded complex was relaxed to its optimum structure by elongating the H–F bond to 0.9600 Å without varying the interhalogen distance. (g) The proper RHF energy (E_5) of the complex was computed at the relaxed geometry. The portion of the RHF binding energy (E_5-E_1) not accounted for by the electrostatic, polarization, and exchange terms involves the charge-transfer energy (ϵ_{CT}) and a contribution due to higher-order component mixing (ϵ_{MIX}). Therefore, the sum of ϵ_{CT} and ϵ_{MIX} was quantified as $E_5-E_4-E_3+E_2$. (h) The BD(T) correlation energies of the separated fragments and the $[FHCl]^-$ complex were determined. The correlation-energy shift in the chloride binding energy was ascribed to the dispersion contribution to the hydrogen bond, ϵ_{DISP}.

Morokuma has formulated a refined procedure[173] whereby the CT and MIX terms are separated by computing the charge-transfer energy directly, but this further decomposition is not of concern here. It is also worth noting that the precise values of the individual components of the Morokuma decomposition depend on the geometric path assumed in the formation of the complex. This issue was highlighted in the early analysis of $[FHF]^-$, in which the 4-31G basis set was used.[176] In the present bond analysis, intramolecular geometry relaxation is ascribed solely to the charge-transfer term.

The values of the QZ(1+)(2*d*1*f*,2*p*1*d*) energy components of the hydrogen bond of $[FHCl]^-$ were found to be $\epsilon_{ES}=-27.33$, $\epsilon_{PL}=-5.16$, $\epsilon_{EX}=18.27$, $\epsilon_{CT}+\epsilon_{MIX}=-4.96$, and $\epsilon_{DISP}=-4.51$ kcal mol^{-1}.[177] The ES interaction is clearly the dominant contributor to the binding energy. The PL enhancement of the electrostatic driving force offsets about 30% of the sizeable exchange repulsion as the adduct is formed. Because the MIX term is small and typically negative for ES-preponderate complexes,[175] the charge-transfer stabilization appears to be less than each of the other bonding contributions. This inference is consistent with several Mulliken population analyses performed here with varying basis sets which indicated that the net charge on Cl^- is reduced by only 0.08–0.10 upon complexation.

In a recent investigation of the $ClCH_2CN+Cl^-$ S_N2 identity exchange reaction, Wladkowski *et al.*[178] presented a simplified bond analysis of the $[ClCH_2CN\cdot Cl]^-$ complex in which the electrostatic potential $\phi[\mathbf{x}]$ surrounding free $ClCH_2CN$ was probed at $\mathbf{x}(Cl^-)$, the position of Cl^- in the adduct. When this approach is applied to the $[FHCl]^-$ adduct at the QZ(1+)(2*d*1*f*,2*p*1*d*) RHF level, it is found that a negative point charge residing at the chloride position of step (b) above is bound by $-e\phi[\mathbf{x}(Cl^-)]=-26.20$ kcal mol^{-1} due to the charge distribution of free hydrogen fluoride. Therefore, a point-charge model accounts nicely for the ϵ_{ES} component of the Morokuma decomposition. Wladkowski *et al.*[178] also suggested that in ES-type chloride-ion adducts, the empirically observed correlation of chloride affinity (CA) with gas-phase acidity for Brønsted acids results from an inverse correlation of the values of the electrostatic potential of the free acid at $\mathbf{x}(Cl^-)$ and $\mathbf{x}(H^+)$, the respective positions of the chloride ion and the acidic proton. The current data support this view in that $(e\phi[\mathbf{x}(Cl^-)], -e\phi[\mathbf{x}(H^+)]; CA)=(26.2, 576; 21.8)$ kcal mol^{-1} for $[FHCl]^-$ as compared to (15.8, 647; 19.6) for $[ClCH_2CN\cdot Cl]^-$ and (8.4, 681; 12.2) for $[CH_3Cl\cdot Cl]^-$.[178]

IV. GLOBAL POTENTIAL ENERGY SURFACE FOR $[FHCl]^-$

In this study stringent conditions were placed on the analytic representation of the global *ab initio* potential energy surface of the $[FHCl]^-$ system. In particular, essentially exact reproduction was required of no less than ten features of the actual surface: (1) optimum geometric structures of HF, HCl, and $[FHCl]^-$; (2) the $HF+Cl^-\rightarrow[FHCl]^-$ complexation energy and the $HF+Cl^-\rightarrow HCl+F^-$ proton-transfer energy; (3) all quadratic force constants and harmonic vibrational frequencies of HF, HCl, and $[FHCl]^-$; (4) the cubic and quartic force constants of HF, HCl, and $[FHCl]^-$, and hence the vibrational anharmonic constants (χ_{ij}) and vibration–rotation interaction constants α_i^B of these species; (5) continuous and smoothly varying higher-order derivatives of the surface throughout the bonding region; (6) the minimum-energy path (MEP) for the proton-transfer reaction, i.e., the optimum value of r(H–F) $+R$(H–Cl) for each fixed value of the progress variable r(H–F) $-R$(H–Cl); (7) the dissociative profile of the $[FHCl]^-$ complex not only to $HF+Cl^-$ and $HCl+F^-$ but also to the atomic fragments $H+F+Cl^-$ and $H+Cl+F^-$; (8) the detailed structure (*ca.* 5 cm^{-1} resolution) of the surface in the space of all geometric configurations lying below the first dissociation threshold ($HF+Cl^-$) near 8150 cm^{-1}; (9) asymptotic long-range ion-dipole binding energies of the form $-\mu R^{-2}$, where μ is the equilibrium dipole moment of the diatomic fragment (HCl or HF) which interacts with its complementary anion (F^- or Cl^-) over a distance R; and (10) barriers to full internal rotation in regions characteristic of a diatomic molecule in the field of a complexing atomic anion, including the decay of these barriers to the asymptotic form $2\mu R^{-2}$ at long distances.

The literature is replete with functional forms used to represent potential energy surfaces of triatomic molecules in general and ion-diatom systems in particular.[67,68,107,179–184] In their recent two-dimensional variational analysis of the stretching vibrations of $[ClHCl]^-$, Botschwina, Sebald, and Burmeister[68] employed a 23-term polynomial function in Morse variables to fit 94 CEPA-1 energy points obtained with a Cl[10*s*10*p*3*d*] and H[5*s*2*p*] basis. In 1990 Epa *et al.*[107] reported a three-dimensional model surface for $[FHF]^-$ constructed from 710 data points computed via the configuration interaction doubles method (CID) using a F[3*s*2*p*1*d*] and H[2*s*1*p*] basis set. The surface was represented as a skeleton two-body potential comprised of Morse functions to which three-body correction terms were added in the form of a polynomial expansion in prolate spheroidal coordinates. In the

previously mentioned investigation of Špirko, Čejchan, and Diercksen,[67] three-dimensional MBPT(4) grids were generated around the equilibrium configurations of $[FHF]^-$ and $[ClHCl]^-$ using basis sets of Cl[7*s*5*p*2*d*], F[5*s*3*p*2*d*], and H[3*s*2*p*] quality; improved stretching potentials for $[FHF]^-$ were also determined at the CCSD and CCSDT-1a levels of theory. The variational vibrational analysis in their study proceeded on an analytic surface represented as an expansion in a set of rectilinear internal displacement variables derived by Plíva.[185] As a final example, the vibrational analyses of several cationic assemblies of alkali metal atoms (Li_3^+, Li_2Na^+, $LiNa_2^+$, $KLiNa^+$, K_2Li^+, and LiH_2^+) by Searles, Nagy-Felsobuki, and co-workers warrant mention.[180–184] In these investigations the use of Padé approximants comprised of polynomial expansions in simple or exponential variants of Dunham, Simons–Parr–Finlan(SPF), or Ogilvie[186] coordinates was developed into an automatic nonlinear triatomic surface-fitting procedure facilitated by singular-value decomposition (SVD) techniques.[180]

Expansions of the potential surface in terms of some (perhaps astutely) selected set of internal coordinates were avoided here in favor of compact, closed-form representations involving smoothly varying functions with appropriate boundary conditions and asymptotic forms. This approach proved quite effective in meeting the formidable requirements outlined above on the analytic representation of the global surface. Moreover, the occurrence of singularities and unphysical features of the surface at highly distorted configurations was thereby prevented. The guiding principle of the effort was to build up the complete surface from precise, global parametrizations of the energy profile, surface curvature, and geometric coordinates along the minimum-energy path (MEP) for the proton-transfer reaction, as defined in criterion (6). The principal technique involved the nesting of flexible functions with several variable parameters within the arguments of simple, smooth functions of appropriate mathematical forms. In this way the smoothness and asymptotic criteria (2, 5, 7, 9, and 10) were achieved while sufficient flexibility was maintained to satisfy conditions (1, 3, 4, 6, and 8). The surface-fitting procedures were implemented with the *Mathematica* package,[187] whose symbolic manipulation and graphical representation facilities proved indispensable. The final surface is represented in terms of the variables $x \equiv S_1 \equiv 2^{-1/2}[r(\text{H–F}) + R(\text{H–Cl})]$, $y \equiv S_2 \equiv 2^{-1/2}[r(\text{H–F}) - R(\text{H–Cl})]$, and $\rho = \pi - \theta(\text{F–H–Cl})$. The stepwise construction of the surface is described below. The explicit functional forms appear in Eqs. (1)–(47), the values of the parameters therein being tabulated in Table VI. Atomic units (hartree, bohr, rad) are assumed in all cases.

A. MEP parametrization

For 25 fixed values of y in the range $[-4.3,3.6]$ bohr, energy cross sections along the symmetric bond displacement coordinate $x = S_1$ were mapped out, and polynomial interpolation of various orders was used to locate the minimum-energy positions $S_1^\circ(y)$. Because the curvature of the surface is always positive for bending displacements from the reference points $(x,y,\rho) = [S_1^\circ(y),y,0]$, all MEP structures are linear. In Fig. 2 the MEP data are plotted, revealing the expected hyperbolic dependence of S_1° on y. To conform to the equilibrium structures of the HF and HCl fragments at long ion-molecule distances, the $S_1^\circ(y)$ function must satisfy the following asymptotic constraints:

$$\lim_{y \to -\infty} S_1^\circ(y) = -y + \sqrt{2}\, r_e(\text{HF}) \tag{1}$$

$$\lim_{y \to +\infty} S_1^\circ(y) = y + \sqrt{2}\, R_e(\text{HCl}). \tag{2}$$

Accordingly, the analytic function selected to represent the MEP is of the form

$$S_1^\circ(y) = f_1[\xi_1(y)] + f_2[\xi_1(y)], \tag{3}$$

where $\xi_1(y)$ is a monotonic function which reduces to y asymptotically,

$$f_1(\xi) = \sqrt{\xi^2 + a_1^2} - \frac{a_1^2}{2\sqrt{\xi^2 + a_1^2}} + \left(\frac{R_e(\text{HCl}) + r_e(\text{HF})}{\sqrt{2}}\right) + \left(\frac{R_e(\text{HCl}) - r_e(\text{HF})}{\sqrt{2}}\right)\tanh[a_2\xi], \tag{4}$$

$f_2(\xi)$ is a fitting function which decays to zero as y approaches $\pm\infty$, and a_1 and a_2 are adjustable parameters. When the first two terms in Eq. (4) are expanded for large ξ, the coefficients of ξ^0 cancel. The composite large-ξ limits of the last two terms in Eq. (4) thus provide intercepts for the linear asymptotes of $f_1(\xi)$ in accord with Eqs. (1) and (2). In the first step of the $S_1^\circ(y)$ fit, $\xi_1(y) = y$ was initially assumed, and the parameters a_1 and a_2 were chosen by inspection to maximize the smoothness of the $S_1^\circ - f_1$ difference points which determine $f_2(\xi)$. The range of $f_2(\xi)$ in the resulting data set was $[-0.2,0.2]$ bohr. Subsequently, a six-parameter nonlinear least-squares fit of the data was performed to the function

$$f_2(\xi) = [a_4(\xi - a_3) + a_5(\xi - a_3)^2 + a_6(\xi - a_3)^3] \times \text{sech}[(\xi - a_3)(a_7 + a_8 \tanh[\xi - a_3])], \tag{5}$$

in which the a_5, a_6, and a_8 terms serve to enhance the flexibility of the predominant form involving the a_3, a_4, and a_7 coefficients (see Table VI).

The explicitly evaluated quartic force field (Table V) of the $[FHCl]^-$ surface at the optimum structure of the ion-molecule complex, $(S_1,S_2) = (x^\circ,y^\circ)$, determines the y derivatives of $S_1^\circ(y)$ at y° through third order. The particular equations are

$$S_1^{\circ\prime}(y^\circ) = -F_{21}F_{11}^{-1}, \tag{6}$$

$$S_1^{\circ\prime\prime}(y^\circ) = -F_{111}F_{21}^2F_{11}^{-3} + 2F_{211}F_{21}F_{11}^{-2} - F_{221}F_{11}^{-1}, \tag{7}$$

and

TABLE VI. Parameters in the analytic representation of the TZ(1+)(3*d*,3*p*) CCSD global surface for the $[FHCl]^-$ system.[a]

E_0	−560.077 285 07	b_3	0.751 304	c_{12}	0.632 73	d_{21}	$2.500\,749 \times 10^3$
ΔE_e	0.063 024	b_4	−1.164 007	c_{13}	−0.009 377	d_{22}	$-6.816\,460 \times 10^3$
x°	3.878 764	b_5	−0.014 985	c_{14}	1.254 8	d_{23}	$-1.267\,033 \times 10^3$
y°	−1.313 098	b_6	−0.030 928	c_{15}	0.028 50	d_{24}	$8.770\,223 \times 10^2$
r_e(HF)	1.729 5	b_7	0.004 277	c_{16}	0.019 35	d_{25}	$-1.487\,607 \times 10^2$
R_e(HCl)	2.404 7	b_8	1.040 289	c_{17}	0.010 90	d_{26}	0.005 362
f_{rr}(HF)	0.626 552	b_9	−0.445 053	c_{18}	1.118 49	d_{27}	−0.032 385 2
f_{RR}(HCl)	0.335 822	b_{10}	−0.175 313	d_1	0.015 44	d_{28}	0.059 418 0
μ_{HF}	0.716 0	b_{11}	−0.225 621	d_2	1.809	d_{29}	0.003 564 6
μ_{HCl}	0.428 8	b_{12}	1.425 557	d_3	23.5	d_{30}	0.013 486 0
D_e(HF)	0.224 691	b_{13}	0.709 351	d_4	3.878 7	d_{31}	−0.023 654 5
Δ(EA)	0.003 969	b_{14}	−1.536 504	d_5	36.518 8	d_{32}	2.995 22
ε	0.20	b_{15}	$1.739\,620 \times 10^{-4}$	d_6	1.512 98	d_{33}	1.634 237
a_1	1.261 09	b_{16}	$-4.567\,615 \times 10^{-4}$	d_7	−0.005 078	d_{34}	2.698 134
a_2	0.40	b_{17}	$5.249\,797 \times 10^{-3}$	d_8	1.628 94	d_{35}	$-9.428\,95 \times 10^{-4}$
a_3	−0.391 190	b_{18}	$9.637\,977 \times 10^{-4}$	d_9	2.049 59	d_{36}	-8.541×10^{-5}
a_4	0.354 570	c_1	−0.598 038	d_{10}	−1.773 55	d_{37}	$5.051\,5 \times 10^{-3}$
a_5	−0.021 543	c_2	1.176 14	d_{11}	$2.708\,197 \times 10^3$	d_{38}	3.114 8
a_6	0.012 942	c_3	0.338 616	d_{12}	$3.373\,390 \times 10^3$	d_{39}	0.499 08
a_7	1.208 935	c_4	0.474 064	d_{13}	$3.110\,463 \times 10^3$	d_{40}	0.148 17
a_8	−0.107 948	c_5	0.024 108	d_{14}	$6.248\,35 \times 10^2$	d_{41}	2.668 63
a_9	$-1.839\,49 \times 10^{-5}$	c_6	−0.237 268	d_{15}	$-4.935\,17 \times 10^2$	d_{42}	0.396 373
a_{10}	$2.037\,16 \times 10^{-4}$	c_7	0.027 475	d_{16}	$5.449\,459 \times 10^2$	d_{43}	−0.392 7
a_{11}	$7.750\,88 \times 10^{-4}$	c_8	0.321 234	d_{17}	$2.873\,983 \times 10^3$		
a_{12}	$6.450\,24 \times 10^{-3}$	c_9	−0.079 06	d_{18}	$4.912\,563 \times 10^3$		
b_1	2.85	c_{10}	0.034 46	d_{19}	$1.102\,788 \times 10^4$		
b_2	2.60	c_{11}	2.104 01	d_{20}	$3.449\,376 \times 10^2$		

[a]Defined in Eqs. (1)–(47) and the accompanying text. All values are given in atomic units.

$$S_1^{\circ\prime\prime\prime}(y^\circ) = 3(F_{211}F_{11}^{-2} - F_{111}F_{21}F_{11}^{-3}) \times (F_{221} - 2F_{211}F_{21}F_{11}^{-1} + F_{111}F_{21}^2F_{11}^{-2}) + F_{1111}F_{21}^3F_{11}^{-4} - 3F_{2111}F_{21}^2F_{11}^{-3} + 3F_{2211}F_{21}F_{11}^{-2} - F_{2221}F_{11}^{-1}, \quad (8)$$

where the force constants F_{ij}, F_{ijk}, and F_{ijkl} involve the symmetry coordinates S_1 and S_2. In order to satisfy these derivative conditions, final modifications of the $S_1^\circ(y)$ function were made by adding a short-range modulation function to the linear component of $\xi_1(y)$:

$$\xi_1(y) = y + [a_9 + a_{10}(y-y^\circ) + a_{11}(y-y^\circ)^2 + a_{12}(y-y^\circ)^3] \times \mathrm{sech}[3(y-y^\circ)]. \quad (9)$$

From the $S_1^\circ(y^\circ)$, $S^\circ{}'_1(y^\circ)$, $S^\circ{}''_1(y^\circ)$, and $S^\circ{}'''_1(y^\circ)$ values, $\xi_1(y^\circ)$, $\xi_1'(y^\circ)$, $\xi_1''(y^\circ)$, and $\xi_1'''(y^\circ)$ were found using chain-rule differentiation, allowing the coefficients a_9–a_{12} in Eq. (9) to be determined analytically. Note in Table VI that the values of a_9–a_{12} are actually very small, indicating the almost negligible effect of the modulation function in $\xi_1(y)$ on the final $S_1^\circ(y)$ fit. The residuals of the fit are plotted underneath the $S_1^\circ(y)$ curve in Fig. 2. The largest residuals (*ca.* 0.002 bohr), which occur for positive values of y, are more a consequence of diminished accuracy accepted in the interpolation procedure for the $S_1^\circ(y)$ points in this region than remaining deficiencies in the fit. In the region between $y=-0.5$ and -2.2 bohr, where the data set is most accurately determined, the rms error of the final $S_1^\circ(y)$ fit is only 0.0003 bohr.

B. MEP energy profile

For each of the 25 $S_1^\circ(y)$ points ascertained from *ab initio* energy calculations via polynomial interpolation schemes, an associated minimum-energy value $E^\circ(y)$ was obtained. The $E^\circ(y)$ data, which constitute the MEP energy profile, are plotted in Fig. 3. Clearly exhibited in the figure are the prodigious ion-molecule complexation energy and the slow decay of the interaction energy characteristic of an ion-dipole system. The functional form invoked to represent the MEP energy profile is

$$E^\circ(y) = E_0 + 2(\Delta E_e)\pi^{-1}\tan^{-1}[g_1[\xi_2(y)]] \times \{(1 + 2\pi^{-1}\tan^{-1}[g_2[\xi_2(y)]])g_3[\xi_2(y)] + 2^{-1}(1+\tanh[\xi_2(y)])\}, \quad (10)$$

where

$$g_1(\xi) = 2(\Delta E_e)\pi^{-1}\left(\frac{\mu_{HCl}}{2}\right)^{-1}\left(\frac{\xi^2}{\tanh[\xi]} + b_1\xi\right)(1+e^{-\xi}), \quad (11)$$

$$g_2(\xi) = 2(\Delta E_e)\pi^{-1}\left(\frac{\mu_{HF}}{2}\right)^{-1}\left(\frac{\xi^2}{\tanh[\xi]} + b_2\xi\right)(1+e^{\xi}), \quad (12)$$

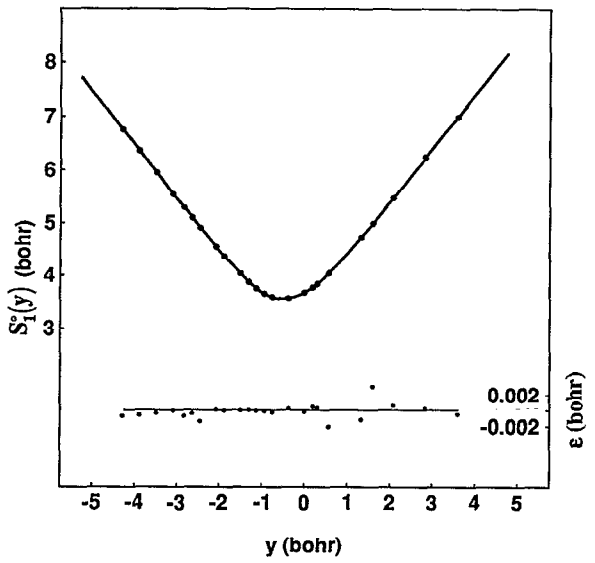

FIG. 2. Optimum values (S_1^e) of the symmetric bond distance coordinate, $S_1=2^{-1/2}[r(\mathrm{H-F})+R(\mathrm{H-Cl})]$, as a function of $y=2^{-1/2}[r(\mathrm{H-F})-R(\mathrm{H-Cl})]$ along the minimum-energy path (MEP) of [FHCl]$^-$. Beneath the curve are plotted the residuals (ϵ) of the fit to the functional form detailed in the text.

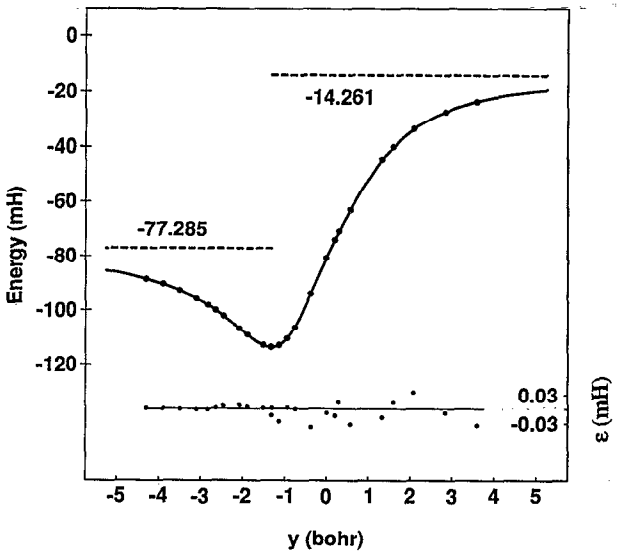

FIG. 3. The energy profile, $E^e(y)$, along the minimum-energy path (MEP) of [FHCl]$^-$. The points are plotted in units of mH relative to an absolute reference value of -560.000 H. The dashed lines locate the HF+Cl$^-$ and HCl+F$^-$ asymptotes. The residuals (ϵ) of the fit to the functional form given in the text are plotted beneath the $E^e(y)$ curve.

and

$$g_3(\xi)=b_3[1+b_5(\xi-b_4)+b_6(\xi-b_4)^2+b_7(\xi-b_4)^3]\times\mathrm{sech}[b_8(\xi-b_4)]+b_9\,\mathrm{sech}[(\xi-b_{10})\times(b_{11}+b_{12}\tanh[\xi-b_{10}])]+2^{-1}(1-\tanh[b_{13}(\xi-b_{14})]). \quad (13)$$

In addition, E_0 is the absolute optimum energy of HF+Cl$^-$, ΔE_e is the proton-transfer energy as before, and the b_i quantities are adjustable parameters. As in the $\xi_1(y)$ case, $\xi_2(y)$ is a monotonic function which is principally linear in y.

The seemingly recondite $E^e(y)$ function is elucidated in Table VII, where asymptotic forms are tabulated for the various components of Eq. (10). The distinguishing characteristic of the inverse tangent functions in the $E^e(y)$ expression is the property $\lim_{\xi\to\pm\infty}\tan^{-1}(\xi)=\pm\pi/2\mp1/\xi$. As $\xi\to-\infty$ and the ion-molecule system approaches the HF+Cl$^-$ limit, $g_1(\xi)$ increases in magnitude exponentially, and thus $\tan^{-1}[g_1(\xi)]$ decays exponentially to $-2^{-1}\pi$. In contrast, the leading term in $g_2(\xi)$ behaves as $-\xi^2$ asymptotically, and consequently $1+2\pi^{-1}\tan^{-1}[g_2(\xi)]$ decays as ξ^{-2}. Thus, the form in Eq. (10) generates the requisite $-\mu_{\mathrm{HF}}R^{-2}$ long-range interaction energy as $\xi\to-\infty$ due to the limiting relation $\xi^2\to y^2\to 2^{-1}R(\mathrm{H\text{-}Cl})^2$. The roles of $g_1(\xi)$ and $g_2(\xi)$ are reversed in the limit $\xi\to+\infty$, as the ξ^2 asymptotic dependence of $g_1(\xi)$ leads to a $-\mu_{\mathrm{HCl}}R^{-2}$ long-range interaction energy. Note also that the shift of the energy asymptote to $E_0+\Delta E_e$, the proper value for HCl+F$^-$, is automatically satisfied by Eq. (10) as $\xi\to+\infty$. Finally, both $g_1(\xi)$ and $g_2(\xi)$ vary as ξ^1 in the vicinity of $\xi=0$, requiring the $E^e(y)$ function to intersect the HF+Cl$^-$ energy asymptote at $\xi=0$. This condition necessitates the predominant linear form $\xi_2(y)=y-y^*$, where the shift parameter y^* is directly determined from the energy profile data as the root of $E^e(y)=E_0$.

The parameters b_1 and b_2 in Eqs. (11) and (12) engender higher-order terms in the multipole expansion of the long-range F$^-\cdots$HCl and Cl$^-\cdots$HF binding energies, respectively. Equivalently, these constants allow the origin of the ion-dipole separation vector (**R**) in the multipole expansion to be shifted from the hydrogen atom to intermediate positions along the respective HCl and HF bond axes. In actuality, the b_1 and b_2 parameters were selected here by graphical inspection to optimize the smoothness and asymptotic characteristics of the data set derived from the $E^e(y)$ points for the fit of $g_3(\xi)$. The flexibility of Eq. (10) needed to fit the $E^e(y)$ data was therefore concentrated in $g_3(\xi)$. By assuming $\xi_2(y)=y-y^*$, a simultaneous nonlinear least-squares fit of b_3–b_{14} to the $g_3(\xi)$ points was performed and found to give excellent results. The resulting $g_3(\xi)$ function reaches a maximum of 1.14 near $\xi=-2.0$ and decays exponentially to 0 and 1 as $\xi\to+\infty$ and $-\infty$, respectively.

The final function employed for $\xi_2(y)$ to complete the specification of $E^e(y)$ was

$$\xi_2(y)=y-y^*+[b_{15}+b_{16}(y-y^e)+b_{17}(y-y^e)^2+b_{18}(y-y^e)^3]\mathrm{sech}[3(y-y^e)], \quad (14)$$

where the coefficients (b_{15}-b_{18}) of the short-range modulation function were selected in order that the total derivatives of $E^e(y)$ at y^e are identical to those required by the known quartic force field:

$$E^{e\prime\prime}(y^e)=F_{22}-F_{21}^2F_{11}^{-1}, \quad (15)$$

TABLE VII. Asymptotic forms of functions comprising $E^\circ(y)$.[a]

	$\xi \to -\infty$	$\xi \to +\infty$
$g_1(\xi)$	$2(\Delta E_e)\pi^{-1}\left(\frac{\mu_{HCl}}{2}\right)^{-1}\left(-\xi^2+b_1\xi\right)e^{-\xi}$	$2(\Delta E_e)\pi^{-1}\left(\frac{\mu_{HCl}}{2}\right)^{-1}\left(\xi^2+b_1\xi\right)$
$tan^{-1}[g_1(\xi)]$	$2^{-1}\pi\left[-1+\left(\frac{\mu_{HCl}}{2\Delta E_e}\right)\left(\frac{e^\xi}{\xi^2}\right)\left(1+\frac{b_1}{\xi}\right)\right]$	$2^{-1}\pi\left[1-\left(\frac{\mu_{HCl}}{2\Delta E_e}\right)\left(\frac{1}{\xi^2}\right)\left(1-\frac{b_1}{\xi}\right)\right]$
$g_2(\xi)$	$2(\Delta E_e)\pi^{-1}\left(\frac{\mu_{HF}}{2}\right)^{-1}\left(-\xi^2+b_2\xi\right)$	$2(\Delta E_e)\pi^{-1}\left(\frac{\mu_{HF}}{2}\right)^{-1}e^{\xi}\left(\xi^2+b_2\xi\right)$
$1+2\pi^{-1}tan^{-1}[g_2(\xi)]$	$\left(\frac{\mu_{HF}}{2\Delta E_e}\right)\left(\frac{1}{\xi^2}\right)\left(1+\frac{b_2}{\xi}\right)$	$2-\left(\frac{\mu_{HF}}{2\Delta E_e}\right)\left(\frac{e^{-\xi}}{\xi^2}\right)\left(1+\frac{b_2}{\xi}\right)$
$g_3(\xi)$	1	0
$E^\circ(\xi)$	$E_0-\left(\frac{\mu_{HF}}{2\xi^2}\right)\left(1+\frac{b_2}{\xi}\right)$	$E_0+\Delta E_e-\left(\frac{\mu_{HCl}}{2\xi^2}\right)\left(1+\frac{b_1}{\xi}\right)$

[a] $E^\circ(y)$ is the MEP energy profile function of Eq. (10).

$$E^{\circ\prime\prime\prime}(y^\circ)=F_{222}-3F_{221}F_{21}F_{11}^{-1}+3F_{211}F_{21}^2F_{11}^{-2}-F_{111}F_{21}^3F_{11}^{-3}, \tag{16}$$

and

$$\begin{aligned}E^{\circ\prime\prime\prime\prime}(y^\circ)=&F_{2222}-4F_{2221}F_{21}F_{11}^{-1}+6F_{2211}F_{21}^2F_{11}^{-2}\\&-4F_{2111}F_{21}^3F_{11}^{-3}+F_{1111}F_{21}^4F_{11}^{-4}\\&-3F_{11}^{-1}(F_{221}-2F_{211}F_{21}F_{11}^{-1})^2\\&+3(4F_{211}F_{111}F_{21}^3F_{11}^{-4}-2F_{221}F_{111}F_{21}^2F_{11}^{-3}\\&-F_{111}^2F_{21}^4F_{11}^{-5}).\end{aligned} \tag{17}$$

As in the case of $\xi_1(y)$, the modulation function for $\xi_2(y)$ has only a very small effect on the overall fit. The residuals of the final $E^\circ(y)$ fit are plotted in Fig. 3 with the MEP energy profile data. The largest residuals do not exceed 7.6 cm^{-1} (0.035 mH) out of a range of 21 810 cm^{-1} and are commensurate with the accuracy of the input data itself in the surrounding regions. Between $y=-0.5$ and -2.2, the region of greatest accuracy in the $E^\circ(y)$ data, the rms error is only 2.6 cm^{-1}.

C. Linear potential function

For each fixed value of y, the potential energy for linear $[FHCl]^-$ structures approaches $+\infty$ as $x\to|y|$, reaches its minimum value $E^\circ(y)$ as $x\to S_1^\circ(y)$, and increases asymptotically to either $E(F+H+Cl^-)$ or $E(F^-+H+Cl)$ as $x\to+\infty$. The energy curves $V_{lin}(x;y)$ along these cross sections for fixed y were represented here as Varshni-type functions in a variable (σ) which acts as the displacement $x-|y|$. In particular, from the Varshni diatomic potential[188]

$$V(r)=V_0+D_e\left\{1-\frac{r_e}{r}e^{-\beta(r^2-r_e^2)}\right\}^2, \tag{18}$$

the generalized function

$$V_{lin}(x;y)=E^\circ(y)+D_e(y)\times\left\{1-\frac{\sigma^\circ(y)}{\sigma(x,y)}e^{-\beta(x,y)[\sigma(x,y)^2-\sigma^\circ(y)^2]}\right\}^2 \tag{19}$$

was constructed, where

$$\sigma[x,y]=x-\sqrt{y^2+\epsilon^2} \tag{20}$$

and

$$\sigma^\circ(y)=\sigma[S_1^\circ(y),y]. \tag{21}$$

The parameter ϵ in Eq. (20) was set to 0.2 bohr, a small value which maintains the principal relation $\sigma=x-|y|$ throughout the ion-molecule bonding region but averts discontinuities in the derivatives of the surface near $y=0$.

Because the experimental electron affinity (EA) of the chlorine atom (3.615 eV) is greater than that of fluorine (3.399 eV),[111] the fragmented system $F+H+Cl^-$ is 4.98 kcal mol^{-1} lower in energy than F^-+H+Cl. Therefore, for negative values of y, which correspond to structures of $FH\cdot Cl^-$ character, it is unequivocal that the proper dissociation energy in Eq. (19) is the sum of the bond energy of hydrogen fluoride, $D_e(HF)$, and the intermediate complexation energy relative to $HF+Cl^-$, viz., $E_0-E^\circ(y)$. For large positive values of y, the potential curve for increasing x remains of $F^-\cdots H\cdots Cl$ character until a seam is encountered 4.98 kcal mol^{-1} below the F^-+H+Cl asymptote. Because this seam involving the different states of the atomic fragments lies over 160 kcal mol^{-1} above the optimum $[FHCl]^-$ structure, it is of no consequence in the vibrational studies here. Accordingly, the final function employed for the dissociation energy along the MEP was

$$D_e(y)=D_e(HF)+E_0-E^\circ(y)+\Delta(EA)\times(1+\tanh[1.5(y-2.8)]), \tag{22}$$

empirical values[111,112] being assumed for $D_e(HF)$ and $\Delta(EA)=EA(Cl)-EA(F)$. Note that the last term on the right side of Eq. (22) provides a smooth transformation of

the effective dissociation limit from $D_e(F+H+Cl^-)$ to $D_e(F^-+H+Cl)$ to the extent of 99.5% within the region $y\in[0.8,4.8]$ bohr. As such, this transformation affects no part of the surface lying lower in energy than the separated species $HF+Cl^-$.

In analogy to the diatomic Varshni relation

$$\beta=\frac{1}{2r_e^2}\left[\sqrt{\frac{f_{rr}r_e^2}{2D_e}}-1\right], \tag{23}$$

in which f_{rr} is the equilibrium quadratic force constant, the dominant contribution (β°) to the $\beta(x,y)$ function in Eq. (19) was expressed as

$$\beta^\circ(y)=\frac{1}{2\sigma^\circ(y)^2}\left(\sqrt{\frac{F^\circ(y)\sigma^\circ(y)^2}{2D_e(y)}}-1\right), \tag{24}$$

where the force constant $F^\circ(y)$ corresponds to $(\partial^2 V_{\rm lin}/\partial x^2)$ evaluated on the MEP at $(S_1^\circ(y),y)$. As in the case of $S_1^\circ(y)$ and $E^\circ(y)$, the function $F^\circ(y)$ is subject to asymptotic constraints, viz.,

$$\lim_{y\to-\infty} F^\circ(y)=2^{-1}f_{rr}(HF) \tag{25}$$

and

$$\lim_{y\to+\infty} F^\circ(y)=2^{-1}f_{RR}(HCl). \tag{26}$$

Hence, the form chosen for $F^\circ(y)$ was

$$F^\circ(y)=4^{-1}[f_{RR}(HCl)+f_{rr}(HF)]+4^{-1}[f_{RR}(HCl)-f_{rr}(HF)]\tanh[h(y)], \tag{27}$$

in which $h(y)$ is a monotonic fitting function which is linear in y at large ion-molecule separations:

$$h(y)=c_1+(y-y^\circ)\left[c_2+c_3(1-\mathrm{sech}[c_4(y-y^\circ)])+\frac{c_5(y-y^\circ)+c_6(y-y^\circ)^2}{1+c_7(y-y^\circ)+c_8(y-y^\circ)^2}\right]. \tag{28}$$

For the 25 values of y at which $S_1^\circ(y)$ and $E^\circ(y)$ data were determined, $F^\circ(y)$ points also resulted from the polynomial interpolation procedures. The c_1 coefficient in Eq. (28) was selected to exactly reproduce the equilibrium quadratic force constant (F_{11}) of $[FHCl]^-$ while the remaining parameters (c_2–c_8) were subsequently determined from a simultaneous nonlinear least-squares fit. Plots of $F^\circ(y)$ and $\beta^\circ(y)$ appear in Fig. 4.

At 0.10 Å intervals of y between −2.835 and −0.378 bohr, additional *ab initio* energy points were computed at successively larger positive and negative x displacements until the energy of the $HF+Cl^-$ asymptote was exceeded. For each of these points, the expression for $V_{\rm lin}(x;y)$ was inverted to find the solutions of Eq. (19) for β. In this way a data set was obtained from which the function $\beta(x,y)$ was fitted, the chosen form being

$$\beta(x,y)=\beta^\circ(y)+\{[c_9+c_{10}e^{-c_{11}(y+c_{12})^2}+c_{13}e^{-c_{14}(y+2.5)^2}+c_{15}(1+\tanh[1.5(y-2.8)])]\delta(x,y)+(c_{16}-c_{17}\tanh[1.5(y-c_{18})])\delta(x,y)^2\}/[10+\delta(x,y)^2], \tag{29}$$

in which c_9–c_{18} are adjustable parameters, and

$$\delta(x,y)=x-S_1^\circ(y) \tag{30}$$

quantifies the deviation of x from the MEP. The term which augments $\beta^\circ(y)$ in Eq. (29) is well behaved as $\delta\to\pm\infty$, and its quadratic form in δ near the MEP allows the full quartic force field along this path to be accurately described. Indeed, the parametric dependence on y of the coefficients of δ and δ^2 was explicitly constructed to yield accurate values of the cubic and quartic force constants of HF, HCl, and $[FHCl]^-$.

The interspersion of linear points at which *ab initio* energy values were determined in the construction of $V_{\rm lin}(x;y)$ is depicted in Fig. 5 in relation to the energy contours for dissociation to $HF+Cl^-$ and $HCl+F^-$. A more extensive contour plot of $V_{\rm lin}(x;y)$ appears in Fig. 6. In Table VIII, the TZ(1+)(3*d*,3*p*) CCSD energy points for all linear structures are tabulated alongside the residuals of the final fit. A more extensive tabulation including the corresponding RHF and MP2 data is provided as supplementary material in the Physics Auxiliary Publication Service (PAPS).[189] The maximum residual for the CCSD points lying below the $HF+Cl^-$ threshold (7979 cm^{-1}) is only 11.1 cm^{-1}, and the rms error in this data set is a mere 3.9 cm^{-1}. Moreover, the accuracy of the analytic representation of the CCSD surface is maintained even for very high energies, *n.b.*, the largest ϵ(CCSD) values in Table VIII involve errors less than 115 cm^{-1} up to 26 500 cm^{-1}.

D. Bending potential and final function

The complete potential energy function for the $[FHCl]^-$ system was expressed as the sum of linear and bending potentials,

$$V(S_1,S_2,\rho)=V_{\rm lin}(S_1;S_2)+V_{\rm bend}(\rho;S_1,S_2), \tag{31}$$

where the bending contribution was represented as

$$V_{\rm bend}(\rho;x,y)=\sum_{n=1}^{4}k_{2n}(x,y)\sin^{2n}\rho+A(y)\sin^8(\rho/2)\times\{[x^2+y^2-(x^2-y^2)\cos(\pi-\rho)]^{-1/2}-2^{-1/2}x^{-1}\}+d_1e^{-3\delta(x,y)^2}\,\mathrm{sech}[d_2(S_1^\circ(y)-3.5)]e^{-\gamma(y)\cos^2\rho}. \tag{32}$$

The second term in Eq. (32) is a fluoride–chloride Coulombic repulsion term involving an effective charge product $A(y)$ multiplied by a difference of inverse F–Cl distances, i.e., $[R_{F\text{–}Cl}(\rho)^{-1}-R_{F\text{–}Cl}(0)^{-1}]$, and damped by a factor of $\sin^8(\rho/2)$. The damping factor retards the steep rise of the Coulombic repulsion potential and allows all

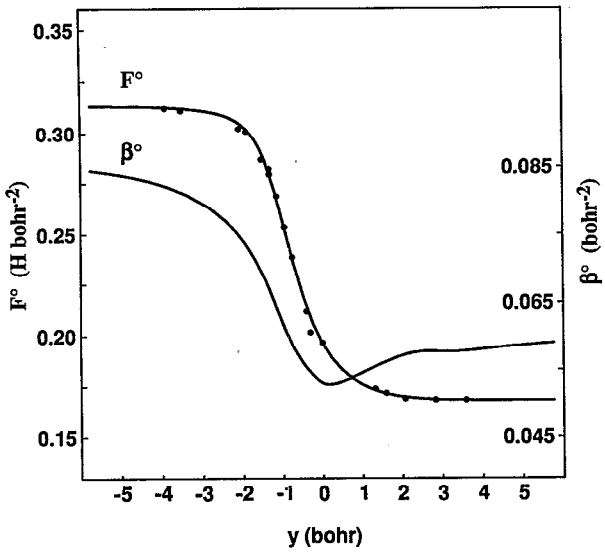

FIG. 4. The quadratic force constant for symmetric bond displacement, $F^\circ(y)$, and the corresponding Varshni exponent, $\beta^\circ(y)$, as functions of $y=2^{-1/2}[r(\mathrm{H-F})-R(\mathrm{H-Cl})]$ along the minimum-energy path (MEP) of $[FHCl]^-$. The slight undulation in β° near $y=3$ bohr is a consequence of the imposed transformation of the modified Varshni function from the $F+H+Cl^-$ to the F^-+H+Cl asymptote.

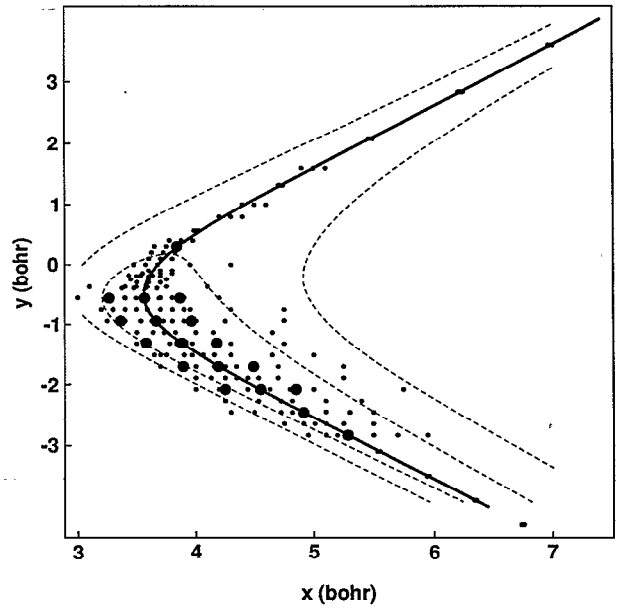

FIG. 5. The interspersion of *ab initio* points used in the construction of the linear potential function of $[FHCl]^-$. As defined in the text, $x=2^{-1/2}[r(\mathrm{H-F})+R(\mathrm{H-Cl})]$ and $y=2^{-1/2}[r(\mathrm{H-F})-R(\mathrm{H-Cl})]$. The dashed contours correspond to the relative energies of the $HF+Cl^-$ and $HCl+F^-$ products, whereas the solid line is the minimum-energy path (MEP). The enlarged data points mark the linear reference configurations selected to map out the bending potential.

contributions lower than tenth order in the angle displacement ρ to be conveniently described by the explicit expansion in even powers of $\sin(\rho)$ appearing first in Eq. (32). The last term in the V_{bend} expression was appended after the determination of the $k_{2n}(x,y)$ coefficients in order to refine the final fit at highly distorted geometries. This alteration is negligible near linearity but peaks sharply at $\rho=2^{-1}\pi$ due to the magnitude of

$$\gamma(y)=d_3-10\,\mathrm{sech}[3.5(S_1^\circ(y)-d_4)]. \tag{33}$$

The Coulombic repulsion term in Eq. (32) is solely responsible for the barrier to internal rotation since all subsequent terms are of periodicity π rather than 2π. For large ion-molecule separations (R), the internal rotation barriers must decay as $2\mu R^{-2}$, a condition which is satisfied by selecting

$$A(y)=2^{-1}\left[\frac{\mu_{\mathrm{HCl}}}{R_e(\mathrm{HCl})}+\frac{\mu_{\mathrm{HF}}}{r_e(\mathrm{HF})}\right]+2^{-1}\left[\frac{\mu_{HCl}}{R_e(\mathrm{HCl})}-\frac{\mu_{HF}}{r_e(\mathrm{HF})}\right]\tanh[1.5(y-2.8)]+d_5e^{-d_6(y-d_7)^2}+d_8\,\mathrm{sech}[d_9(y-d_{10})], \tag{34}$$

because the accompanying factor $[R_{\mathrm{F-Cl}}(\pi)^{-1}-R_{\mathrm{F-Cl}}(0)^{-1}]$ in Eq. (32) is equivalent to $2r_<(R_>^2-r_<^2)^{-1}$, where $r_<=\min[R(\mathrm{H\text{–}Cl}),r(\mathrm{H\text{–}F})]$ and $R_>=\max[R(\mathrm{H\text{–}Cl}),r(\mathrm{H\text{–}F})]$. Note that the transformation from $HF+Cl^-$ to $HCl+F^-$ asymptotic behavior is achieved by the same switching function employed for $D_e(y)$. The fitting parameters d_5–d_{10} in Eq. (34) were derived from high-energy *ab initio* points explicitly computed

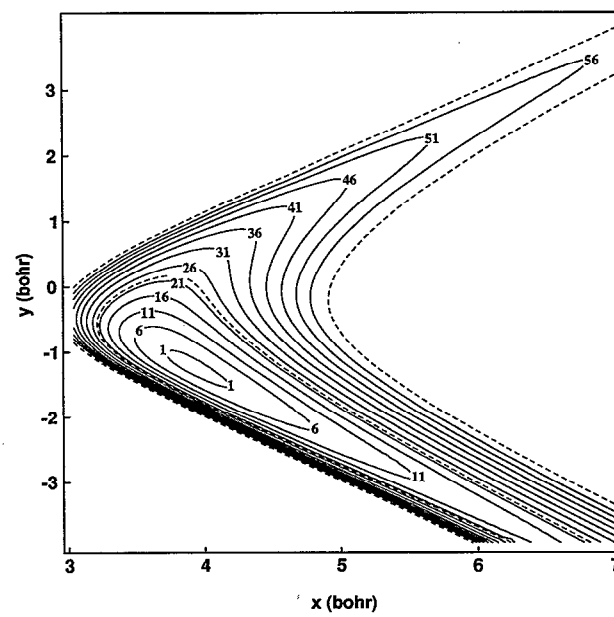

FIG. 6. A contour plot of the linear potential function of $[FHCl]^-$ with respect to $x=2^{-1/2}[r(\mathrm{H-F})+R(\mathrm{H-Cl})]$ and $y=2^{-1/2}[r(\mathrm{H-F})-R(\mathrm{H-Cl})]$. As indicated by affixed labels, the first contour line is 1 kcal mol^{-1} above the local minimum of the complex, and subsequent contours appear every 5 kcal mol^{-1}. The relative energies of the $HF+Cl^-$ and $HCl+F^-$ products are shown by dashed contour lines.

TABLE VIII. TZ(1+)(3*d*,3*p*) CCSD relative energy points (in cm^{-1}) for linear structures of $[FHCl]^-$.[a]

k	S_1	S_2	E(CCSD)	ε(CCSD)[b]	k	S_1	S_2	E(CCSD)	ε(CCSD)[b]	k	S_1	S_2	E(CCSD)	ε(CCSD)[b]	k	S_1	S_2	E(CCSD)	ε(CCSD)[b]
1	6.73552	−4.30000	5502.88	−0.71	53	4.34637	−1.88973	1024.44	0.72	105	3.73221	−1.13384	177.83	0.35	157	3.60000	−0.20000	5735.12	−6.70
2	6.74552	−4.30000	5496.66	−0.11	54	4.25000	−1.88973	1523.76	0.71	106	3.63772	−1.13384	630.94	0.15	158	3.49841	−0.19841	6029.00	−2.20
3	6.75552	−4.30000	5497.33	0.43	55	4.13000	−1.88973	3356.06	−1.45	107	3.50000	−1.13380	2610.53	−0.51	159	3.63307	−0.18897	5832.50	−7.68
4	6.33842	−3.90000	5098.75	−0.54	56	4.00000	−1.88973	7398.77	−11.13	108	4.75000	−0.93638	16496.48	−15.32	160	3.53307	−0.18897	5955.86	−3.44
5	6.34842	−3.90000	5094.40	−0.04	57	5.25000	−1.70075	17041.86	−31.68	109	4.25000	−0.94486	7009.87	3.46	161	3.43307	−0.18897	6608.64	0.31
6	6.35842	−3.90000	5096.90	0.41	58	4.70000	−1.70008	6041.14	9.41	110	4.00000	−0.94486	3202.61	2.06	162	3.80000	−0.15000	6747.49	−8.78
7	5.94000	−3.50000	4592.29	−0.46	59	4.50000	−1.70008	2866.53	3.88	111	3.90000	−0.94486	2048.14	1.51	163	3.70000	−0.15000	6251.30	−8.61
8	5.95000	−3.50000	4588.73	−0.15	60	4.34637	−1.70076	1171.69	1.03	112	3.80000	−0.94486	1201.68	1.13	164	3.55000	−0.15000	6237.12	−2.92
9	5.96000	−3.50000	4592.00	0.12	61	4.25189	−1.70076	621.26	0.40	113	3.72276	−0.94486	813.14	0.84	165	3.80000	−0.10000	7015.97	−7.75
10	5.53400	−3.10000	3958.77	−0.37	62	4.15740	−1.70075	575.26	0.22	114	3.62828	−0.94486	730.01	0.29	166	3.70000	−0.10000	6582.58	−6.96
11	5.54400	−3.10000	3950.29	−0.33	63	4.00000	−1.70076	2025.87	−1.45	115	3.53379	−0.94486	1181.65	−0.62	167	3.60000	−0.10000	6534.09	−3.17
12	5.55400	−3.10000	3948.76	−0.30	64	3.90000	−1.70008	4275.90	−5.71	116	3.40000	−0.94486	3006.04	−2.20	168	4.30000	0.00000	12766.36	113.07
13	5.95000	−2.83459	12155.20	−6.76	65	3.70000	−1.70008	13485.02	−34.70	117	3.25000	−0.94486	7287.77	−1.40	169	3.95000	0.00000	8569.84	3.65
14	5.70000	−2.83460	7522.51	−2.79	66	5.00000	−1.51178	14639.21	−13.11	118	4.75000	−0.75589	17995.61	−7.00	170	3.67500	0.00000	7252.32	−1.63
15	5.50000	−2.83460	4711.94	−2.70	67	4.65000	−1.51178	7614.71	9.10	119	4.30000	−0.75589	9639.45	1.87	171	3.57499	0.00000	7498.13	0.83
16	5.29124	−2.83459	3433.77	−0.11	68	4.30000	−1.51178	1965.46	2.15	120	3.95000	−0.75590	4222.87	1.55	172	3.47500	0.00000	8280.85	−3.28
17	5.19675	−2.83459	3736.51	1.10	69	4.15740	−1.51178	594.80	0.54	121	3.90000	−0.75590	3621.70	1.41	173	3.80000	0.10000	8093.40	−0.42
18	5.10226	−2.83459	4819.86	0.81	70	4.06291	−1.51178	183.41	0.31	122	3.80000	−0.75590	2615.13	1.11	174	3.70000	0.10000	7997.90	1.89
19	4.95000	−2.83459	8801.45	−8.37	71	3.96843	−1.51178	301.09	0.20	123	3.70000	−0.75590	1929.35	0.67	175	3.60000	0.10000	8349.55	0.89
20	5.50000	−2.64562	6891.90	−0.36	72	3.90000	−1.51178	798.91	−0.22	124	3.59048	−0.75589	1649.55	−0.25	176	3.82500	0.20000	8733.93	2.54
21	5.25000	−2.64562	3686.52	−2.29	73	3.75000	−1.51178	3483.04	−4.01	125	3.49599	−0.75589	1909.86	−1.58	177	3.72500	0.20000	8763.24	3.20
22	5.10226	−2.64562	3017.31	0.46	74	3.70000	−1.51178	4989.09	−6.74	126	3.40151	−0.75589	2754.83	−3.28	178	3.62500	0.20000	9260.36	−4.16
23	5.00778	−2.64562	3331.99	2.81	75	3.65000	−1.51178	6872.21	−10.56	127	3.30000	−0.75590	4476.54	−4.76	179	3.85000	0.30000	9388.24	2.88
24	4.91329	−2.64562	4429.06	4.04	76	3.90549	−1.33982	4.67	0.33	128	3.20000	−0.75590	7206.36	−4.13	180	3.75000	0.30000	9576.89	−0.29
25	4.75000	−2.64562	8861.57	−3.70	77	3.87876	−1.33982	15.31	0.32	129	4.20000	−0.56092	9410.02	6.99	181	3.65000	0.30000	10262.55	−18.15
26	5.50000	−2.45660	9763.92	7.37	78	3.85204	−1.33982	72.29	0.31	130	3.90000	−0.56092	5157.09	−1.97	182	3.97500	0.40000	10136.85	1.25
27	5.30000	−2.45660	6205.21	1.53	79	3.91885	−1.32646	28.31	0.33	131	3.80000	−0.56092	4123.70	−3.18	183	3.87500	0.40000	10087.11	−0.79
28	5.10000	−2.45000	3605.91	−1.72	80	3.89213	−1.32646	1.18	0.33	132	3.70000	−0.56092	3375.72	−3.75	184	3.77500	0.40000	10473.76	−11.25
29	4.91329	−2.45664	2558.98	1.28	81	3.86540	−1.32646	17.61	0.33	133	3.69000	−0.56690	3274.63	−3.59	185	4.02658	0.56692	11137.36	−7.41
30	4.81881	−2.45665	2892.04	4.05	82	3.83868	−1.32646	80.67	0.31	134	3.59048	−0.56692	2929.76	−3.76	186	4.00658	0.56692	11154.69	−8.60
31	4.72432	−2.45665	4010.28	5.88	83	4.75000	−1.32281	12106.49	0.84	135	3.49600	−0.56692	3026.92	−3.74	187	3.98658	0.56692	11188.95	−10.10
32	4.50000	−2.45660	11251.57	−9.88	84	4.30000	−1.32281	3796.06	4.40	136	3.40151	−0.56692	3637.48	−3.48	188	4.40000	0.80000	13009.90	3.58
33	4.30000	−2.45660	26413.36	−106.92	85	4.15000	−1.32281	1730.23	1.63	137	3.40000	−0.56092	3691.21	−3.46	189	4.30000	0.80000	12611.31	−8.49
34	5.40000	−2.26767	10908.57	11.27	86	3.96843	−1.32281	195.88	0.36	138	3.25000	−0.56092	6030.59	−0.93	190	4.20000	0.80000	12554.07	−16.43
35	5.10000	−2.26767	5455.40	3.25	87	3.87394	−1.32281	4.84	0.33	139	3.00000	−0.56092	15321.68	23.02	191	4.59999	1.00000	14194.90	10.40
36	4.81881	−2.26767	2313.33	0.04	88	3.77945	−1.32281	382.20	0.17	140	3.67000	−0.40000	4406.86	−8.70	192	4.50000	0.99999	13746.11	−4.95
37	4.72432	−2.26767	2062.42	1.81	89	3.60000	−1.32281	3248.58	−2.11	141	3.57499	−0.39994	4176.78	−7.41	193	4.40000	1.00003	13622.39	−13.55
38	4.53535	−2.26767	3575.79	5.40	90	3.50000	−1.32281	6520.10	−5.16	142	3.47500	−0.40000	4388.15	−4.82	194	4.74247	1.32281	15136.20	−2.82
39	4.25000	−2.26767	14483.65	−26.87	91	3.90549	−1.31310	21.42	0.33	143	3.37500	−0.40000	5179.08	−1.27	195	4.72357	1.32281	15130.21	−3.80
40	5.75000	−2.07870	21389.52	−63.23	92	3.87876	−1.31310	0.00	0.33	144	4.10000	−0.37795	8927.47	11.73	196	4.70467	1.32281	15137.84	−4.80
41	5.00000	−2.07870	6263.76	8.01	93	3.85204	−1.31310	22.41	0.33	145	3.75000	−0.37795	5016.72	−9.11	197	5.10000	1.60001	16375.80	6.75
42	4.80000	−2.07870	3267.36	1.99	94	3.91885	−1.29974	73.46	0.34	146	3.59048	−0.37795	4356.61	−7.97	198	5.00000	1.60000	16192.01	2.78
43	4.62983	−2.07870	1752.22	0.68	95	3.89213	−1.29974	16.74	0.33	147	3.49600	−0.37795	4480.08	−5.40	199	4.90000	1.60000	16384.72	−0.68
44	4.53535	−2.07870	1540.58	1.54	96	3.86540	−1.29974	1.22	0.33	148	3.40151	−0.37794	5096.88	−1.94	200	5.49836	2.07870	17589.84	7.01
45	4.44086	−2.07870	1948.35	2.65	97	3.83868	−1.29974	29.82	0.33	149	3.10000	−0.37794	11827.71	15.11	201	5.47946	2.07870	17581.02	7.31
46	4.26000	−2.07870	5144.49	−0.02	98	3.90549	−1.28637	65.30	0.34	150	3.70000	−0.30000	5249.33	−10.32	202	5.46057	2.07870	17585.43	7.65
47	4.20000	−2.07870	7144.64	−4.65	99	3.87876	−1.28637	14.39	0.34	151	3.60000	−0.30000	4962.83	−8.40	203	6.25425	2.83459	18969.29	−1.71
48	4.00000	−2.07870	18806.10	−56.88	100	3.85204	−1.28637	4.96	0.34	152	3.50000	−0.30006	5119.12	−4.70	204	6.23535	2.83459	18962.52	−1.61
49	5.25000	−1.88973	14065.90	−1.09	101	4.65000	−1.13380	12438.76	−0.38	153	3.75000	−0.25000	5847.17	−10.44	205	6.21646	2.83459	18968.93	−1.53
50	4.70000	−1.88973	3769.26	4.99	102	4.15000	−1.13380	3478.48	3.04	154	3.60000	−0.25000	5347.05	−7.82	206	7.01014	3.59048	19784.31	−6.79
51	4.53535	−1.88973	1810.00	1.35	103	4.00000	−1.13380	1570.59	1.17	155	3.45000	−0.25000	5860.90	−1.42	207	6.99124	3.59048	19778.80	−7.20
52	4.44086	−1.88973	1172.72	0.66	104	3.82670	−1.13384	286.43	0.43	156	3.70000	−0.20000	5920.54	−9.74	208	6.97235	3.59048	19786.46	−7.66

[a]Referenced to the absolute total energy (in hartree) $E(CCSD) = -560.113\,637\,67$ computed at the optimum CCSD geometry of $[FHCl]^-$. S_1 and S_2 in bohr.

[b]Residuals of the analytic fit in cm^{-1}.

at $\rho=\pi$ and/or $2^{-1}\pi$. The function $A(y)$ and the barrier to internal rotation, $B(y)$, are plotted in Fig. 7 in the entrance channel of the MEP.

In order to ascertain the k_{2n} coefficients, in which the flexibility of the bending potential near linearity is concentrated, eighteen linear reference points were judiciously chosen from which bending displacements were executed every 5° until the computed *ab initio* energy exceeded the $HF+Cl^-$ dissociation limit. These reference structures correspond to the enlarged points plotted in Fig. 5. From the energy values for $\rho=5°$, the quadratic bending force constants ($2k_2$) at the reference structures were evaluated by a finite-difference formula, and the results were fit to the functional form

$$k_2(x,y)=\left(\frac{\mu_{HF}}{4x^2}\right)\left\{1+\left(\frac{1}{x^6}\right)\left[\sum_{n=0}^{5}\ell_n(x,y)(x-x^\circ)^n\right]\right\}, \tag{35}$$

where

$$\ell_0(x,y)=\Omega_2(x,y;d_{11},d_{12},d_{13},1)+\Omega_4(x,y;d_{14},d_{15},1), \tag{36}$$

$$\ell_1(x,y)=\Omega_2(x,y;d_{16},d_{17},d_{18},1)+\Omega_4(x,y;d_{19},0,1), \tag{37}$$

$$\ell_2(x,y)=\Omega_2(x,y;d_{20},d_{21},d_{22},1), \tag{38}$$

and

$$\ell_i(x,y)=\Omega_2(x,y;d_{20+i},0,0,0) \tag{39}$$

for $i=\{3,4,5\}$, in which

$$\Omega_2(x,y;\alpha_0,\alpha_1,\alpha_2,\alpha_3)\equiv\frac{\alpha_0+\alpha_1\delta(x,y)+\alpha_2\delta(x,y)^2}{1+\alpha_3\delta(x,y)^2} \tag{40}$$

and

$$\Omega_4(x,y;\alpha_1,\alpha_2,\alpha_3)\equiv\frac{\alpha_1\delta(x,y)^3+\alpha_2\delta(x,y)^4}{1+\alpha_3\delta(x,y)^4}. \tag{41}$$

Note that $k_2(x,y)$ is constrained to yield the correct long-range ion-dipole form of the bending force constant in the $HF+Cl^-$ entrance channel. The fitting procedure used for Eq. (35) involved a determination of k_2 vs x along a set of three parallel curves encompassing the MEP, viz., those defined by constant values of $\delta(x,y)=+0.3$, 0.0, and -0.3 bohr. The collections of ℓ_n parameters for the three curves were then interpolated by appropriately behaved functions of $\delta(x,y)$, yielding the d_{11}–d_{25} constants of Eqs. (36)–(39).

The higher-order bending force constants in Eq. (32) were ascertained at each linear reference structure in a sequential manner by performing least-squares fits to data points for progressively larger values of ρ while fixing all previously determined lower-order constants. As in the k_2 case, the functional dependence of the k_4, k_6, and k_8 coefficients was constructed by considering families of curves of constant $\delta(x,y)$. The final functions given by the procedure were

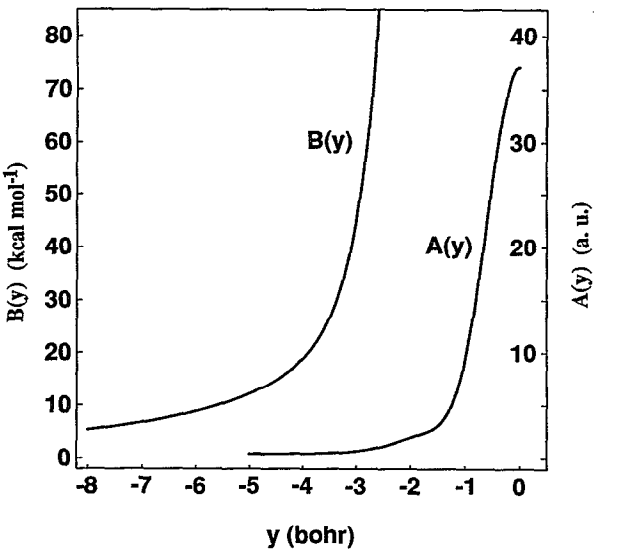

FIG. 7. The effective charge product $A(y)$ and the barrier to internal rotation $B(y)$ in the entrance channel of the minimum-energy path (MEP) for $[FHCl]^-$.

$$k_4(x,y)=[m_0(x,y)+m_1(x,y)(x-m_2(x,y))]\times\Gamma[x-m_2(x,y);0.1]^{-2}, \tag{42}$$

$$k_6(x,y)=m_3(x,y)\Gamma[x-m_4(x,y);0.1]^{-2}, \tag{43}$$

and

$$k_8(x,y)=0.025\,\Gamma[x-m_5(x,y);0.1]^{-2}, \tag{44}$$

where

$$m_i(x,y)=\Omega_2(x,y;d_{26+3i},d_{27+3i},d_{28+3i},1) \quad \text{for } i=\{0,1,2,3\}, \tag{45}$$

$$m_i(x,y)=\Omega_2(x,y;d_{26+3i},d_{27+3i},d_{28+3i},0) \quad \text{for } i=\{4,5\}, \tag{46}$$

and

$$\Gamma(\eta;\eta^\circ)\equiv 2^{-1}\sqrt{\eta^2+5^{-1}[\eta^\circ e^{-(\eta/\eta^\circ)^2}]^2}\times[1+\tanh(2\eta/\eta^\circ)]. \tag{47}$$

The function $\Gamma(\eta;\eta^\circ=0.1)$ is indistinguishable from η in the bonding region of the $[FHCl]^-$ surface but transforms to an asymptotically decaying function for $\eta\leqslant\eta^\circ$, thus averting abrupt singularities in Eqs. (42)–(44).

In Table IX the TZ(1+)(3*d*,3*p*) CCSD energy points for all nonlinear structures are listed with the ϵ(CCSD) residuals. As before, the corresponding RHF and MP2 data are provided as supplementary material in PAPS.[189] For the CCSD points lying below the $HF+Cl^-$ dissociation limit with distortions less than 90°, the rms error of the analytic fit is 9.3 cm^{-1}. Among several tests of the smoothness of the analytic bending potential was the construction of contour plots for excursions of the chloride ion around the HF monomer held rigid at the equilibrium configura-

tion of the ion-molecule complex. These contour plots are depicted in Fig. 8, where the bending potential is seen to be well behaved even near the $HF+Cl^-$ dissociation limit.

V. VIBRATIONAL EIGENSPECTRUM OF $[FHCl]^-$

The analytic representation of the global surface of $[FHCl]^-$ in a form which exhibits all requisite asymptotic characteristics provides for the variational determination of the complete vibrational eigenspectrum of $[FHCl]^-$ to near the $HF+Cl^-$ dissociation limit. This achievement facilitates an analysis of highly excited eigenstates of the system and thus actuates the investigation of several contemporary issues of vibrational dynamics: (1) the adiabatic separation of protonic and interhalogen motions,[108] (2) occurrences and patterns of anharmonic resonances, (3) the "entropy" of wave function mixing,[190] especially for states with extreme motion in a particular mode,[191] (4) the density of vibrational states at high energies,[191–195] and (5) signatures of quantum ergodicity[194,195] in the spacing distribution of adjacent energy levels. This section is focused on the analysis of such phenomena in the $[FHCl]^-$ complex. The chemical interpretation of the vibrational structure of $[FHCl]^-$ is discussed above in Sec. III.

A. Vibrational methodology

The Jacobi coordinates $(\Re,r,\tau)$ for the interaction of Cl^- with HF are a near optimal set of curvilinear internal variables for the current vibrational analysis because they not only provide a natural description of the dissociation channel but also closely mimic the normal modes at equilibrium. As denoted here, $\Re$ is the distance from the Cl^- ion to the center of mass of the HF fragment, r is the H–F distance, and τ is the angle subtended by the two radial direction vectors, $\hat{\Re}$ and $\hat{\mathbf{r}}$. When represented in a symmetric-top basis $|JKM\rangle$, the exact vibrational kinetic energy operator, $\hat{T}^{JM}_{\rm vib}(K',K) = \langle JK'M|\hat{T}|JKM\rangle$, expressed in Jacobi coordinates is[165]

$$\hat{T}^{JM}_{\rm vib}(K',K) = -\frac{\hbar^2}{2}\left[\frac{1}{\mu_1\Re^2}\left(\frac{\partial}{\partial\Re}\Re^2\frac{\partial}{\partial\Re}\right)+\frac{1}{\mu_2 r^2}\left(\frac{\partial}{\partial r}r^2\frac{\partial}{\partial r}\right)+\left(\frac{1}{\mu_1\Re^2}+\frac{1}{\mu_2 r^2}\right)\left(\frac{1}{\sin\tau}\frac{\partial}{\partial\tau}\sin\tau\frac{\partial}{\partial\tau}\right)\right]+\delta_{K',K}\hbar^2\left[\frac{J(J+1)-2K^2}{2\mu_1\Re^2}\right.$$
$$\left.+\frac{K^2}{2}\csc^2\tau\left(\frac{1}{\mu_1\Re^2}+\frac{1}{\mu_2 r^2}\right)\right]+\frac{\hbar^2}{2\mu_1\Re^2}\left[\delta_{K',K+1}\lambda^+_{JK}\left(-\frac{\partial}{\partial\tau}+K\cot\tau\right)+\delta_{K',K-1}\lambda^-_{JK}\left(\frac{\partial}{\partial\tau}+K\cot\tau\right)\right], \quad (48)$$

in which $\lambda^{\pm}_{JK}=[J(J+1)-K(K\pm1)]^{1/2}$, the reduced masses μ_1 and μ_2 refer to the (HF)–Cl^- and H–F subsystems, respectively, the body-fixed quantization axis (z) is assumed to lie along the radial vector $\hat{\Re}$, and (J,K,M) is the conventional set of quantum numbers for the total angular momentum $\mathbf{J}$ and its projections on the body- and space-fixed z axes.

Algorithmic details[160–164] of the vibrational methods employed here have been described in a previous communication.[160] In brief, rovibrational eigenfunctions are constructed from contracted state functions of the form

$$\Phi^{JPM\ell}_m(r,\Re,\tau;\omega) = \sqrt{\alpha_J}\,[D^J_{MK}(\omega)+P(-1)^{J+K}D^J_{M,-K}(\omega)]$$
$$\times\sum_{(v_1v_2v_3)\in\mathscr{A}} c^{JP\ell}_{m,v_1v_2v_3}\left(\frac{f^{JP\ell}_{v_1}(\Re)}{\Re}\right)$$
$$\times g^{JP\ell}_{v_2}(\tau)\left(\frac{h^{JP\ell}_{v_3}(r)}{r}\right), \quad (49)$$

where $\ell=|K|$, P specifies the parity (±1), $\alpha_J=(8\pi^2)^{-1}(2J+1)$, ω signifies the three Euler angles of rotation, $D^J_{MK}(\omega)$ is a Wigner rotation matrix[196] which yields the symmetric-top wave function $\langle\omega|JKM\rangle$ when normalized by $\alpha_J^{1/2}$, and $f^{JP\ell}_{v_1}$, $g^{JP\ell}_{v_2}$, and $h^{JP\ell}_{v_3}$ are members of selected orthonormal sets of single-mode vibrational functions. For linear molecules, ℓ corresponds to the usual vibrational angular momentum quantum number. The contraction coefficients $c^{JP\ell}_{m,v_1v_2v_3}$ in Eq. (49) are determined by neglecting the coupling of different K values in Eq. (48) and diagonalizing each $JP\ell$ block of the Hamiltonian matrix in the uncontracted configuration space $\mathscr{A}$. The final eigenfunctions Ψ^{JPM}_n are then found by solving the full secular equation in the $\Phi^{JPM\ell}_m$ basis to ascertain the rotationally induced mixing coefficients $C^{JP}_{n,m\ell}$ in the expansion

$$\Psi^{JPM}_n(r,\Re,\tau;\omega) = \sum_m\sum_{\ell=\ell^\circ}^{J} C^{JP}_{n,m\ell}\Phi^{JPM\ell}_m(r,\Re,\tau;\omega), \quad (50)$$

where $\ell^\circ=0$ if $P=(-1)^J$, and $\ell^\circ=1$ if $P=(-1)^{J+1}$. Only $J=0$ and 1 vibrational levels were computed for $[FHCl]^-$. Because the coupling matrix elements between $(J^P,\ell)=(1^-,0)$ and $(1^-,1)$ states are minuscule, the resultant rms rotational ℓ-type doubling of the $(1^\pm,1)$ manifolds is only 0.016 cm^{-1} for the lowest 265 vibrational levels. Therefore, the recontraction step of Eq. (50) has essentially no effect on the vibrational eigenvalues reported here.

The determination of the single-mode basis functions was initiated by converging the vibrational self-consistent-field (VSCF) procedure[197,198] on the lowest state of each $JP\ell$ manifold, providing the final $g^{JP\ell}_{v_2}$ set and preliminary radial functions as the spectrum of occupied and virtual modals for each coordinate. The VSCF angular modals $(g^{JP\ell}_{v_2})$ were represented as linear combinations of associ-

TABLE IX. TZ(1+)(3*d*,3*p*) CCSD relative energy points (in cm^{-1}) for nonlinear structures of $[FHCl]^-$.[a]

k	ρ	E(CCSD)	ε(CCSD)
	$(S_1, S_2) = (3.56492, -0.56692)$		
1	0.00000	2911.33	-3.77
2	0.08700	2964.59	-3.99
3	0.17500	3128.70	-4.54
4	0.26200	3404.99	-5.14
5	0.34900	3801.78	-5.36
6	0.43600	4327.84	-4.50
7	0.52400	5002.59	-2.05
8	0.61100	5824.87	0.91
9	0.69800	6820.15	0.57
10	0.78500	8013.18	-9.70
11	0.87300	9454.80	-38.20
	$(S_1, S_2) = (3.86492, -0.56692)$		
12	0.00000	4721.83	-2.33
13	0.08700	4763.47	-2.55
14	0.17500	4891.48	-3.21
15	0.26200	5106.07	-4.20
16	0.34900	5412.89	-5.16
17	0.43600	5817.89	-5.54
18	0.52400	6334.95	-5.07
19	0.61100	6961.66	-4.90
20	0.69800	7715.27	-8.71
21	0.78500	8611.59	-23.28
22	0.87300	9685.04	-59.35
	$(S_1, S_2) = (3.26492, -0.56692)$		
23	0.00000	5678.10	-1.56
24	0.08700	5751.53	-2.01
25	0.17500	5977.71	-3.19
26	0.26200	6358.24	-4.67
27	0.34900	6904.57	-5.62
28	0.43600	7629.39	-4.50
29	0.52400	8561.03	0.45
	$(S_1, S_2) = (3.66273, -0.94486)$		
30	0.00000	704.62	0.52
31	0.08700	751.02	0.48
32	0.17500	893.42	0.24
33	0.26200	1131.61	-0.34
34	0.34900	1471.29	-1.01
35	0.43600	1918.61	-0.97
36	0.52400	2488.71	0.57
37	0.61100	3179.11	3.16
38	0.69800	4009.31	4.47
39	0.78500	4997.53	1.39
40	0.87300	6182.60	-6.65
41	0.96000	7570.12	-13.82
42	1.04700	9215.31	-11.19
	$(S_1, S_2) = (3.96273, -0.94486)$		
43	0.00000	2741.09	1.83
44	0.08700	2779.03	1.86
45	0.17500	2895.15	1.80
46	0.26200	3088.50	1.41
47	0.34900	3362.68	0.80
48	0.43600	3721.60	0.55
49	0.52400	4176.14	1.30
50	0.61100	4722.88	2.82
51	0.69800	5375.42	3.41
52	0.78500	6145.61	0.44
53	0.87300	7060.42	-8.02
54	0.96000	8120.48	-21.54
55	1.04700	9364.10	-42.03
	$(S_1, S_2) = (3.36273, -0.94486)$		
56	0.00000	3818.79	-2.47
57	0.08700	3879.41	-2.65
58	0.17500	4065.70	-3.26
59	0.26200	4377.99	-4.29
60	0.34900	4824.59	-5.39
61	0.43600	5414.76	-5.64
62	0.52400	6170.16	-4.18
63	0.61100	7089.81	-1.69
64	0.69800	8202.59	-0.78
65	0.78500	9536.34	-3.72
66	0.87300	11147.30	-6.14
	$(S_1, S_2) = (3.87877, -1.31310)$		
67	0.00000	0.00	0.33
68	0.08700	35.52	0.31
69	0.17500	144.11	0.14
70	0.26200	324.57	-0.35
71	0.34900	579.82	-0.91
72	0.43600	913.01	-0.72
73	0.52400	1333.72	1.09
74	0.61100	1838.27	4.40
75	0.69800	2438.68	7.57
76	0.78500	3145.19	8.14
77	0.87300	3981.65	4.94
78	0.96000	4947.36	0.41
79	1.04700	6075.36	-1.34
80	1.13400	7398.11	-0.67
81	1.22200	8978.64	-1.99
	$(S_1, S_2) = (4.17877, -1.31310)$		
82	0.00000	2166.69	2.14
83	0.08700	2197.38	2.05
84	0.17500	2291.05	1.67
85	0.26200	2446.14	0.85
86	0.34900	2664.45	-0.24
87	0.43600	2947.72	-0.98
88	0.52400	3303.02	-0.63
89	0.61100	3726.01	0.95
90	0.69800	4225.41	2.81
91	0.78500	4808.01	3.34
92	0.87300	5491.15	1.56
93	0.96000	6271.54	-1.78
94	1.04700	7172.69	-6.36
95	1.13400	8216.84	-18.04
96	1.22200	9449.63	-49.88
	$(S_1, S_2) = (3.57877, -1.31310)$		
97	0.00000	3616.75	-2.33
98	0.08700	3659.94	-2.37
99	0.17500	3792.26	-2.58
100	0.26200	4012.89	-3.02
101	0.34900	4326.45	-3.30
102	0.43600	4738.00	-2.53
103	0.52400	5260.91	0.13
104	0.61100	5892.41	4.27
105	0.69800	6649.72	8.05
106	0.78500	7548.48	9.80
107	0.87300	8622.44	12.32
	$(S_1, S_2) = (4.19277, -1.70075)$		
108	0.00000	525.03	0.28
109	0.08700	550.92	0.31
110	0.17500	629.86	0.26
111	0.26200	760.36	-0.06
112	0.34900	943.62	-0.65
113	0.43600	1180.66	-1.21
114	0.52400	1476.83	-1.42
115	0.61100	1827.82	-1.59
116	0.69800	2240.08	-3.05
117	0.78500	2718.21	-7.48
118	0.87300	3275.17	-15.09
119	0.96000	3906.64	-21.78
120	1.04700	4629.56	-19.97
121	1.13400	5458.76	-5.88
122	1.22200	6426.01	7.57
123	1.30900	7536.60	-1.10
124	1.39600	8837.24	13.62
	$(S_1, S_2) = (4.49277, -1.70075)$		
125	0.00000	2763.07	3.68
126	0.08700	2786.50	3.65
127	0.17500	2857.90	3.49
128	0.26200	2975.76	3.10
129	0.34900	3140.88	2.57
130	0.43600	3353.81	2.24
131	0.52400	3618.74	2.48
132	0.61100	3931.14	3.18
133	0.69800	4295.88	3.53
134	0.78500	4715.99	2.48
135	0.87300	5201.49	0.13
136	0.96000	5747.03	-0.40
137	1.04700	6365.31	6.29
138	1.13400	7066.57	21.71
139	1.22200	7874.59	33.01
	$(S_1, S_2) = (3.89277, -1.70075)$		
140	0.00000	4510.20	-6.23
141	0.08700	4539.65	-6.47
142	0.17500	4629.56	-7.32
143	0.26200	4778.56	-8.91
144	0.34900	4988.53	-11.11
145	0.43600	5261.40	-13.45
146	0.52400	5604.25	-15.55
147	0.61100	6013.25	-17.75
148	0.69800	6497.17	-21.59
149	0.78500	7063.04	-28.69
150	0.87300	7728.22	-37.93
151	0.96000	8489.93	-41.06
	$(S_1, S_2) = (4.55118, -2.07870)$		
152	0.00000	1537.07	1.35
153	0.08700	1556.38	1.38
154	0.17500	1615.19	1.42
155	0.26200	1712.21	1.32
156	0.34900	1847.99	1.04
157	0.43600	2022.80	0.73
158	0.52400	2239.82	0.41
159	0.61100	2494.92	-0.38
160	0.69800	2791.59	-2.89
161	0.78500	3131.63	-8.69
162	0.87300	3522.24	-18.42
163	0.96000	3957.99	-29.18
164	1.04700	4447.65	-34.10
165	1.13400	4997.37	-25.52
166	1.22200	5622.93	-6.94
167	1.30900	6321.33	-2.68
168	1.39600	7114.30	-17.25
	$(S_1, S_2) = (4.85118, -2.07870)$		
169	0.00000	3934.98	3.21
170	0.08700	3953.03	3.22
171	0.17500	4008.03	3.24
172	0.26200	4098.76	3.22
173	0.34900	4225.73	3.28
174	0.43600	4389.13	3.68
175	0.52400	4591.80	4.67
176	0.61100	4829.66	6.06
177	0.69800	5105.61	7.10
178	0.78500	5420.76	6.81
179	0.87300	5781.05	5.05
180	0.96000	6180.55	4.26
181	1.04700	6626.20	10.19
182	1.13400	7122.21	29.03
183	1.22200	7681.05	58.29
184	1.30900	8298.05	78.09
	$(S_1, S_2) = (4.25118, -2.07870)$		
185	0.00000	5404.22	-0.53
186	0.08700	5425.17	-0.41
187	0.17500	5489.03	-0.10
188	0.26200	5594.45	0.30
189	0.34900	5742.19	0.81
190	0.43600	5932.76	1.64
191	0.52400	6169.97	2.84
192	0.61100	6449.83	3.73
193	0.69800	6776.78	2.72
194	0.78500	7153.62	-2.16
195	0.87300	7589.40	-11.56
196	0.96000	8079.30	-21.52
	$(S_1, S_2) = (4.91122, -2.45664)$		
197	0.00000	2559.19	1.33
198	0.08700	2574.21	1.35
199	0.17500	2619.96	1.35
200	0.34900	2800.96	1.23
201	0.78500	3788.98	-1.94
202	0.87266	4083.16	-7.87
	$(S_1, S_2) = (5.28553, -2.83459)$		
203	0.00000	3433.33	-0.02
204	0.08700	3445.53	-0.04
205	0.17500	3482.70	-0.11
206	0.34900	3629.69	-0.25
207	0.78500	4428.31	2.33
208	0.87266	4663.89	0.81
	$(S_1, S_2) = (3.83796, 0.30000)$		
209	0.00000	9387.89	2.84
210	0.08700	9421.91	-0.24
211	0.17500	9526.98	-8.81
212	0.34900	9960.22	-32.55
213	0.78500	12667.49	-57.90
214	0.87266	13577.66	-107.78
	$(S_1, S_2) = (6.74542, -4.30000)$		
215	[illegible]1	5497.79	-0.14
216	[illegible]0	6055.25	0.86

Highly distorted structures: [k, S_1, S_2, ρ, E(CCSD), ε(CCSD)] = (217, 3.83796, 0.30000, 1.57080, 31935.41, -24691.00); (218, 3.56488, -0.56688, 3.14159, 5339407, –); (219, 3.[illegible], -0.94486, 3.14159, 1200794,–); (220, 3.87877, -1.31310, 3.14159, 332181.33, -745.53); (221, 4.19277, -1.70075, 3.14159, 136708.08, 803.90); (222, 4.55118, -2.07870, 1.65759, 10308.26, 1256.10); (223, 4.55118, -2.07870, 3.14159, 74563.70, -940.60); (224, 4.91123, -2.45664, 1.57080, 7896.51, 464.97); (225, 4.91122, -2.45664, 3.14159, 40047.16, 378.80); (226, 5.28554, -2.83459, 1.57080, 7518.57, 529.37); (227, 5.28553, -2.83459, 3.14159, 22790.22, -438.28); (228, 6.74542, -4.30000, 1.57080, 7641.69, 469.62).

[a]S_1 and S_2 in bohr, ρ in rad. See also footnote a of Table VIII.

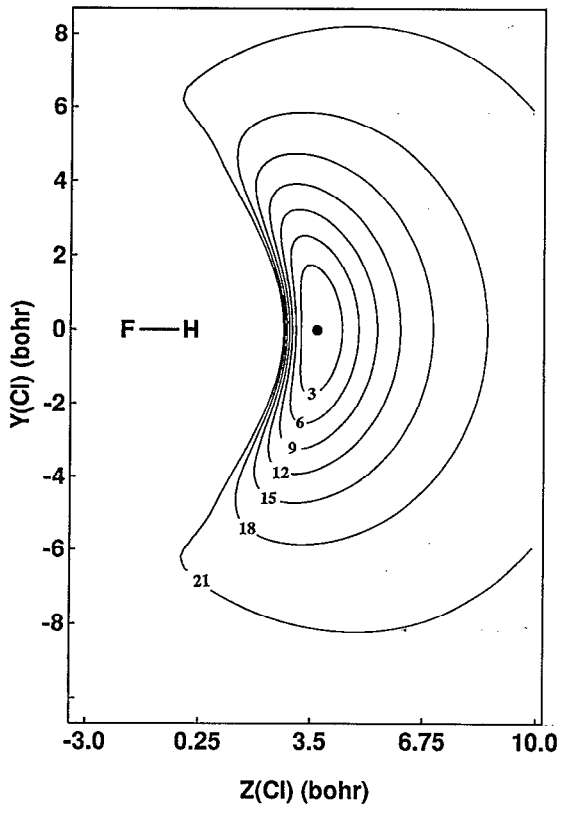

FIG. 8. Energy contours for the excursion of the chloride ion about the HF moiety in the $[FHCl]^-$ complex. Contour lines are drawn and labeled every 3 kcal mol^{-1} above the local minimum. The origin of the Cartesian (Y,Z) axis system for Cl^- coincides with the hydrogen nucleus. The H–F distance is assumed fixed at 0.9600 Å, the equilibrium separation in the complex.

ated Legendre functions $P_L^K(\cos\tau)$ with the maximum value of L (52 for $J=0$) and quadrature parameters selected automatically.[160] The VSCF equations for the radial modes were solved numerically to high precision by means of the finite-difference boundary value method.[164] The mesh size and range were also selected automatically,[160] and the finite-difference approximation of the second-derivative operator involved 27 points. The total number of grid points generated in the $J=0$ case was 703 and 76 for $\Re$ and r, respectively. In order to improve the description of highly excited stretching states, the VSCF radial functions were contracted by computing state-averaged natural modals.[161] In this procedure, the configuration space $\mathscr{A}$ in Eq. (49) was chosen by restricting the excitations to stretching modes alone and including all such states [574 $(J=0)$] lying less than 0.07 a.u. $(J=0)$ above the ground vibrational level $[E_{zp}^{\mathrm{SCF}}(J=0)=2583.6\ \mathrm{cm}^{-1}]$, according to the sum of the VSCF eigenvalues.[160] An average density matrix was constructed over all configuration interaction roots [132 $(J=0)$] with excitation energy less than 0.05 a.u. $(J=0)$, and all natural modals with occupation numbers greater than 10^{-6} were selected for subsequent calculations.[199]

Because the dissociation energy of the $[FHCl]^-$ complex to $HF+Cl^-$ is relatively small and motion along the $\Re$ coordinate extends far into the dissociation channel for higher vibrational levels, some modifications of the procedures described previously[160] were required in the computation of matrix elements of the potential energy function, $\langle v_1' v_2' v_3' | V(\Re,\tau,r) | v_1 v_2 v_3 \rangle$. For each coordinate Gauss–Legendre quadrature nodes were used with weights derived as before, and the number of points was determined automatically using an accuracy criterion of 10^{-5}. In integrations over radial modes, ten separate quadratures over equally spaced intervals were employed with independent adjustment of the number of points within each partition. For $J=0$ the total number of points for integrations over $\Re$, τ, r was 58, 28, and 56, respectively, and the associated quadrature errors were shown by test results to affect the vibrational eigenvalues by less than 0.1 cm^{-1}. Because the weight functions in the radial quadratures included coefficients of $\Re^{-2}$ and r^{-2}, terms in the Hamiltonian involving these factors were integrated exactly. It was found advantageous to order the quadratures so that integrations were performed last over the coordinate $(\Re)$ with the largest number of basis functions and quadrature points. Finally, to minimize numerical instabilities in converging highly excited bound-state wave functions, the system was effectively placed in a box by the addition of a potential term (in atomic units) $V_{\mathrm{box}}(R) = e^{4(R-R_0)}$, where R is the H–Cl distance and $R_0=15$ bohr. Variation of the onset parameter R_0 between 10 and 15 bohr in preliminary test calculations for $J=0$ revealed that the effect of the box constraint on the lowest 150 energy levels was less than the uncertainties arising from quadrature errors or limitations of the configuration space.

In the determination of the final vibrational wave functions, the selection of the configuration space $\mathscr{A}$ in Eq. (49) was accomplished by an energy selection criterion[160] based on VSCF eigenvalues for the angular mode and diagonal elements of the VSCF Hamiltonian in the natural modal basis for the radial modes. In the $J=0$ case, the excitation energy cutoff was placed at $E_{zp}^{\mathrm{SCF}} + 0.07$ a.u., giving a Hamiltonian matrix of total dimension 2123 involving 96, 20, and 8 active single-mode functions $f_{v_1}^{JP\ell}(\Re)$, $g_{v_2}^{JP\ell}(\tau)$, and $h_{v_3}^{JP\ell}(r)$, respectively.[200] The somewhat insignificant recontraction step of Eq. (50) for $J^P=1^-$ was implemented using an energy cutoff of 0.046 a.u. and thus included 296 and 246 state functions $(\Phi_m^{JPM\ell})$ for $\ell=0$ and 1, respectively. The majority of the CPU time required for the vibrational analysis was spent in the diagonalization of the Hamiltonian matrices for each value of $JP\ell$. All selection criteria in this investigation were ascertained on the basis of systematic convergence studies, which provided the following maximum uncertainty estimates (ϵ, cm^{-1}) for the roots of the $J=0$ Hamiltonian between states n_1 and n_2: $\epsilon(n_1-n_2)=0.001$ (1–15), 0.07 (16–45), 0.75 (46–80), 3.2 (81–150), and 8.1 (151–200). Energy levels and wave function components are given in Tables X and XI for the lowest 150 vibrational states of $[FHCl]^-$ with $J=0$ and $(J^P,\ell)=(1^+,0)$, respectively. The configuration interaction coefficients therein refer to state functions comprised of the natural modals of *each* coordinate for the *specific*

eigenstate listed. The underlying quartic force field of $[FHCl]^-$ and the spectroscopic constants derived from it are given above in Table V. Finally, for reference in future spectroscopic studies, selected variationally determined vibrational levels of $[FDCl]^-$ lying below 3100 cm^{-1} are listed in Table XII.

B. Vibrational adiabaticity and anharmonic resonances

The $[FHCl]^-$ complex constitutes a prototypical example of vibrational adiabaticity since a large separation in time scales of classical motion occurs between the chloride stretching mode with $\nu_1=247$ cm^{-1} and the protonic bending and stretching vibrations with $(\nu_2, \nu_3)=(876, 2884)$ cm^{-1}. Myriad authors have developed mathematical formalisms for treating the vibrational dynamics of such systems, and Epa and Thorson[108] in particular have applied the adiabatic approximation to the hydrogen bihalide system $[FHF]^-$. At low energies the vibrationally adiabatic picture predicts the existence of uniform progressions of chloride stretching states appearing on families of widely separated, effective one-dimensional potentials, $V_{\text{eff}}(\Re; v_2, v_3)$, which depend on the quantum numbers for the high-frequency vibrations. At higher vibrational energies avoided crossings between these effective potentials are encountered at certain values of $\Re$, and mixing of adiabatic chloride stretching states results. Epa and Thorson[108] have provided several plots which depict the effects of such avoided crossings on the effective potentials for the symmetric vibrational stretching mode of $[FHF]^-$. In the presence of intertwining effective potential curves, it is necessary to solve a set of coupled-channel adiabatic equations[108] to ascertain the strength of the resulting anharmonic resonances and the extent of wave function mixing. To the degree that the nonadiabatic coupling is strong, direct variational methods of full dimensionality are required to compute reliable wave functions effectively.

The character of rigorously determined vibrational wave functions is conveniently quantified by "entropy of mixing" data for a given eigenstate. For each coordinate q, the entropy of mixing component for the nth state $(S^q_{\text{mix},n})$ is defined by[190]

$$S^q_{\text{mix},n}=-\sum_i n_i^q \ln(n_i^q), \tag{51}$$

where $\{n_i^q\}$ is the set of occupation numbers for the natural modals of each coordinate. Note that if one of the occupation numbers is unity and the rest are zero for a given coordinate, then the associated entropy component vanishes. Here a total entropy of mixing is defined for ease of analysis,

$$S_{\text{mix},n}=\sum_q S^q_{\text{mix},n}, \tag{52}$$

and for each eigenstate in Tables X and XI the computed value for $S_{\text{mix},n}$ is listed.

The interplay of vibrational adiabaticity and resonance *inter*actions is elucidated in Figs. 9–12 by wave function contour plots for series of $|v_1\ 0\ 0\rangle$, $|v_1\ 0\ 1\rangle$, and $|v_1\ 0\ 2\rangle$ states, and also in Figs. 13 and 14 by plots of $S_{\text{mix},n}$ values and adjacent-level spacings, $\delta(v_1)\equiv E_{v_1}-E_{v_1-1}$, for the $|v_1\ 0\ 0\rangle$ and $|v_1\ 0\ 1\rangle$ progressions. It is useful to focus first on the $|v_1\ 0\ 0\rangle$ states. The nodal patterns (Figs. 9 and 10) exhibited by these states are remarkably regular, and vibrational adiabaticity is clearly demonstrated in that the spatial extent of the wave function lobes in the direction of the antisymmetric stretching coordinate (y) is virtually constant not only within each eigenstate but also throughout the entire vibrational progression. The (v_1,v_1-1) level spacings (Fig. 13) within this series of states start at 247.2 cm^{-1} and decrease uniformly to 44.7 cm^{-1} at $v_1=49$. The first several members are predicted to form a linear progression $\delta(v_1)=\nu_1+2(v_1-1)\chi_{11}=251.9-5.78\ v_1$ cm^{-1} (cf. Table V) according to second-order perturbation theory, and indeed this formula reproduces the observed spacings within 2 cm^{-1} through $v_1=18$.

Apart from a small disturbance at $v_1=13$, $S_{\text{mix},n}$ increases in an incremental fashion for the lowest 20 $|v_1\ 0\ 0\rangle$ states. While not unexpected, this behavior contrasts that observed spectroscopically[191] in the 14 000–20 000 cm^{-1} region of the S_0 surface of HFCO, where there appears to exist a series of vibrational states $(2_16_v;\ v=13, 15, 17, 19)$ which become *unmixed* as the motion in the out-of-plane bending mode (ν_6) becomes more extreme. The first sharp resonance in the $|v_1\ 0\ 0\rangle$ series for $[FHCl]^-$ occurs between the $|20\ 0\ 0\rangle$ and $|11\ 2\ 0\rangle$ configurations, whose eigenstates lie 3827.6 and 3832.9 cm^{-1}, respectively, above the ground vibrational state. For larger values of v_1, a periodic phasing and dephasing of resonance interactions between $|v_1\ 0\ 0\rangle$ and $|v_1'\ 2\ 0\rangle$ configurations is observed, as shown strikingly by the $S_{\text{mix},n}$ plot in Fig. 13. The associated displacements in the $\delta(v_1)$ series are generally less than 4 cm^{-1}. For example, a strong mixing of the $|36\ 0\ 0\rangle$ and $|24\ 2\ 0\rangle$ configurations is found in the eigenstate at 5518.4 cm^{-1}, and $\delta(36)=80.8$ and $\delta(37)=73.0$ cm^{-1} are thus displaced by $+1.4$ and -3.8 cm^{-1}, respectively, from the values given by a linear interpolation of the $\delta(35)$ and $\delta(38)$ spacings. It is noteworthy that the mixing with configurations of the type $|v_1'\ 0\ 1\rangle$ is quite small for eigenstates in the $|v_1\ 0\ 0\rangle$ progression which have as many as 50 quanta in the chloride stretching mode.

Regularity of nodal patterns and evidence of vibrational adiabaticity is essentially maintained in the wave functions for the $|v_1\ 0\ 1\rangle$ and $|v_1\ 0\ 2\rangle$ states, as revealed in the contour plots of Figs. 11 and 12. In particular, the multinode structure extending into the $HF+Cl^-$ dissociation channel for the $|v_1\ 0\ 0\rangle$ states becomes bi- and trifurcated as quanta are added to the H–F antisymmetric stretching mode. For the wave functions of higher-lying $|v_1\ 0\ 1\rangle$ and $|v_1\ 0\ 2\rangle$ eigenstates, small, irregular undulations at large (HF)–Cl^- separations become noticeable which arise from moderate mixing of the dominant configurations with more highly oscillatory wave functions with fewer multifurcated lobes. The level-spacing data depicted in Fig. 14 for the $|v_1\ 0\ 1\rangle$ progression are consistent with the corresponding wave function plots in that broad patterns of regularity are observed but with diminished extent vis-à-vis the $|v_1\ 0\ 0\rangle$ series. The observed $\delta(v_1=1)$

TABLE X. Vibrational states $[(J,\ell)=(0,0)]$ of nonrotating $[FHCl]^-$.[a]

k	E_k	S_{mix}	Wave function components			k	E_k	S_{mix}	Wave function components			k	E_k	S_{mix}	Wave function components		
1	0.00	0.03	0.999 | 0 0 0⟩	0.035 | 0 2 1⟩	0.026 | 1 0 1⟩	51	4294.45	0.66	0.964 | 14 2 0⟩	0.199 | 11 4 0⟩	0.106 | 11 2 1⟩	101	5591.40	0.74	0.954 | 37 0 0⟩	0.261 | 27 2 0⟩	0.097 | 22 0 1⟩
2	247.20	0.05	0.998 | 1 0 0⟩	0.048 | 0 0 1⟩	0.035 | 1 2 1⟩	52	4344.47	0.39	0.981 | 24 0 0⟩	0.124 | 17 2 0⟩	0.114 | 17 0 1⟩	102	5602.09	2.03	0.864 | 11 0 1⟩	0.360 | 23 2 0⟩	0.151 | 11 0 0⟩
3	488.30	0.07	0.997 | 2 0 0⟩	0.061 | 1 0 1⟩	0.034 | 2 2 1⟩	53	4344.91	0.95	0.947 | 6 4 0⟩	0.210 | 5 4 0⟩	0.159 | 6 2 1⟩	103	5611.73	2.21	0.834 | 25 2 0⟩	0.387 | 11 0 1⟩	0.199 | 22 4 0⟩
4	723.27	0.09	0.997 | 3 0 0⟩	0.071 | 2 0 1⟩	0.034 | 3 2 1⟩	54	4437.07	0.87	0.952 | 15 2 0⟩	0.204 | 15 2 0⟩	0.104 | 15 2 1⟩	104	5632.60	1.42	0.898 | 15 4 0⟩	0.368 | 10 6 0⟩	0.105 | 15 2 1⟩
5	952.11	0.10	0.996 | 4 0 0⟩	0.079 | 3 0 1⟩	0.034 | 4 2 1⟩	55	4462.91	0.42	0.978 | 25 0 0⟩	0.151 | 20 2 0⟩	0.105 | 20 0 1⟩	105	5648.51	2.91	0.751 | 1 0 2⟩	0.395 | 4 2 1⟩	0.287 | 1 2 1⟩
6	1174.85	0.12	0.995 | 5 0 0⟩	0.085 | 4 0 1⟩	0.033 | 5 2 1⟩	56	4474.65	0.84	0.960 | 6 0 1⟩	0.139 | 8 0 1⟩	0.121 | 6 2 1⟩	106	5665.33	0.50	0.972 | 38 0 0⟩	0.193 | 31 2 0⟩	0.084 | 31 0 1⟩
7	1391.51	0.13	0.994 | 6 0 0⟩	0.091 | 5 0 1⟩	0.034 | 5 2 0⟩	57	4512.25	0.92	0.946 | 7 4 0⟩	0.235 | 6 6 0⟩	0.156 | 7 2 1⟩	107	5684.50	3.65	0.545 | 4 2 1⟩	0.336 | 3 0 0⟩	0.292 | 4 6 1⟩
8	1602.14	0.14	0.994 | 7 0 0⟩	0.096 | 4 0 1⟩	0.039 | 4 2 0⟩	58	4548.45	1.63	0.828 | 0 6 0⟩	0.502 | 0 2 1⟩	0.145 | 0 0 2⟩	108	5702.68	1.05	0.931 | 26 2 0⟩	0.296 | 23 4 0⟩	0.145 | 32 0 0⟩
9	1677.52	0.22	0.989 | 0 2 0⟩	0.144 | 0 0 1⟩	0.026 | 1 2 1⟩	59	4573.35	1.74	0.736 | 18 2 0⟩	0.645 | 26 0 0⟩	0.142 | 13 4 0⟩	109	5736.17	0.51	0.972 | 39 0 0⟩	0.198 | 32 2 0⟩	0.082 | 32 0 1⟩
10	1806.79	0.16	0.993 | 8 0 0⟩	0.100 | 5 0 1⟩	0.043 | 5 2 0⟩	60	4579.52	1.69	0.747 | 26 0 0⟩	0.636 | 16 2 0⟩	0.125 | 13 4 0⟩	110	5739.01	2.81	0.744 | 7 6 0⟩	0.410 | 6 2 1⟩	0.277 | 7 2 1⟩
11	1904.98	0.25	0.988 | 1 2 0⟩	0.138 | 1 0 1⟩	0.049 | 0 2 1⟩	61	4672.13	1.21	0.930 | 8 4 0⟩	0.253 | 5 6 0⟩	0.148 | 7 0 1⟩	111	5748.15	1.34	0.899 | 16 4 0⟩	0.378 | 13 6 0⟩	0.099 | 16 2 1⟩
12	2005.54	0.17	0.992 | 9 0 0⟩	0.104 | 6 0 1⟩	0.048 | 6 2 0⟩	62	4680.69	2.79	0.574 | 0 2 1⟩	0.474 | 0 6 0⟩	0.383 | 0 6 1⟩	112	5779.91	1.00	0.930 | 0 8 0⟩	0.314 | 0 4 1⟩	0.135 | 1 10 0⟩
13	2126.01	0.27	0.987 | 2 2 0⟩	0.132 | 2 0 1⟩	0.062 | 1 2 1⟩	63	4686.45	0.51	0.972 | 27 0 0⟩	0.187 | 20 2 0⟩	0.090 | 20 0 1⟩	113	5790.55	1.59	0.888 | 27 2 0⟩	0.321 | 28 0 0⟩	0.189 | 29 0 0⟩
14	2198.46	0.18	0.992 | 10 0 0⟩	0.107 | 7 0 1⟩	0.052 | 7 2 0⟩	64	4707.17	2.30	0.801 | 17 2 0⟩	0.473 | 7 0 1⟩	0.163 | 10 4 0⟩	114	5804.54	0.98	0.937 | 40 0 0⟩	0.264 | 31 2 0⟩	0.179 | 16 0 1⟩
15	2340.59	0.30	0.986 | 3 2 0⟩	0.126 | 3 0 1⟩	0.072 | 2 4 0⟩	65	4716.60	2.28	0.808 | 7 0 1⟩	0.470 | 17 2 0⟩	0.155 | 8 4 0⟩	115	5810.85	1.39	0.925 | 12 0 1⟩	0.192 | 21 2 0⟩	0.133 | 21 0 0⟩
16	2385.63	0.19	0.991 | 11 0 0⟩	0.110 | 8 0 1⟩	0.057 | 8 2 0⟩	66	4788.23	1.96	0.854 | 1 6 0⟩	0.340 | 0 2 1⟩	0.249 | 1 2 1⟩	116	5848.07	2.62	0.787 | 8 6 0⟩	0.332 | 7 4 0⟩	0.203 | 5 2 1⟩
17	2548.72	0.33	0.984 | 4 2 0⟩	0.121 | 4 0 1⟩	0.086 | 3 4 0⟩	67	4793.00	0.40	0.979 | 28 0 0⟩	0.149 | 21 2 0⟩	0.106 | 21 0 1⟩	117	5858.34	1.45	0.883 | 17 4 0⟩	0.402 | 14 6 0⟩	0.122 | 13 2 0⟩
18	2567.15	0.21	0.990 | 12 0 0⟩	0.111 | 9 0 1⟩	0.065 | 9 2 0⟩	68	4826.91	1.05	0.934 | 9 4 0⟩	0.274 | 8 6 0⟩	0.141 | 9 2 1⟩	118	5867.49	1.04	0.922 | 41 0 0⟩	0.352 | 27 2 0⟩	0.102 | 21 4 0⟩
19	2743.02	0.32	0.985 | 13 0 0⟩	0.115 | 10 2 0⟩	0.097 | 10 0 1⟩	69	4837.74	0.82	0.951 | 18 2 0⟩	0.240 | 15 4 0⟩	0.105 | 15 2 1⟩	119	5879.29	1.49	0.880 | 28 2 0⟩	0.383 | 35 0 0⟩	0.233 | 27 0 0⟩
20	2750.59	0.44	0.978 | 5 2 0⟩	0.106 | 5 0 1⟩	0.091 | 5 4 0⟩	70	4895.66	0.40	0.980 | 29 0 0⟩	0.147 | 22 2 0⟩	0.106 | 22 0 1⟩	120	5912.84	3.32	0.719 | 5 2 1⟩	0.396 | 7 6 0⟩	0.243 | 3 0 2⟩
21	2883.72	0.31	0.985 | 0 0 1⟩	0.159 | 0 2 0⟩	0.041 | 1 0 0⟩	71	4900.56	2.64	0.560 | 2 2 1⟩	0.491 | 2 2 0⟩	0.369 | 1 2 1⟩	121	5930.03	1.81	0.875 | 1 8 0⟩	0.282 | 1 4 1⟩	0.201 | 0 10 0⟩
22	2913.58	0.24	0.989 | 14 0 0⟩	0.115 | 11 0 1⟩	0.075 | 11 2 0⟩	72	4945.02	1.21	0.938 | 8 0 1⟩	0.205 | 15 2 0⟩	0.121 | 8 0 2⟩	122	5931.00	0.56	0.968 | 42 0 0⟩	0.214 | 35 2 0⟩	0.073 | 35 0 1⟩
23	2946.01	0.39	0.981 | 6 2 0⟩	0.111 | 6 0 1⟩	0.110 | 5 2 0⟩	73	4961.98	1.36	0.920 | 19 2 0⟩	0.204 | 14 0 0⟩	0.200 | 8 0 1⟩	123	5959.06	1.62	0.870 | 27 2 0⟩	0.400 | 22 4 0⟩	0.201 | 27 0 0⟩
24	3078.76	0.24	0.989 | 15 0 0⟩	0.116 | 12 0 1⟩	0.077 | 12 2 0⟩	74	4975.67	1.15	0.925 | 10 4 0⟩	0.299 | 7 6 0⟩	0.137 | 10 2 1⟩	124	5964.17	1.88	0.842 | 18 4 0⟩	0.429 | 20 2 0⟩	0.232 | 23 2 0⟩
25	3135.12	0.46	0.978 | 7 2 0⟩	0.097 | 6 4 0⟩	0.093 | 6 2 1⟩	75	4987.55	2.67	0.670 | 2 6 0⟩	0.434 | 2 2 1⟩	0.369 | 1 2 1⟩	125	5984.00	3.13	0.710 | 2 0 2⟩	0.528 | 9 6 0⟩	0.215 | 6 4 0⟩
26	3163.05	1.10	0.935 | 1 0 1⟩	0.221 | 0 4 0⟩	0.217 | 1 4 0⟩	76	4994.74	0.44	0.976 | 30 0 0⟩	0.166 | 25 2 0⟩	0.098 | 25 0 1⟩	126	5991.57	0.54	0.969 | 43 0 0⟩	0.209 | 36 2 0⟩	0.074 | 36 0 1⟩
27	3214.84	1.14	0.925 | 0 4 0⟩	0.271 | 0 0 1⟩	0.195 | 1 0 1⟩	77	5078.95	1.27	0.907 | 20 2 0⟩	0.335 | 23 0 0⟩	0.191 | 18 4 0⟩	127	5994.65	3.75	0.595 | 9 2 0⟩	0.447 | 2 0 2⟩	0.252 | 6 2 2⟩
28	3238.72	0.25	0.988 | 16 0 0⟩	0.117 | 13 0 1⟩	0.081 | 13 2 0⟩	78	5090.89	0.90	0.935 | 31 0 0⟩	0.322 | 20 2 0⟩	0.101 | 18 0 1⟩	128	6010.04	1.01	0.949 | 13 0 1⟩	0.197 | 8 0 1⟩	0.091 | 23 2 1⟩
29	3318.30	0.44	0.978 | 8 2 0⟩	0.133 | 7 4 0⟩	0.098 | 8 0 1⟩	79	5109.28	2.23	0.846 | 3 6 0⟩	0.363 | 1 2 1⟩	0.190 | 2 4 0⟩	129	6037.44	1.52	0.886 | 30 2 0⟩	0.357 | 32 0 0⟩	0.230 | 29 0 0⟩
30	3393.58	0.26	0.987 | 17 0 0⟩	0.118 | 14 0 1⟩	0.086 | 14 2 0⟩	80	5118.00	1.19	0.921 | 11 4 0⟩	0.311 | 8 6 0⟩	0.126 | 11 2 1⟩	130	6050.17	0.91	0.935 | 44 0 0⟩	0.320 | 29 2 0⟩	0.081 | 23 4 0⟩
31	3406.76	1.68	0.867 | 1 4 0⟩	0.341 | 2 0 1⟩	0.282 | 1 0 1⟩	81	5171.21	1.12	0.944 | 9 0 1⟩	0.145 | 13 0 1⟩	0.116 | 13 2 1⟩	131	6064.10	1.48	0.881 | 19 4 0⟩	0.409 | 16 6 0⟩	0.091 | 16 4 1⟩
32	3452.71	1.65	0.874 | 2 0 1⟩	0.341 | 1 4 0⟩	0.262 | 2 4 0⟩	82	5180.74	0.79	0.950 | 32 0 0⟩	0.260 | 22 2 0⟩	0.123 | 17 0 1⟩	132	6070.03	1.98	0.854 | 2 8 0⟩	0.291 | 1 6 0⟩	0.190 | 2 4 1⟩
33	3495.46	0.50	0.975 | 9 2 0⟩	0.146 | 8 4 0⟩	0.099 | 8 2 1⟩	83	5194.97	2.86	0.734 | 2 2 1⟩	0.465 | 3 6 0⟩	0.230 | 2 0 2⟩	133	6094.92	2.81	0.744 | 10 6 0⟩	0.371 | 7 4 0⟩	0.204 | 5 2 1⟩
34	3543.47	0.28	0.987 | 18 0 0⟩	0.118 | 15 0 1⟩	0.093 | 15 2 0⟩	84	5196.16	1.63	0.895 | 21 2 0⟩	0.284 | 22 0 0⟩	0.169 | 20 0 0⟩	134	6103.37	1.08	0.916 | 45 0 0⟩	0.369 | 27 2 0⟩	0.105 | 20 4 0⟩
35	3611.38	0.90	0.952 | 2 4 0⟩	0.194 | 2 0 1⟩	0.149 | 1 0 1⟩	85	5254.97	1.13	0.921 | 12 4 0⟩	0.325 | 9 6 0⟩	0.122 | 12 2 1⟩	135	6114.20	1.53	0.872 | 31 2 0⟩	0.400 | 37 0 0⟩	0.238 | 33 2 0⟩
36	3666.20	0.60	0.969 | 10 2 0⟩	0.156 | 9 2 0⟩	0.099 | 9 2 1⟩	86	5269.76	0.48	0.974 | 33 0 0⟩	0.180 | 24 2 0⟩	0.092 | 24 0 1⟩	136	6148.93	3.19	0.714 | 6 2 1⟩	0.394 | 7 6 0⟩	0.216 | 6 6 0⟩
37	3688.56	0.34	0.983 | 19 0 0⟩	0.117 | 16 2 0⟩	0.111 | 16 0 1⟩	87	5290.67	2.13	0.850 | 4 6 0⟩	0.338 | 3 2 1⟩	0.185 | 4 2 1⟩	137	6157.70	0.58	0.966 | 46 0 0⟩	0.226 | 37 2 0⟩	0.066 | 37 0 1⟩
38	3715.70	0.81	0.961 | 3 0 1⟩	0.130 | 3 2 0⟩	0.118 | 2 2 0⟩	88	5304.70	0.95	0.941 | 22 2 0⟩	0.269 | 18 4 0⟩	0.125 | 29 0 0⟩	138	6161.20	1.73	0.866 | 20 4 0⟩	0.414 | 15 6 0⟩	0.131 | 6 2 1⟩
39	3805.69	0.75	0.961 | 3 4 0⟩	0.185 | 3 2 1⟩	0.135 | 2 6 0⟩	89	5324.56	1.18	0.908 | 0 0 2⟩	0.373 | 0 2 1⟩	0.111 | 3 2 1⟩	139	6184.05	1.47	0.901 | 32 2 0⟩	0.320 | 27 2 0⟩	0.173 | 30 0 0⟩
40	3827.59	1.24	0.883 | 20 0 0⟩	0.444 | 11 2 0⟩	0.101 | 11 0 1⟩	90	5355.21	0.45	0.976 | 34 0 0⟩	0.171 | 27 2 0⟩	0.096 | 27 0 1⟩	140	6202.33	2.57	0.807 | 3 8 0⟩	0.351 | 2 6 0⟩	0.194 | 3 4 1⟩
41	3832.90	1.38	0.871 | 11 2 0⟩	0.449 | 20 0 0⟩	0.130 | 8 4 0⟩	91	5385.60	1.94	0.870 | 13 4 0⟩	0.252 | 12 2 0⟩	0.208 | 11 0 1⟩	141	6204.44	1.65	0.917 | 14 0 1⟩	0.167 | 11 0 0⟩	0.129 | 11 0 2⟩
42	3964.05	0.38	0.981 | 21 0 0⟩	0.130 | 14 2 0⟩	0.111 | 14 0 1⟩	92	5390.46	2.01	0.885 | 10 0 1⟩	0.288 | 13 4 0⟩	0.168 | 14 2 0⟩	142	6209.48	0.71	0.958 | 47 0 0⟩	0.238 | 36 2 0⟩	0.106 | 21 0 1⟩
43	3972.44	1.42	0.926 | 4 0 1⟩	0.268 | 4 4 0⟩	0.137 | 10 2 0⟩	93	5407.39	3.08	0.604 | 5 6 0⟩	0.400 | 5 2 1⟩	0.335 | 4 2 1⟩	143	6224.80	2.48	0.797 | 11 6 0⟩	0.417 | 8 8 0⟩	0.227 | 8 2 1⟩
44	3991.73	1.40	0.877 | 12 2 0⟩	0.431 | 5 4 0⟩	0.110 | 13 0 0⟩	94	5411.09	1.51	0.908 | 23 2 0⟩	0.258 | 19 2 0⟩	0.155 | 10 2 1⟩	144	6250.32	2.32	0.752 | 27 2 0⟩	0.500 | 24 4 0⟩	0.351 | 40 0 0⟩
45	3994.89	2.13	0.835 | 4 4 0⟩	0.392 | 12 2 0⟩	0.300 | 4 0 1⟩	95	5437.61	0.53	0.971 | 35 0 0⟩	0.200 | 28 2 0⟩	0.084 | 28 0 1⟩	145	6254.00	2.44	0.757 | 22 4 0⟩	0.466 | 24 2 0⟩	0.333 | 44 0 0⟩
46	4095.23	0.33	0.984 | 22 0 0⟩	0.116 | 15 2 0⟩	0.115 | 15 0 1⟩	96	5471.15	2.86	0.579 | 3 2 1⟩	0.461 | 3 6 0⟩	0.389 | 4 6 1⟩	146	6260.11	1.45	0.865 | 48 0 0⟩	0.455 | 31 2 0⟩	0.169 | 24 4 0⟩
47	4145.57	0.64	0.966 | 13 2 0⟩	0.190 | 12 4 0⟩	0.105 | 12 2 1⟩	97	5509.33	2.16	0.778 | 24 2 0⟩	0.450 | 26 0 0⟩	0.391 | 15 2 0⟩	147	6288.87	2.27	0.842 | 3 0 2⟩	0.333 | 7 2 1⟩	0.247 | 3 2 1⟩
48	4171.04	1.08	0.942 | 5 4 0⟩	0.126 | 4 0 0⟩	0.126 | 4 2 0⟩	98	5512.51	2.03	0.837 | 14 4 0⟩	0.370 | 14 2 0⟩	0.287 | 34 0 0⟩	148	6304.85	0.82	0.945 | 49 0 0⟩	0.296 | 37 2 0⟩	0.081 | 21 4 0⟩
49	4221.99	0.33	0.984 | 23 0 0⟩	0.117 | 18 2 0⟩	0.116 | 18 0 1⟩	99	5518.45	1.57	0.837 | 36 0 0⟩	0.504 | 24 2 0⟩	0.163 | 17 4 0⟩	149	6317.74	3.79	0.647 | 6 8 0⟩	0.417 | 6 4 0⟩	0.224 | 2 4 1⟩
50	4228.98	0.91	0.956 | 5 0 1⟩	0.142 | 5 4 0⟩	0.108 | 5 2 0⟩	100	5580.24	2.26	0.846 | 6 6 0⟩	0.227 | 5 6 0⟩	0.179 | 3 2 1⟩	150	6318.78	1.52	0.889 | 34 2 0⟩	0.354 | 36 2 0⟩	0.226 | 37 0 0⟩

[a]Variational eigenstates of the TZ(1+)(3*d*,3*p*) CCSD surface for which there is no total or vibrational angular momentum ($\ell=0$). Energy levels (E_k) are tabulated in cm^{-1} relative to the ground vibrational state, which lies 2575.64 cm^{-1} above the minimum of the surface in the final calculations. As defined in the text, S_{mix} is the "entropy of mixing" for each eigenstate. In the lists of wave function components, the three largest configuration interaction coefficients are given in the basis of configuration state functions $|v_1v_2v_3\rangle$ comprised of natural modals for *each* coordinate determined for the *specific* eigenstate of concern. The quantum numbers for the natural modals are ambiguous in some cases. The current assignments were made by counting nodes between oscillations with local maxima at least 20% of the absolute maximum. Adjustments have been made for the leading configurations of roots 60 and 146 to clarify the progression placements.

TABLE XI. Vibrational states $[(J^P,\ell)=(1^+,1)]$ of nonrotating $[FHCl]^-$.[a]

k	E_k	S_{mix}	Wave function components			k	E_k	S_{mix}	Wave function components			k	E_k	S_{mix}	Wave function components		
1	876.16	0.03	0.999 | 0 1 0⟩	0.035 | 0 3 1⟩	0.026 | 1 1 1⟩	51	4959.39	0.66	0.964 | 14 3 0⟩	0.199 | 11 5 0⟩	0.106 | 11 3 1⟩	101	6172.78	1.83	0.887 | 11 1 1⟩	0.332 | 23 3 0⟩	0.150 | 6 1 2⟩
2	1113.02	0.05	0.998 | 1 1 0⟩	0.048 | 0 1 1⟩	0.035 | 1 3 1⟩	52	5002.11	0.39	0.981 | 24 1 0⟩	0.124 | 17 3 0⟩	0.114 | 17 1 1⟩	102	6201.52	1.99	0.862 | 25 3 0⟩	0.340 | 11 1 1⟩	0.201 | 23 5 0⟩
3	1343.61	0.07	0.997 | 2 1 0⟩	0.061 | 1 1 1⟩	0.034 | 2 3 1⟩	53	5065.91	0.95	0.947 | 6 5 0⟩	0.210 | 5 5 0⟩	0.159 | 6 3 1⟩	103	6210.29	1.47	0.897 | 15 5 0⟩	0.364 | 10 7 0⟩	0.103 | 15 3 1⟩
4	1567.92	0.09	0.997 | 3 1 0⟩	0.071 | 2 1 1⟩	0.034 | 3 3 1⟩	54	5071.48	0.87	0.952 | 15 3 0⟩	0.204 | 15 3 0⟩	0.104 | 15 3 1⟩	104	6218.15	0.60	0.966 | 37 1 0⟩	0.212 | 28 3 0⟩	0.086 | 24 1 1⟩
5	1785.99	0.10	0.996 | 4 1 0⟩	0.079 | 3 1 1⟩	0.034 | 4 3 1⟩	55	5110.45	0.42	0.978 | 25 1 0⟩	0.151 | 20 3 0⟩	0.105 | 20 1 1⟩	105	6227.90	2.91	0.752 | 1 1 2⟩	0.393 | 4 3 1⟩	0.286 | 1 3 1⟩
6	1997.82	0.12	0.995 | 5 1 0⟩	0.085 | 4 1 1⟩	0.033 | 5 3 1⟩	56	5158.17	0.84	0.960 | 6 1 1⟩	0.139 | 8 1 1⟩	0.121 | 6 3 1⟩	106	6260.16	3.65	0.547 | 4 3 1⟩	0.347 | 3 1 0⟩	0.296 | 4 7 1⟩
7	2203.49	0.13	0.994 | 6 1 0⟩	0.091 | 5 1 1⟩	0.034 | 5 3 0⟩	57	5170.64	0.92	0.946 | 7 5 0⟩	0.235 | 6 7 0⟩	0.156 | 7 3 1⟩	107	6275.85	1.10	0.927 | 26 3 0⟩	0.298 | 22 5 0⟩	0.163 | 33 1 0⟩
8	2403.04	0.14	0.994 | 7 1 0⟩	0.096 | 4 1 1⟩	0.039 | 4 3 0⟩	58	5197.87	1.63	0.828 | 0 7 0⟩	0.502 | 0 3 1⟩	0.145 | 0 1 2⟩	108	6295.91	0.61	0.965 | 38 1 0⟩	0.223 | 29 3 0⟩	0.090 | 21 1 1⟩
9	2476.56	0.22	0.989 | 0 3 0⟩	0.144 | 0 1 1⟩	0.026 | 1 3 1⟩	59	5208.48	1.74	0.737 | 18 3 0⟩	0.643 | 26 1 0⟩	0.142 | 13 5 0⟩	109	6298.12	2.80	0.744 | 7 7 0⟩	0.410 | 6 3 1⟩	0.278 | 7 3 1⟩
10	2596.55	0.16	0.993 | 8 1 0⟩	0.100 | 5 1 1⟩	0.043 | 5 3 0⟩	60	5270.61	1.69	0.749 | 24 1 0⟩	0.634 | 16 3 0⟩	0.125 | 13 5 0⟩	110	6316.02	1.32	0.901 | 16 5 0⟩	0.375 | 13 7 0⟩	0.098 | 16 3 1⟩
11	2693.48	0.25	0.988 | 1 3 0⟩	0.138 | 1 1 1⟩	0.049 | 0 3 1⟩	61	5302.69	1.21	0.930 | 8 5 0⟩	0.253 | 5 7 0⟩	0.147 | 7 1 1⟩	111	6325.30	0.99	0.931 | 0 9 0⟩	0.312 | 0 5 1⟩	0.134 | 1 11 0⟩
12	2784.12	0.17	0.992 | 9 1 0⟩	0.104 | 6 1 1⟩	0.048 | 6 3 0⟩	62	5319.31	2.78	0.575 | 0 3 1⟩	0.476 | 0 7 0⟩	0.382 | 0 7 1⟩	112	6357.03	1.70	0.889 | 27 3 0⟩	0.217 | 17 1 0⟩	0.199 | 14 1 1⟩
13	2903.83	0.27	0.987 | 2 3 0⟩	0.132 | 2 1 1⟩	0.062 | 1 3 1⟩	63	5347.08	0.51	0.972 | 27 1 0⟩	0.188 | 22 3 0⟩	0.089 | 22 1 1⟩	113	6365.50	1.51	0.916 | 12 1 1⟩	0.242 | 25 3 0⟩	0.127 | 15 1 2⟩
14	2965.83	0.18	0.992 | 10 1 0⟩	0.107 | 7 1 1⟩	0.052 | 7 3 0⟩	64	5366.91	2.29	0.802 | 17 3 0⟩	0.472 | 7 1 1⟩	0.162 | 10 5 0⟩	114	6369.94	0.66	0.961 | 39 1 0⟩	0.231 | 28 3 0⟩	0.103 | 20 1 1⟩
15	3107.60	0.30	0.986 | 3 3 0⟩	0.126 | 3 1 1⟩	0.072 | 2 5 0⟩	65	5370.99	2.27	0.809 | 7 1 1⟩	0.469 | 17 3 0⟩	0.154 | 8 5 0⟩	115	6370.93	2.59	0.791 | 8 7 0⟩	0.331 | 7 5 0⟩	0.205 | 5 3 1⟩
16	3141.79	0.19	0.991 | 11 1 0⟩	0.110 | 8 1 1⟩	0.057 | 8 3 0⟩	66	5436.65	1.96	0.854 | 1 7 0⟩	0.340 | 0 3 1⟩	0.249 | 1 3 1⟩	116	6372.66	1.38	0.890 | 17 5 0⟩	0.396 | 14 7 0⟩	0.103 | 13 3 0⟩
17	3304.80	0.33	0.984 | 4 3 0⟩	0.121 | 4 1 1⟩	0.086 | 3 5 0⟩	67	5446.29	0.40	0.979 | 28 1 0⟩	0.149 | 21 3 0⟩	0.105 | 21 1 1⟩	117	6412.69	1.09	0.927 | 28 3 0⟩	0.302 | 26 5 0⟩	0.155 | 35 1 0⟩
18	3312.13	0.21	0.990 | 12 1 0⟩	0.111 | 9 1 1⟩	0.065 | 9 3 0⟩	68	5459.86	1.05	0.934 | 9 5 0⟩	0.275 | 8 7 0⟩	0.141 | 9 3 1⟩	118	6419.74	3.30	0.723 | 5 3 1⟩	0.396 | 7 7 0⟩	0.246 | 3 1 2⟩
19	3476.85	0.32	0.985 | 13 1 0⟩	0.115 | 10 3 0⟩	0.097 | 10 1 1⟩	69	5517.26	0.82	0.952 | 18 3 0⟩	0.240 | 15 5 0⟩	0.105 | 15 3 1⟩	119	6438.94	0.58	0.967 | 40 1 0⟩	0.213 | 31 3 0⟩	0.089 | 23 1 1⟩
20	3495.61	0.44	0.978 | 5 3 0⟩	0.106 | 5 1 1⟩	0.091 | 5 5 0⟩	70	5546.19	0.39	0.980 | 29 1 0⟩	0.146 | 22 3 0⟩	0.106 | 22 1 1⟩	120	6439.81	1.77	0.878 | 1 9 0⟩	0.280 | 1 5 1⟩	0.201 | 0 11 0⟩
21	3636.23	0.31	0.985 | 0 1 1⟩	0.159 | 0 3 0⟩	0.041 | 1 1 0⟩	71	5551.23	2.64	0.560 | 2 3 1⟩	0.491 | 2 3 0⟩	0.368 | 1 3 1⟩	121	6462.15	1.48	0.882 | 18 5 0⟩	0.402 | 15 7 0⟩	0.139 | 26 3 0⟩
22	3679.94	0.24	0.989 | 14 1 0⟩	0.114 | 11 1 1⟩	0.075 | 11 3 0⟩	72	5568.28	1.20	0.938 | 8 1 1⟩	0.203 | 15 3 0⟩	0.121 | 8 1 2⟩	122	6464.92	1.34	0.912 | 29 3 0⟩	0.315 | 23 5 0⟩	0.161 | 28 1 0⟩
23	3790.32	0.39	0.981 | 6 3 0⟩	0.111 | 6 1 1⟩	0.110 | 5 3 0⟩	73	5586.41	1.35	0.921 | 19 3 0⟩	0.205 | 14 1 0⟩	0.198 | 8 1 1⟩	123	6468.77	3.03	0.750 | 2 1 2⟩	0.497 | 9 7 0⟩	0.221 | 2 3 1⟩
24	3818.79	0.24	0.989 | 15 1 0⟩	0.116 | 12 1 1⟩	0.077 | 12 3 0⟩	74	5597.84	1.16	0.925 | 10 5 0⟩	0.299 | 7 7 0⟩	0.137 | 10 3 1⟩	124	6504.98	3.68	0.642 | 9 7 0⟩	0.392 | 2 1 2⟩	0.275 | 8 1 2⟩
25	3858.01	0.46	0.978 | 7 3 0⟩	0.097 | 6 5 0⟩	0.093 | 6 3 1⟩	75	5633.78	2.67	0.670 | 2 7 0⟩	0.434 | 2 3 1⟩	0.369 | 1 3 1⟩	125	6516.48	1.04	0.947 | 13 1 1⟩	0.201 | 10 1 1⟩	0.094 | 25 3 1⟩
26	3939.25	1.10	0.935 | 1 1 1⟩	0.220 | 0 5 0⟩	0.217 | 1 5 0⟩	76	5657.18	0.44	0.977 | 30 1 0⟩	0.163 | 25 3 0⟩	0.099 | 25 1 1⟩	126	6526.28	0.64	0.964 | 41 1 0⟩	0.213 | 31 3 0⟩	0.109 | 20 1 1⟩
27	3946.28	1.14	0.925 | 0 5 0⟩	0.271 | 0 1 1⟩	0.195 | 1 1 1⟩	77	5689.23	1.16	0.921 | 20 3 0⟩	0.298 | 21 1 0⟩	0.181 | 20 1 0⟩	127	6549.49	1.70	0.857 | 30 3 0⟩	0.430 | 23 5 0⟩	0.184 | 24 1 0⟩
28	4029.84	0.25	0.988 | 16 1 0⟩	0.117 | 13 1 1⟩	0.081 | 13 3 0⟩	78	5711.22	0.77	0.950 | 31 1 0⟩	0.278 | 22 3 0⟩	0.099 | 18 1 1⟩	128	6553.55	2.25	0.801 | 19 5 0⟩	0.459 | 24 3 0⟩	0.258 | 18 3 0⟩
29	4083.14	0.44	0.978 | 8 3 0⟩	0.133 | 7 5 0⟩	0.098 | 8 1 1⟩	79	5715.90	2.23	0.846 | 3 7 0⟩	0.362 | 1 3 1⟩	0.190 | 2 5 0⟩	129	6559.90	2.17	0.841 | 2 9 0⟩	0.289 | 1 7 0⟩	0.184 | 2 7 1⟩
30	4094.09	0.26	0.987 | 17 1 0⟩	0.118 | 14 1 1⟩	0.086 | 14 3 0⟩	80	5759.62	1.20	0.921 | 11 5 0⟩	0.311 | 8 7 0⟩	0.126 | 11 3 1⟩	130	6569.26	2.91	0.723 | 10 7 0⟩	0.286 | 9 5 0⟩	0.247 | 9 3 0⟩
31	4141.73	1.68	0.867 | 1 5 0⟩	0.341 | 2 1 1⟩	0.282 | 1 1 1⟩	81	5791.35	1.10	0.946 | 9 1 1⟩	0.147 | 13 1 1⟩	0.112 | 16 3 1⟩	131	6587.69	0.61	0.965 | 42 1 0⟩	0.220 | 32 3 0⟩	0.092 | 25 1 1⟩
32	4195.67	1.65	0.874 | 2 1 1⟩	0.341 | 1 5 0⟩	0.262 | 2 5 0⟩	82	5794.66	1.03	0.924 | 32 1 0⟩	0.338 | 20 3 0⟩	0.128 | 15 1 1⟩	132	6602.87	3.48	0.547 | 23 3 0⟩	0.436 | 15 3 1⟩	0.309 | 10 7 0⟩
33	4222.15	0.50	0.975 | 9 3 0⟩	0.146 | 8 5 0⟩	0.099 | 8 3 1⟩	83	5802.09	2.79	0.745 | 2 3 1⟩	0.473 | 3 7 0⟩	0.235 | 2 1 2⟩	133	6606.46	3.10	0.688 | 29 3 0⟩	0.435 | 6 3 1⟩	0.231 | 7 3 0⟩
34	4317.92	0.28	0.987 | 18 1 0⟩	0.118 | 15 1 1⟩	0.093 | 15 3 0⟩	84	5836.62	1.65	0.879 | 21 3 0⟩	0.359 | 26 1 0⟩	0.195 | 22 5 0⟩	134	6628.93	1.74	0.867 | 20 5 0⟩	0.410 | 17 7 0⟩	0.110 | 21 3 0⟩
35	4354.18	0.90	0.952 | 2 5 0⟩	0.194 | 2 1 1⟩	0.149 | 1 1 1⟩	85	5858.53	1.13	0.922 | 12 5 0⟩	0.323 | 9 7 0⟩	0.122 | 12 3 1⟩	135	6632.11	2.58	0.833 | 14 1 1⟩	0.396 | 3 9 0⟩	0.136 | 5 7 0⟩
36	4357.33	0.60	0.969 | 10 3 0⟩	0.157 | 9 3 0⟩	0.099 | 9 3 1⟩	86	5870.51	0.53	0.971 | 33 1 0⟩	0.196 | 24 3 0⟩	0.085 | 24 1 1⟩	136	6643.64	3.28	0.717 | 3 9 0⟩	0.449 | 14 1 1⟩	0.313 | 2 7 0⟩
37	4369.26	0.33	0.983 | 19 1 0⟩	0.117 | 16 3 0⟩	0.111 | 16 1 1⟩	87	5870.75	2.12	0.850 | 4 7 0⟩	0.338 | 3 3 1⟩	0.184 | 4 3 1⟩	137	6656.88	0.74	0.954 | 43 1 0⟩	0.262 | 30 3 0⟩	0.095 | 26 1 1⟩
38	4485.63	0.81	0.961 | 3 1 1⟩	0.130 | 3 3 0⟩	0.118 | 2 3 0⟩	88	5941.64	0.99	0.938 | 22 3 0⟩	0.272 | 20 5 0⟩	0.139 | 29 1 0⟩	138	6664.50	2.29	0.814 | 11 7 0⟩	0.425 | 8 9 0⟩	0.218 | 4 3 1⟩
39	4501.31	0.75	0.961 | 3 5 0⟩	0.185 | 3 3 1⟩	0.135 | 2 7 0⟩	89	5951.98	1.18	0.908 | 0 1 2⟩	0.373 | 0 3 1⟩	0.111 | 3 3 1⟩	139	6678.56	1.33	0.908 | 32 3 0⟩	0.320 | 30 3 0⟩	0.204 | 35 1 0⟩
40	4509.69	1.24	0.882 | 20 1 0⟩	0.446 | 11 3 0⟩	0.101 | 11 1 1⟩	90	5954.89	0.46	0.976 | 34 1 0⟩	0.172 | 27 3 0⟩	0.094 | 27 1 1⟩	140	6681.06	1.51	0.877 | 21 5 0⟩	0.420 | 20 7 0⟩	0.110 | 24 3 0⟩
41	4610.61	1.39	0.870 | 11 3 0⟩	0.451 | 20 1 0⟩	0.129 | 8 5 0⟩	91	5971.72	2.27	0.832 | 13 5 0⟩	0.400 | 12 1 1⟩	0.277 | 10 7 0⟩	141	6686.73	2.14	0.854 | 3 1 2⟩	0.319 | 7 3 1⟩	0.249 | 3 3 1⟩
42	4620.50	0.38	0.981 | 21 1 0⟩	0.130 | 14 3 0⟩	0.111 | 14 1 1⟩	92	6005.92	2.39	0.843 | 10 1 1⟩	0.380 | 13 5 0⟩	0.182 | 15 3 0⟩	142	6708.95	1.18	0.903 | 44 1 0⟩	0.393 | 31 3 0⟩	0.098 | 18 5 0⟩
43	4658.18	1.42	0.926 | 4 1 1⟩	0.267 | 4 5 0⟩	0.138 | 10 3 0⟩	93	6011.32	3.06	0.606 | 5 7 0⟩	0.402 | 5 3 1⟩	0.335 | 4 3 1⟩	143	6718.69	3.27	0.727 | 4 9 0⟩	0.266 | 1 5 1⟩	0.231 | 1 5 0⟩
44	4676.94	1.38	0.882 | 12 3 0⟩	0.420 | 5 5 0⟩	0.110 | 13 1 0⟩	94	6043.91	1.42	0.915 | 23 3 0⟩	0.260 | 18 3 0⟩	0.139 | 10 3 1⟩	144	6733.56	1.72	0.858 | 33 3 0⟩	0.416 | 40 1 0⟩	0.229 | 30 5 0⟩
45	4731.13	2.10	0.841 | 4 5 0⟩	0.380 | 12 3 0⟩	0.299 | 4 1 1⟩	95	6060.99	0.46	0.976 | 35 1 0⟩	0.172 | 28 3 0⟩	0.094 | 28 1 1⟩	145	6739.35	3.43	0.702 | 12 7 0⟩	0.441 | 9 9 0⟩	0.229 | 6 3 1⟩
46	4800.77	0.33	0.984 | 22 1 0⟩	0.116 | 15 3 0⟩	0.115 | 15 1 1⟩	96	6067.08	2.86	0.579 | 3 3 1⟩	0.461 | 3 7 0⟩	0.389 | 4 7 1⟩	146	6754.29	1.54	0.873 | 22 5 0⟩	0.427 | 19 7 0⟩	0.114 | 19 3 0⟩
47	4838.50	0.64	0.966 | 13 3 0⟩	0.190 | 12 5 0⟩	0.105 | 12 3 1⟩	97	6077.84	2.00	0.754 | 20 3 0⟩	0.588 | 15 3 0⟩	0.187 | 11 7 0⟩	147	6755.36	3.14	0.613 | 0 5 1⟩	0.451 | 0 9 0⟩	0.350 | 0 3 2⟩
48	4847.32	1.08	0.942 | 5 5 0⟩	0.127 | 4 1 0⟩	0.125 | 4 3 0⟩	98	6129.58	2.14	0.738 | 15 5 0⟩	0.594 | 22 3 0⟩	0.217 | 12 7 0⟩	148	6780.26	3.52	0.692 | 7 3 1⟩	0.385 | 9 7 0⟩	0.213 | 7 7 0⟩
49	4873.67	0.33	0.984 | 23 1 0⟩	0.117 | 18 3 0⟩	0.116 | 18 1 1⟩	99	6131.04	0.49	0.973 | 36 1 0⟩	0.184 | 29 3 0⟩	0.088 | 29 1 1⟩	149	6785.52	1.54	0.916 | 15 1 1⟩	0.166 | 10 3 1⟩	0.158 | 10 1 1⟩
50	4938.32	0.91	0.956 | 5 1 1⟩	0.142 | 5 5 0⟩	0.108 | 5 3 0⟩	100	6141.87	2.25	0.846 | 6 7 0⟩	0.230 | 5 7 0⟩	0.182 | 3 3 1⟩	150	6788.24	1.91	0.693 | 32 3 0⟩	0.665 | 45 1 0⟩	0.191 | 25 5 0⟩

[a]Variational eigenstates of the TZ(1+)(3*d*,3*p*) CCSD surface with positive parity and one quantum of vibrational angular momentum ($\ell=1$) but no external rotation. See the footnote to Table X for pertinent information. Because the effects of rotational ℓ-type doubling are minuscule for $[FHCl]^-$, the energy levels of odd-parity states are not given in the table.

TABLE XII. Selected vibrational levels (cm^{-1}) of nonrotating $[FDCl]^-$.[a]

$(v_1\ v_2^{\ell}\ v_3)$	$n=$ 0	1	2	3
$(n\ 0^0\ 0)$	0.0	241.7	477.7	707.9
$(n\ 1^1\ 0)$	628.7	863.5	1092.3	1315.2
$(n\ 2^0\ 0)$	1220.6	1448.7	1670.8	1886.9
$(n\ 3^1\ 0)$	1810.5	2031.6	2246.5	2455.4
$(n\ 4^0\ 0)$	2367.3	2581.6	2789.8	2992.2
$(n\ 0^0\ 1)$	2173.5	2436.8	2694.6	2944.3
$(n\ 1^1\ 1)$	2834.8	3088.7	–	–

[a]Relative to the ground vibrational state, which lies 1905.49 cm^{-1} above the minimum of the surface.

separation is 279.3 cm^{-1}, whereas the spacing progression derived from the anharmonic constants of Table V is $\delta(v_1)=\nu_1+\chi_{31}+2(v_1-1)\chi_{11}=268.8-5.78\ v_1\ cm^{-1}$. Therefore, the quartic force field of $[FHCl]^-$ qualitatively explains the shift of the $|v_1\ 0\ 1\rangle$ spacing progression upward from the analogous $|v_1\ 0\ 0\rangle$ curve but fails to quantitatively predict the position of the first member of the series. Nevertheless, while variations within the progression are substantial, several points ($v_1=8$, 10, 11, 13, and 14) lie within 3 cm^{-1} of the idealized linear form. In general, the $S_{\mathrm{mix},n}$ values in the $|v_1\ 0\ 1\rangle$ series are much larger

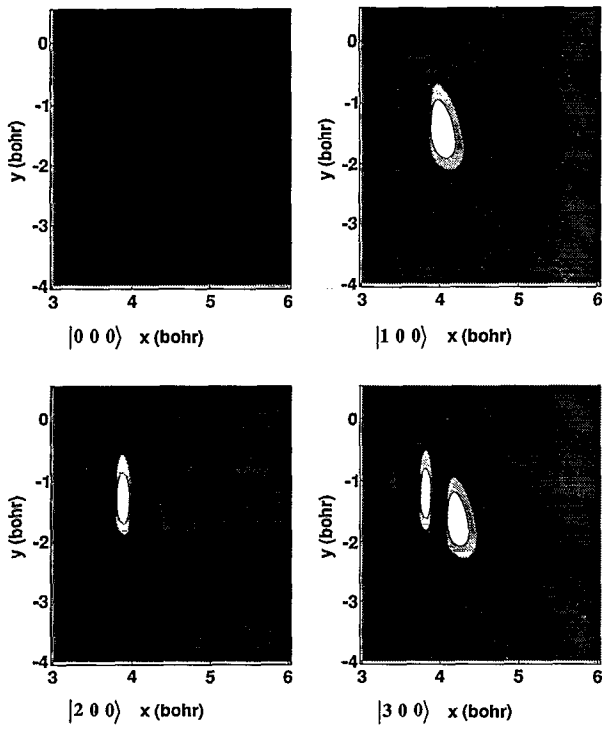

FIG. 9. Contour plots in the stretching space for ($J=0$) vibrational wave functions of $[FHCl]^-$ within the progression $|v_1\ v_2\ v_3\rangle=|0\ 0\ 0\rangle$, $|1\ 0\ 0\rangle$, $|2\ 0\ 0\rangle$, and $|3\ 0\ 0\rangle$. The plots depict the functional dependence on the symmetric (x) and antisymmetric (y) stretching coordinates (in bohr) under the constraint of linearity. Contour lines are shown for the following values (in atomic units) of the normalized wave functions: 0.45, 0.10, −0.10, and −0.45. Positive and negative regions are illustrated using successively lighter and darker shading, respectively, superimposed on an intermediate gray background.

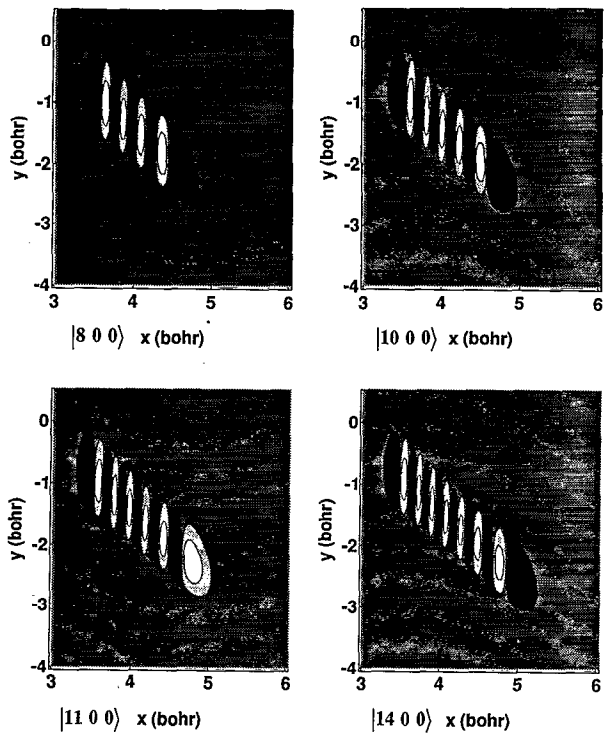

FIG. 10. Contour plots in the stretching space for ($J=0$) vibrational wave functions of $[FHCl]^-$ within the progression $|v_1\ v_2\ v_3\rangle=|8\ 0\ 0\rangle$, $|10\ 0\ 0\rangle$, $|11\ 0\ 0\rangle$, and $|14\ 0\ 0\rangle$. See the caption to Fig. 9 for details.

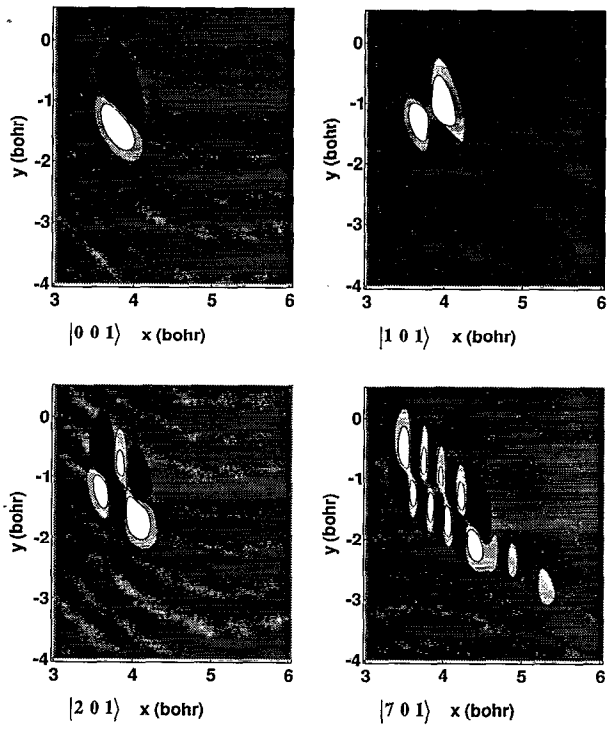

FIG. 11. Contour plots in the stretching space for ($J=0$) vibrational wave functions of $[FHCl]^-$ within the progression $|v_1\ v_2\ v_3\rangle=|0\ 0\ 1\rangle$, $|1\ 0\ 1\rangle$, $|2\ 0\ 1\rangle$, and $|7\ 0\ 1\rangle$. See the caption to Fig. 9 for details.

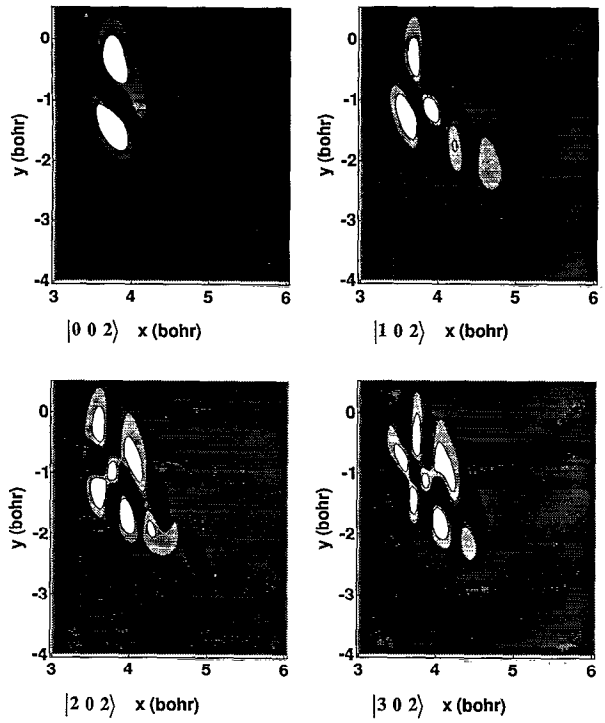

FIG. 12. Contour plots in the stretching space for (J=0) vibrational wave functions of $[FHCl]^-$ within the progression $|v_1\ v_2\ v_3\rangle = |0\ 0\ 2\rangle$, $|1\ 0\ 2\rangle$, $|2\ 0\ 2\rangle$, and $|3\ 0\ 2\rangle$. See the caption to Fig. 9 for details.

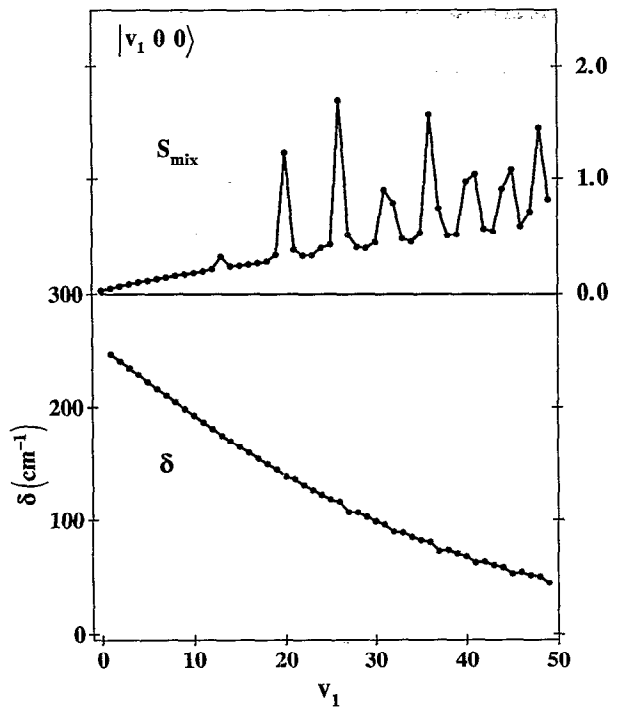

FIG. 13. Spacings between adjacent energy levels (δ) and the "entropy of mixing" within eigenstates (S_{mix}) in the $|v_1\ 0\ 0\rangle$ progression of $[FHCl]^-$.

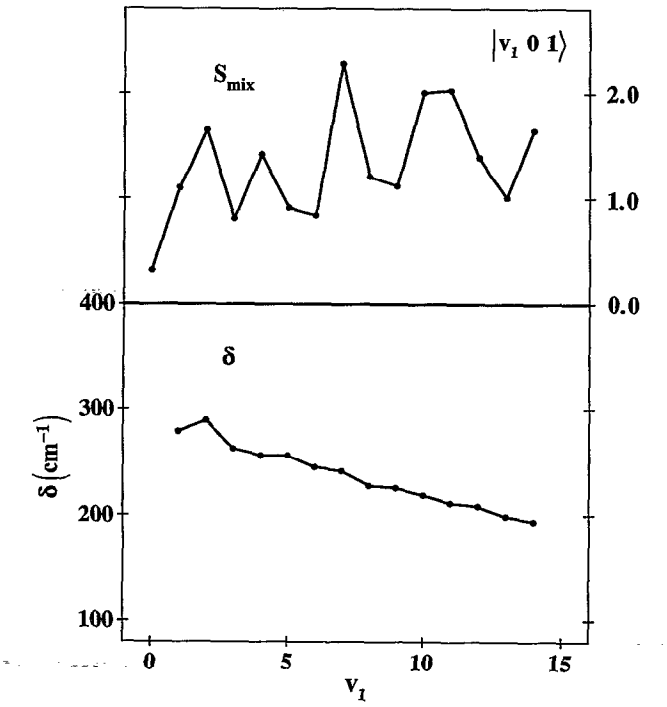

FIG. 14. Spacings between adjacent energy levels (δ) and the "entropy of mixing" within eigenstates (S_{mix}) in the $|v_1\ 0\ 1\rangle$ progression of $[FHCl]^-$.

and more erratic than their $|v_1\ 0\ 0\rangle$ counterparts. The $|1\ 0\ 1\rangle$ and $|2\ 0\ 1\rangle$ eigenstates have sizeable components from configurations of $|v_1'\ 4\ 0\rangle$ type, and the $|7\ 0\ 1\rangle$ state forms a resonant pair with $|17\ 2\ 0\rangle$ at (4707.2, 4716.6) cm^{-1}. In brief, the breakdown of the adiabatic approximation in these cases is quite severe.

C. Density of vibrational states

In statistical theories of chemical reaction rates, a central role is assumed by the density of vibrational states, $\rho(E,J)$, of molecular complexes. However, the accurate *a priori* determination of $\rho(E,J)$ and its integral $W(E,J)$, the total number of accessible states, is a formidable challenge at high energies. In Stark-level crossing experiments on D_2CO at 28 370 cm^{-1}, Polik *et al.*[193] observed more than 1200 resonances within a 0.2 cm^{-1} range between highly excited S_0 vibronic states and J=1, 2, 3, and 4 levels in the $4^1\ S_1$ manifold. The density of vibrational states of all symmetries on the S_0 surface was found to be 440±110 states per cm^{-1}, a number six times greater than that given by a direct-count algorithm incorporating first-order anharmonic terms. In stimulated emission pumping (SEP) spectra of HFCO in the 16 000 cm^{-1} region, Choi and Moore[191] observed roughly 10 a'' vibrational states per cm^{-1}, whereas a direct count of a'' levels using a complete set of anharmonic constants predicted about 2.6 states per cm^{-1}. These discrepancies and others[194,195] led Choi and Moore to conclude that "a better method to calculate the density of states of highly excited molecules has to be developed." In approaching this issue, systematic compari-

sons are needed between the number of highly excited vibrational states obtained by converged variational procedures and conventional extrapolations based on harmonic and anharmonic molecular force fields. A brief comparison of state counts by various procedures in the case of $[FHCl]^-$ is thus warranted.

In Fig. 15 the number of accessible states of $[FHCl]^-$ without angular momentum, $W(E,J=0)$, is shown as a function of *total* vibrational energy for three direct-count methods. Method A utilizes the rigorous variational results directly, B assumes the anharmonic expression

$$E(v_1,v_2^{\ell},v_3)=\sum_i \omega_i\left(v_i+\frac{d_i}{2}\right)+\sum_{i>j}\chi_{ij}\left(v_i+\frac{d_i}{2}\right)\times\left(v_j+\frac{d_j}{2}\right)+\chi_{\ell_2\ell_2}\ell^2, \tag{53}$$

with spectroscopic constants from Table V, and C involves only the harmonic terms in Eq. (53). At 7500 cm^{-1} the variational and anharmonic state counts (71) are identical, but the harmonic estimate (46) reveals that this approximation has already deteriorated significantly. Near 8000 cm^{-1} the anharmonic procedure becomes invalid because the negative, diagonal anharmonic contribution for the chloride stretching mode overtakes the harmonic term at $v_1=43$ and causes a turnover in the energy-level pattern. Consequently, curve B in Fig. 15 is truncated shortly after it departs from curve A, and corresponding state counts at higher energies cannot be made unless an extrapolation of lower-energy results is invoked.

The variational data for $W(E,J=0)$ clearly exhibit an exponential dependence and are closely fit by the function $W_{\rm var}[E(cm^{-1}),J=0]=1.110\,18\,e^{E/1807.8}$ above 5000 cm^{-1}. In contrast, the harmonic data in the 5000–9000 cm^{-1} region are not described well by an exponential function but can be reproduced by the quadratic form $W_{\rm harm}[E(cm^{-1}),J=0]=[(E-2588.8)/713.63]^2$. Upon differentiation these functions yield the following expressions for the density of states: $\rho_{\rm var}[E(cm^{-1}),J=0]=6.141\times10^{-4}\,e^{E/1807.8}$ and $\rho_{\rm harm}[E(cm^{-1}),J=0]=3.927\times10^{-6}E$. Therefore, at $E=10\,000$ cm^{-1}, for example, the harmonic approximation already underestimates the variational density of states by a factor of 3.9. The $W(E,J)$ data for $J=1$ are very similar to the results for $J=0$ and thus are not explicitly given here. Above 5000 cm^{-1} the variational results for $(J,\ell)=(1^{\pm1},1)$ are well fit by the functions $W_{\rm var}[E(cm^{-1}),J=1]=0.3962\,e^{E/1573.4}$ and $\rho_{\rm var}[E(cm^{-1}),J=1]=2.518\times10^{-4}\,e^{E/1573.4}$. All of the expressions provided here for the variational state counts should be useful in unimolecular dissociation studies of the $[FHCl]^-$ complex.

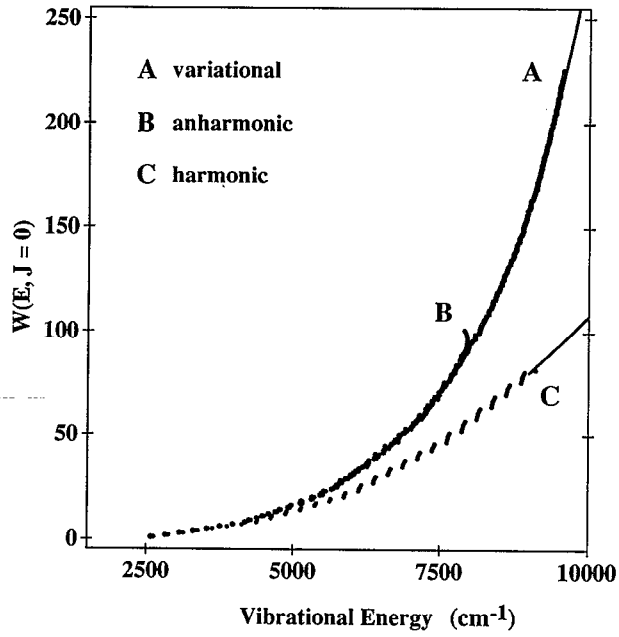

FIG. 15. The number of accessible $J=0$ states of $[FHCl]^-$ vs total vibrational energy as computed by direct counting on the spectrum of energy levels from the variational (A), anharmonic (B), and harmonic (C) procedures. Curves A and B are virtually indistinguishable until a turnover is encountered in the chloride stretching levels of the anharmonic expression near 8000 cm^{-1}. Extrapolations above 9000 cm^{-1} are also shown based on the equations presented in the text.

D. Signatures of quantum ergodicity

The development of stimulated emission pumping (SEP) techniques over the past decade has made possible eigenstate-resolved studies of highly excited vibrational states which were previously inaccessible through conventional spectroscopic methods. The detailed vibrational structure provided by SEP spectroscopy has prompted searches for signatures of quantum ergodicity in the highly excited vibrational states of small molecules, as exemplified by the experiments of Abramson *et al.*[194,195] in which curious clumps spanning about 1.5 cm^{-1} and consisting of 50–75 vibrational levels each were observed at intervals of roughly 10 cm^{-1} in the SEP spectra of acetylene near 27 900 cm^{-1}. Among various tests for ergodicity in quantum dynamics is the distribution of nearest-neighbor level spacings. In classical systems exhibiting chaotic behavior, extensive mixing occurs among all nuclear degrees of freedom, and the available phase space is fully sampled. In such cases the quantum mechanical eigenspectrum displays repulsions among energy levels and a uniform pattern of spacings in which accidental degeneracies are of vanishingly small probability. In ergodic systems the spacing distribution, $P(s)$, is anticipated to be of the idealized form first suggested by Wigner[201]

$$P_w(s)=\left(\frac{\pi s}{2\bar{s}^2}\right)\exp\left(-\frac{\pi s^2}{4\bar{s}^2}\right), \tag{54}$$

where $\bar{s}$ is the average level spacing in the spectrum. In contrast, if the classical dynamics of a system is dominated by quasiperiodic trajectories which are stable against intramolecular vibrational energy redistribution (IVR), a random distribution of quantum mechanical levels occurs which gives rise to a Poisson distribution of energy spacings, viz.,[194,195]

$$P_p(s)=\left(\frac{1}{\bar{s}}\right)\exp\left(-\frac{s}{\bar{s}}\right). \tag{55}$$

Recently Choi and Light[190] have computed highly excited vibrational eigenstates of H_2O for two different analytic forms of the ground-state potential energy surface with the aid of DVR techniques. Dissimilarities in the spacing distributions for the two surfaces were apparent with the peculiar result that a Wigner-type profile was found in one case and a Poisson-type profile in the other. Here a preliminary analysis of the spacing distribution of excited vibrational states of $[FHCl]^-$ is reported, thus adding another molecule to the set of test results for quantum ergodicity.

The highly excited vibrational eigenstates of $[FHCl]^-$ were analyzed by computing the magnitude of each state separation relative to the local average spacing for $2L+1$ encompassing intervals, i.e., a data set $\{t_n\}$ for the relative spacing distribution was constructed using the relation[190]

$$t_n\equiv\left(\frac{s}{\bar{s}}\right)_n=(2L+1)\left(\frac{E_{n+1}-E_n}{E_{n+L+1}-E_{n-L}}\right). \tag{56}$$

The range of total vibrational energy in the analysis started at 5000 cm^{-1} and extended beyond the highest levels reported in Tables X and XI to the limit of well-converged eigenvalues near 9500 cm^{-1}. Specifically, for $J=0$ the spacings between all roots in the range $17\leqslant n\leqslant 224-L$ were included in the statistics. By sorting the N values within the $\{t_n\}$ set according to size, a lexically-ordered collection of points $\{(t_k,f(t_k)=k/N),k=1,2,...,N\}$ was obtained which samples the integrated probability distribution function

$$f(t)=\int_0^t P(t')dt'. \tag{57}$$

In Fig. 16 a plot of the observed $J=0$ data for $f(t)$ is shown, as extracted from the vibrational eigenspectrum using a local averaging parameter of $L=8$. These statistical data were found to be remarkably invariant to L, at least for values between 5 and 12. Moreover, the distribution for $J=1$ levels cannot be distinguished from that in Fig. 16 without close inspection and thus is not displayed here.

The observed integrated probability distribution points are nicely enveloped by the analytic Wigner and Poisson forms, $f_w(t)=1-e^{-\pi t^2/4}$ and $f_p(t)=1-e^{-t}$, respectively. However, the points exhibit a decay profile for $t\to 0$ and an asymptotic tail for $t\to\infty$ which are more closely described by the Poisson distribution. In fact, if the fractional Poisson character is employed as an adjustable parameter in a least-squares fit of the observed distribution, the function $f_{obs}(t)=0.672\ f_p(t)+0.328\ f_w(t)$ is obtained, which is seen to provide an excellent fit to the data in Fig. 16. Differentiation of this expression for $f_{obs}(t)$ gives the probability distribution function $P_{obs}(t)$, which is also plotted in Fig. 16 alongside the idealized Poisson profile $P_p(t)$. The principal Poisson character of the observed level spacing of $[FHCl]^-$ presumably arises from a preponderance of eigenstates with regular nodal patterns, such as those depicted in Figs. 9–12. This conclusion is supported by the fact that most of the leading configuration interaction coefficients for the eigenstates listed in Tables X and XI are larger than 0.80. Nevertheless, the same list of wave function components reveals that intermingled among these classically quasiperiodic levels are eigenstates which exhibit strong resonances and add a significant ergodic component to the spacing distribution.

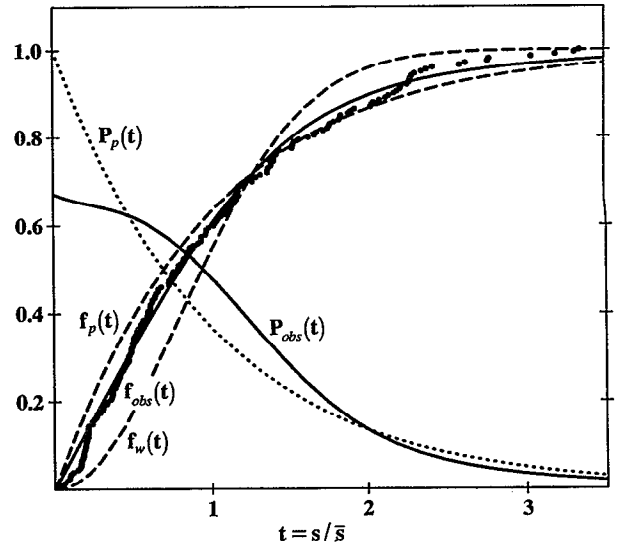

FIG. 16. Probability distribution curves $P(t)$ and integrated probability functions $f(t)$ for level spacings among $J=0$ states of $[FHCl]^-$ with total vibrational energies between 5000 and 9500 cm^{-1}. Solid lines indicate observed (*obs*) data, while dashed or dotted lines illustrate idealized Poisson (p) or Wigner (w) distributions.

VI. SYNOPSIS

In Sec. I an apologia is given for detailed studies of the $[FHCl]^-$ anion in view of its relevance to transition state spectroscopy experiments and the unique vibrational dynamics of hydrogen bihalide systems. These considerations have prompted the report here of three connected studies of $[FHCl]^-$ performed with the *ab initio* electronic structure methods summarized in Sec. II. In the first study (Sec. III) chemical and physical aspects of the $[FHCl]^-$ complex were definitively characterized, including central thermochemical and spectroscopic issues as well as the nature of the bonding in the complex. After careful calibrations of *ab initio* methods, a flexible global surface for $[FHCl]^-$ was constructed (Sec. IV) which exhibits the necessary asymptotic properties for the study of vibrational dynamics at high energies. Subsequently, a rigorous variational determination of several hundred of the lowest $J=0$ and $J=1$ eigenstates of $[FHCl]^-$ was performed (Sec. V) followed by an analysis of vibrational adiabaticity, anharmonic resonances, densities of high-lying states, and signatures of quantum ergodicity. In several respects the collective scope and rigor of the studies reported here is unprecedented for polyatomic molecular anions.

[1] D. M. Neumark, Annu. Rev. Phys. Chem. **43**, 153 (1992).
[2] R. B. Metz, S. E. Bradforth, and D. M. Neumark, Adv. Chem. Phys. **81**, 1 (1992).
[3] P. R. Brooks, Chem. Rev. **88**, 407 (1988).
[4] A. H. Zewail, Science **242**, 1645 (1988).
[5] M. Gruebele and A. H. Zewail, Phys. Today **43**(5), 24 (1990).
[6] G. C. Schatz, Annu. Rev. Phys. Chem. **39**, 317 (1988).
[7] D. G. Truhlar and A. Kuppermann, J. Chem. Phys. **52**, 3841 (1970).
[8] R. D. Levine and S. Wu, Chem. Phys. Lett. **11**, 557 (1971).
[9] G. C. Schatz and A. Kuppermann, Phys. Rev. Lett. **35**, 1266 (1975).
[10] J.-C. Nieh and J. J. Valentini, Phys. Rev. Lett. **60**, 519 (1988).
[11] J.-C. Nieh and J. J. Valentini, J. Chem. Phys. **92**, 1083 (1990).
[12] F. Webster and J. C. Light, J. Chem. Phys. **85**, 4744 (1986).
[13] W. H. Miller, Annu. Rev. Phys. Chem. **41**, 245 (1990).
[14] J. J. Valentini, Faraday Discuss. Chem. Soc. **91**, 392 (1991).
[15] T. Seideman and M. Shapiro, J. Chem. Phys. **88**, 5525 (1988).
[16] T. Seideman, J. L. Krause, and M. Shapiro, Faraday Discuss. Chem. Soc. **91**, 271 (1991).
[17] D. A. V. Kliner, D. E. Adelman, and R. N. Zare, J. Chem. Phys. **94**, 1069 (1991).
[18] D. E. Manolopoulos and R. E. Wyatt, Chem. Phys. Lett. **159**, 123 (1989).
[19] M. D'Mello, D. E. Manolopoulos, and R. E. Wyatt, J. Chem. Phys. **94**, 5985 (1991).
[20] J. M. Launay and M. LeDourneuf, Chem. Phys. Lett. **163**, 178 (1989).
[21] M. Zhao, D. G. Truhlar, D. W. Schwenke, and D. J. Kouri, J. Phys. Chem. **94**, 7074 (1990).
[22] M. Mladenovic, M. Zhao, D. G. Truhlar, D. W. Schwenke, Y. Sun, and D. J. Kouri, Chem. Phys. Lett. **146**, 358 (1988).
[23] M. Mladenovic, M. Zhao, D. G. Truhlar, D. W. Schwenke, Y. Sun, and D. J. Kouri, J. Phys. Chem. **92**, 7035 (1988).
[24] J. Z. H. Zhang and W. H. Miller, Chem. Phys. Lett. **153**, 465 (1988).
[25] J. Z. H. Zhang and W. H. Miller, J. Chem. Phys. **91**, 1528 (1989).
[26] J. Z. H. Zhang and W. H. Miller, Chem. Phys. Lett. **159**, 130 (1989).
[27] M. J. Redmon and R. E. Wyatt, Chem. Phys. Lett. **63**, 209 (1979).
[28] G. C. Schatz, J. M. Bowman, and A. Kuppermann, J. Chem. Phys. **63**, 674 (1975).
[29] S. L. Latham, J. F. McNutt, R. E. Wyatt, and M. J. Redmon, J. Chem. Phys. **69**, 3746 (1978).
[30] J. N. L. Connor, W. Jakubetz, and J. Manz, Mol. Phys. **35**, 1301 (1978).
[31] J. M. Launay and M. L. Dourneuf, J. Phys. B **15**, L455 (1982).
[32] D. M. Neumark, A. M. Wodtke, G. N. Robinson, C. C. Hayden, and Y. T. Lee, J. Chem. Phys. **82**, 3045 (1985).
[33] D. M. Neumark, A. M. Wodtke, G. N. Robinson, C. C. Hayden, K. Shobatake, R. K. Sparks, T. P. Schaefer, and Y. T. Lee, J. Chem. Phys. **82**, 3067 (1985).
[34] J. D. Kress, Z. Bačić, G. A. Parker, and R. T Pack, Chem. Phys. Lett. **157**, 484 (1989).
[35] Z. Bačić, J. D. Kress, G. A. Parker, and R. T Pack, J. Chem. Phys. **92**, 2344 (1990).
[36] C. Yu, D. J. Kouri, M. Zhao, and D. G. Truhlar, Chem. Phys. Lett. **157**, 491 (1989).
[37] C. Yu, D. J. Kouri, M. Zhao, D. G. Truhlar, and D. W. Schwenke, Int. J. Quantum Chem. Symp. **23**, 45 (1989).
[38] J. Z. H. Zhang and W. H. Miller, J. Chem. Phys. **92**, 1811 (1990).
[39] D. E. Manolopoulos, M. D'Mello, and R. E. Wyatt, J. Chem. Phys. **93**, 403 (1990).
[40] M. D'Mello, D. E. Manolopoulos, and R. E. Wyatt, Chem. Phys. Lett. **168**, 113 (1990).
[41] D. E. Manolopoulos, M. D'Mello, R. E. Wyatt, and R. B. Walker, Chem. Phys. Lett. **169**, 482 (1990).
[42] J. M. Launay and M. LeDourneuf, Chem. Phys. Lett. **169**, 473 (1990).
[43] D. Neuhauser, R. S. Judson, R. L. Jaffe, M. Baer, and D. J. Kouri, Chem. Phys. Lett. **176**, 546 (1991).
[44] J. M. Launay, Theor. Chim. Acta **79**, 183 (1991).
[45] R. B. Metz, T. Kitsopoulos, A. Weaver, and D. M. Neumark, J. Chem. Phys. **88**, 1463 (1988).
[46] A. Weaver, R. B. Metz, S. E. Bradforth, and D. M. Neumark, J. Phys. Chem. **92**, 5558 (1988).
[47] I. M. Waller, T. N. Kitsopoulos, and D. M. Neumark, J. Phys. Chem. **94**, 2240 (1990).
[48] S. E. Bradforth, A. Weaver, D. W. Arnold, R. B. Metz, and D. M. Neumark, J. Chem. Phys. **92**, 7205 (1990).
[49] R. B. Metz, A. Weaver, S. E. Bradforth, T. N. Kitsopoulos, and D. M. Neumark, J. Phys. Chem. **94**, 1377 (1990).
[50] C. M. Ellison and B. S. Ault, J. Phys. Chem. **83**, 832 (1979).
[51] Matrix-isolation studies place the symmetric stretching fundamental of $[IHI]^-$ near 130 cm^{-1} (see Table I).
[52] G. C. Schatz, J. Chem. Phys. **90**, 3582 (1989).
[53] G. C. Schatz, J. Chem. Phys. **90**, 4847 (1989).
[54] G. C. Schatz, J. Chem. Soc. Faraday Trans. **86**, 1729 (1990).
[55] G. C. Schatz, J. Phys. Chem. **94**, 6157 (1990).
[56] G. C. Schatz, S. Florance, T. J. Lee, and C. W. Bauschlicher, Jr., Chem. Phys. Lett. **202**, 495 (1993). See also R. C. Mayrhofer and J. M. Bowman, J. Chem. Phys. (submitted for publication).
[57] B. Gazdy and J. M. Bowman, J. Chem. Phys. **91**, 4615 (1989).
[58] E. J. Heller, J. Chem. Phys. **68**, 3891 (1978).
[59] R. Kosloff, J. Phys. Chem. **92**, 2087 (1988).
[60] R. H. Bisseling, R. Kosloff, and J. Manz, J. Chem. Phys. **83**, 993 (1985).
[61] R. H. Bisseling, P. L. Gertitschke, R. Kosloff, and J. Manz, J. Chem. Phys. **88**, 6191 (1988).
[62] A. J. Lorquet, J. C. Lorquet, J. Delwiche, and M. J. Hubin-Franskin, J. Chem. Phys. **76**, 4692 (1982).
[63] O. Hahn, J. M. G. Llorente, and H. S. Taylor, J. Chem. Phys. **94**, 2608 (1991).
[64] O. Hahn and H. S. Taylor, J. Chem. Phys. **96**, 5915 (1992).
[65] C. L. Janssen, W. D. Allen, H. F. Schaefer III, and J. M. Bowman, Chem. Phys. Lett. **131**, 352 (1986).
[66] V. Špirko, G. H. F. Diercksen, A. J. Sadlej, and M. Urban, Chem. Phys. Lett. **161**, 519 (1989).
[67] V. Špirko, A. Čejchan, and G. H. F. Diercksen, Chem. Phys. **151**, 45 (1991).
[68] P. Botschwina, P. Sebald, and R. Burmeister, J. Chem. Phys. **88**, 5246 (1988).
[69] S. Ikuta, T. Saitoh, and O. Nomura, J. Chem. Phys. **91**, 3539 (1989).
[70] J. C. Weisshaar, T. S. Zwier, and S. R. Leone, J. Chem. Phys. **75**, 4873 (1981).
[71] T. S. Zwier, V. M. Bierbaum, G. B. Ellison, and S. R. Leone, J. Chem. Phys. **72**, 5426 (1980).
[72] J. Emsley, Chem. Soc. Rev. **9**, 91 (1980).
[73] B. S. Ault, Acc. Chem. Res. **15**, 103 (1982).
[74] L. Andrews, Annu. Rev. Phys. Chem. **30**, 79 (1979).
[75] J. W. Larson and T. B. McMahon, J. Am. Chem. Soc. **105**, 2944 (1983).
[76] J. W. Larson and T. B. McMahon, Inorg. Chem. **23**, 2029 (1984).
[77] J. W. Larson and T. B. McMahon, J. Am. Chem. Soc. **106**, 517 (1984).
[78] J. W. Larson and T. B. McMahon, Can. J. Chem. **62**, 675 (1984).
[79] G. Caldwell and P. Kebarle, Can. J. Chem. **63**, 1399 (1985).
[80] J. C. Evans and G. Y.-S. Lo, J. Phys. Chem. **71**, 3942 (1967).
[81] J. C. Evans and G. Y.-S. Lo, J. Phys. Chem. **70**, 543 (1966).
[82] J. C. Evans and G. Y.-S. Lo, J. Phys. Chem. **70**, 11 (1966).
[83] J. C. Evans and G. Y.-S. Lo, J. Phys. Chem. **70**, 20 (1966).
[84] J. C. Evans and G. Y.-S. Lo, J. Phys. Chem. **73**, 448 (1969).
[85] B. S. Ault, J. Phys. Chem. **83**, 837 (1979).
[86] B. S. Ault and L. Andrews, J. Chem. Phys. **64**, 1986 (1976).
[87] B. S. Ault and L. Andrews, J. Chem. Phys. **63**, 2466 (1975).
[88] C. M. Ellison and B. S. Ault, J. Phys. Chem. **83**, 832 (1979).
[89] K. Kawaguchi and E. Hirota, J. Chem. Phys. **84**, 2953 (1986).
[90] K. Kawaguchi and E. Hirota, J. Chem. Phys. **87**, 6838 (1987).
[91] K. Kawaguchi, J. Chem. Phys. **88**, 4186 (1988).
[92] R. D. Hunt and L. Andrews, J. Chem. Phys. **87**, 6819 (1987).
[93] J. W. Nibler and G. C. Pimentel, J. Chem. Phys. **47**, 710 (1967).
[94] L. W. Schroeder and J. A. Ibers, Inorg. Chem. **7**, 594 (1968).
[95] V. Bondybey, G. C. Pimentel, and P. N. Noble, J. Chem. Phys. **55**, 540 (1971).
[96] D. E. Milligan and M. E. Jacox, J. Chem. Phys. **55**, 2550 (1971).
[97] M. J. Frisch, J. E. Del Bene, J. S. Binkley, and H. F. Schaefer III, J. Chem. Phys. **84**, 2279 (1986).
[98] P. Botschwina, in *Structure/Reactivity and Thermochemistry of Ions*, edited by P. Ausloos and S. G. Lias (Reidel, Dordrecht, 1987), p. 261.
[99] A. B. Sannigrahi and S. D. Peyerimhoff, J. Mol. Struct. THEOCHEM **122**, 127 (1985).
[100] P. Botschwina, in *Fundamental Gas-Phase Ion Chemistry*, NATO ASI Ser. C **347**, 231 (1991).
[101] S. Ikuta, T. Saitoh, and O. Nomura, J. Chem. Phys. **93**, 2530 (1990).

[102] A. B. Sannigrahi and S. D. Peyerimhoff, J. Mol. Struct. THEOCHEM **165**, 55 (1988).
[103] A. B. Sannigrahi and S. D. Peyerimhoff, Chem. Phys. Lett. **112**, 267 (1984).
[104] A. B. Sannigrahi and S. D. Peyerimhoff, Chem. Phys. Lett. **164**, 348 (1989).
[105] A. B. Sannigrahi and S. D. Peyerimhoff, J. Mol. Struct. THEOCHEM **209**, 15 (1990).
[106] A. B. Sannigrahi and M. Peric, J. Mol. Struct. THEOCHEM **209**, 9 (1990).
[107] V. C. Epa, J. H. Choi, M. Klobukowski, and W. R. Thorson, J. Chem. Phys. **92**, 466 (1990).
[108] V. C. Epa and W. R. Thorson, J. Chem. Phys. **92**, 473 (1990); **93**, 3773 (1990).
[109] K. Yamashita and K. Morokuma, in *Institute for Molecular Science Annual Review* (Okazaki, Japan, 1987), p. 15.
[110] W. D. Allen and A. G. Császár, J. Chem. Phys. **98**, 2983 (1993).
[111] H. Hotop and W. C. Lineberger, J. Phys. Chem. Ref. Data **4**, 539 (1975).
[112] S. Bourcier, *Spectroscopic Data Relative to Diatomic Molecules*, Tables of Constants and Numerical Data, Vol. 17 (Pergamon, New York, 1970).
[113] S. Huzinaga, J. Chem. Phys. **42**, 1293 (1965).
[114] T. H. Dunning, Jr., J. Chem. Phys. **55**, 716 (1971).
[115] A. D. McLean and G. S. Chandler, J. Chem. Phys. **72**, 5639 (1980).
[116] T. H. Dunning, Jr., J. Chem. Phys. **90**, 1007 (1989).
[117] R. Ahlrichs and P. R. Taylor, J. Chim. Phys. **78**, 315 (1981).
[118] M. J. Frisch, J. A. Pople, and J. S. Binkley, J. Chem. Phys. **80**, 3265 (1984).
[119] Gaussian exponents of nHF(+)(*extpol*) basis set: **F** $\{\alpha_s$: 1277672, 191300.7, 43534.31, 12331.35, 4023.248, 1452.587, 566.6280, 235.0575, 102.5020, 46.53321, 21.82785, 10.51179, 5.093690, 2.176174, 0.989967, 0.440127, 0.191072, 0.082950$\}$; $\{\alpha_p$: 1687.718, 399.6517, 129.8267, 49.57826, 20.86193, 9.365564, 4.409977, 2.128376, 1.028288, 0.490757, 0.230073, 0.103766, 0.046800$\}$; $\{\alpha_d$: 123.132, 42.362, 14.574, 5.014, 1.725, 0.586$\}$; $\{\alpha_f$: 34.292, 11.052, 3.562, 1.148$\}$. **Cl** $\{\alpha_s$: 3249104, 486495.6, 110712.5, 31359.44, 10230.97, 3693.568, 1440.549, 597.3637, 260.2796, 118.0074, 55.20054, 26.21200, 11.81335, 5.718663, 2.774713, 1.332335, 0.584347, 0.244902, 0.094408, 0.036394$\}$; $\{\alpha_p$: 4618.003, 1093.668, 355.1296, 135.5096, 57.09366, 25.74903, 12.10980, 5.814367, 2.829132, 1.347763, 0.626745, 0.275482, 0.113358, 0.042389$\}$; $\{\alpha_d$: 150.417, 50.139, 16.713, 5.571, 1.857, 0.619, 0.206$\}$; $\{\alpha_f$: 32.724, 10.908, 3.636, 1.212, 0.404$\}$. **H** $\{\alpha_s$: 188.614, 28.2766, 6.42483, 1.81504, 0.59106, 0.21215, 0.07989, 0.03310$\}$; $\{\alpha_p$: 0.292, 0.838, 2.292$\}$; $\{\alpha_d$: 0.662, 2.062$\}$; $\{\alpha_f$: 1.397$\}$.
[120] H. Partridge, J. Chem. Phys. **90**, 1043 (1989).
[121] H. Partridge, J. Chem. Phys. **87**, 6643 (1987).
[122] H. Partridge, *Near Hartree–Fock Quality Gaussian Type Orbital Basis Sets for the First- and Third-Row Atoms*, NASA Technical Memorandum 101044 (1989).
[123] H. Partridge, *Near Hartree–Fock Quality GTO Basis Sets for the Second-Row Atoms*, NASA Technical Memorandum 89449 (1987).
[124] F. B. van Duijneveldt, IBM Research Report No. RJ 945 (IBM Research Laboratory, San Jose, CA, 1971).
[125] C. C. J. Roothaan, Rev. Mod. Phys. **23**, 69 (1951).
[126] J. A. Pople and R. K. Nesbet, J. Chem. Phys. **22**, 571 (1954).
[127] W. J. Hehre, L. Radom, P. v. R. Schleyer, and J. A. Pople, *Ab initio Molecular Orbital Theory* (Wiley-Interscience, New York, 1986).
[128] A. Szabo and N. S. Ostlund, *Modern Quantum Chemistry* (McGraw-Hill, New York, 1989).
[129] R. J. Bartlett, Annu. Rev. Phys. Chem. **32**, 359 (1981).
[130] G. D. Purvis and R. J. Bartlett, J. Chem. Phys. **76**, 1910 (1982).
[131] J. Paldus, in *New Horizons of Quantum Chemistry*, edited by P.-O. Löwdin and B. Pullmann (Reidel, Dordrecht, 1983), p. 31.
[132] R. J. Bartlett, C. E. Dykstra, and J. Paldus, in *Advanced Theories and Computational Approaches to the Electronic Structure of Molecules*, edited by C. E. Dykstra (Reidel, Dordrecht, 1984), p. 127.
[133] G. E. Scuseria, A. C. Scheiner, T. J. Lee, J. E. Rice, and H. F. Schaefer III, J. Chem. Phys. **86**, 2881 (1987).
[134] A. C. Scheiner, G. E. Scuseria, J. E. Rice, T. J. Lee, and H. F. Schaefer III, J. Chem. Phys. **87**, 5361 (1987).
[135] C. Møller and M. S. Plesset, Phys. Rev. **46**, 618 (1934).
[136] J. A. Pople, J. S. Binkley, and R. Seeger, Int. J. Quant. Chem. Symp. **10**, 1 (1976).
[137] R. Krishnan and J. A. Pople, Int. J. Quant. Chem. **14**, 91 (1978).
[138] R. Krishnan, M. J. Frisch, and J. A. Pople, J. Chem. Phys. **72**, 4244 (1980).
[139] K. Raghavachari, G. W. Trucks, J. A. Pople, and M. Head-Gordon, Chem. Phys. Lett. **157**, 479 (1989).
[140] G. E. Scuseria and T. J. Lee, J. Chem. Phys. **93**, 5851 (1990).
[141] K. Raghavachari, J. A. Pople, E. S. Replogle, and M. Head-Gordon, J. Phys. Chem. **94**, 5579 (1990).
[142] T. J. Lee, R. Kobayashi, N. C. Handy, and R. D. Amos, J. Chem. Phys. **96**, 8931 (1992).
[143] TITAN is a set of electronic structure programs written by T. J. Lee, A. P. Rendell, and J. E. Rice.
[144] *PSI 2.0* (PSITECH Inc., Watkinsville, GA, 1991).
[145] GAUSSIAN 92, Revision A, M. J. Frisch, G. W. Trucks, M. Head-Gordon, P. M. W. Gill, M. W. Wong, J. B. Foresman, B. G. Johnson, H. B. Schlegel, M. A. Robb, E. S. Replogle, R. Gomperts, J. L. Andres, K. Raghavachari, J. S. Binkley, C. Gonzalez, R. L. Martin, D. J. Fox, D. J. Defrees, J. Baker, J. J. P. Stewart, and J. A. Pople, Gaussian Inc., Pittsburgh, PA (1992).
[146] J. F. Gaw and N. C. Handy, Annu. Rept. R. Soc. Chem. C **81**, 291 (1984).
[147] H. F. Schaefer III and Y. Yamaguchi, J. Mol. Struct. THEOCHEM **135**, 369 (1986).
[148] *Geometrical Derivatives of Energy Surfaces and Molecular Properties*, edited by P. Jørgensen and J. Simons (Reidel, Dordrecht, 1986).
[149] P. Pulay, Mol. Phys. **17**, 197 (1969).
[150] P. Pulay, in *Modern Theoretical Chemistry*, edited by H. F. Schaefer III (Plenum, New York, 1977), Vol. 4, p. 153.
[151] Y. Osamura, Y. Yamaguchi, P. Saxe, M. A. Vincent, J. F. Gaw, and H. F. Schaefer III, Chem. Phys. **72**, 131 (1982).
[152] Y. Osamura, Y. Yamaguchi, P. Saxe, D. J. Fox, M. A. Vincent, and H. F. Schaefer III, J. Mol. Struct. THEOCHEM **103**, 183 (1983).
[153] H. H. Nielsen, Rev. Mod. Phys. **23**, 90 (1951).
[154] I. M. Mills, in *Molecular Spectroscopy: Modern Research*, edited by K. N. Rao and C. W. Mathews (Academic, New York, 1972), Vol. 1, p. 115.
[155] D. Papoušek and M. R. Aliev, *Molecular Vibrational–Rotational Spectra* (Elsevier, Amsterdam, 1982).
[156] J. K. G. Watson, in *Vibrational Spectra and Structure*, edited by J. R. Durig (Elsevier, Amsterdam, 1977), Vol. 6, p. 1.
[157] J. K. G. Watson, J. Chem. Phys. **48**, 4517 (1968).
[158] D. A. Clabo, Jr., W. D. Allen, R. B. Remington, Y. Yamaguchi, and H. F. Schaefer III, Chem. Phys. **123**, 187 (1988).
[159] W. D. Allen, Y. Yamaguchi, A. G. Császár, D. A. Clabo, Jr., R. B. Remington, and H. F. Schaefer III, Chem. Phys. **145**, 427 (1990).
[160] D. W. Schwenke, Comput. Phys. Comm. **70**, 1 (1992).
[161] D. W. Schwenke, J. Chem. Phys. **96**, 3426 (1992).
[162] D. W. Schwenke and D. G. Truhlar, Comput. Phys. Commun. **34**, 57 (1984); D. G. Truhlar, J. Comput. Phys. **10**, 123 (1972); D. W. Schwenke, M. Mladenovic, M. Zhao, D. G. Truhlar, Y. Sun, and D. J. Kouri, in *Supercomputer Algorithms for Reactivity, Dynamics and Kinetics of Small Molecules*, edited by A. Lagana (Kluwer, Dordrecht, 1989), p. 131.
[163] R. A. Sack and A. F. Donovan, Numer. Math. **18**, 465 (1972).
[164] D. G. Rush, Trans. Faraday Soc. **64**, 2013 (1968).
[165] B. T. Sutcliffe and J. Tennyson, Mol. Phys. **58**, 1053 (1986).
[166] K. P. Huber and G. Herzberg, *Constants of Diatomic Molecules* (Van Nostrand, Princeton, NJ, 1979).
[167] I. N. Levine, *Molecular Spectroscopy* (Wiley, New York, 1975), pp. 149–160.
[168] J. S. Muenter and W. Klemperer, J. Chem. Phys. **52**, 6033 (1970); E. W. Kaiser, J. Chem. Phys. **53**, 1686 (1970).
[169] T. J. Lee and P. R. Taylor, Int. J. Quant. Chem. Symp. **23**, 199 (1989).
[170] A. Bondi, J. Phys. Chem. **68**, 441 (1964).
[171] *JANAF Thermochemical Tables*, 3rd ed., J. Phys. Chem. Ref. Data **14**, Supp. No. 1 (1985).
[172] K. Morokuma, Acc. Chem. Res. **10**, 294 (1977).
[173] K. Kitaura and K. Morokuma, Int. J. Quantum Chem. **10**, 325 (1976).
[174] H. Umeyama, K. Morokuma, and S. Yamabe, J. Am. Chem. Soc. **99**, 330 (1977); K. Morokuma, J. Chem. Phys. **55**, 1236 (1971).
[175] H. Umeyama and K. Morokuma, J. Am. Chem. Soc. **99**, 1316 (1977).
[176] H. Umeyama, K. Kitaura, and K. Morokuma, Chem. Phys. Lett. **36**, 11 (1975).

[177] See, also, L. B. Shevardina and V. M. Pinchuk, J. Struct. Chem. **30**, 545 (1989), which summarizes a Morokuma analysis on $[FHCl]^-$ performed with a small F[4*s*2*p*1*d*], H[3*s*1*p*], Cl[5*s*2*p*1*d*] basis set. The results, $\epsilon_{ES}=-38.5$, $\epsilon_{PL}=-8.7$, $\epsilon_{EX}=25.9$, $\epsilon_{CT}+\epsilon_{MIX}=-7.9$, and $\Delta E_{RHF}=-28.1$ kcal mol^{-1}, are vitiated by severe basis set deficiencies but are in broad, qualitative agreement with the analysis reported here.
[178] B. D. Wladkowski, K. F. Lim, W. D. Allen, and J. I. Brauman, J. Am. Chem. Soc. **114**, 9136 (1992).
[179] J. N. Murrell, S. Carter, S. C. Farantos, P. Huxley, and A. J. C. Varandas, *Molecular Potential Energy Functions* (Wiley, Chicester, 1984).
[180] D. J. Searles and E. I. v. Nagy-Felsobuki, Comp. Phys. Commun. **67**, 527 (1992).
[181] D. J. Searles and E. I. v. Nagy-Felsobuki, Phys. Rev. A **43**, 3365 (1991).
[182] D. J. Searles and E. I. v. Nagy-Felsobuki, J. Chem. Phys. **95**, 1107 (1991).
[183] F. Wang, D. J. Searles, and E. I. v. Nagy-Felsobuki, J. Mol. Struct. **272**, 73 (1992).
[184] F. Wang, D. J. Searles, and E. I. v. Nagy-Felsobuki, J. Phys. Chem. **96**, 6158 (1992).
[185] J. Plíva, Coll. Czech. Chem. Comm. **23**, 1846 (1958).
[186] J. F. Ogilvie, Proc. R. Soc. London, Ser. A **378**, 287 (1981).
[187] *Mathematica*, Version 2.102 enhanced, Copyright © 1988-92 by Wolfram Research, Inc.
[188] Y. P. Varshni, Rev. Mod. Phys. **29**, 664 (1957).
[189] See AIP document no. PAPS JCPSA-99-3865-9 for 9 pages of the complete set of RHF, MP2, and CCSD energy points obtained in the construction of the global surface of $[FHCl]^-$. Order by PAPS number and journal reference from American Institute of Physics, Physics Auxiliary Publication Service, 500 Sunnyside Boulevard, Woodbury, NY 11797-2999. The price is $1.50 for each microfiche (60 pages) or $5.00 for photocopies of up to 30 pages, and $0.15 for each additional page over 30 pages. Airmail additional. Make checks payable to the American Institute of Physics.
[190] S. E. Choi and J. C. Light, J. Chem. Phys. **97**, 7031 (1992).
[191] Y. S. Choi and C. B. Moore, J. Chem. Phys. **94**, 5414 (1991).
[192] W. H. Green, Jr., C. B. Moore, and W. F. Polik, Annu. Rev. Phys. Chem. **43**, 591 (1992).
[193] W. F. Polik, D. R. Guyer, and C. B. Moore, J. Chem. Phys. **92**, 3453 (1990).
[194] E. Abramson, R. W. Field, D. Imre, K. K. Innes, and J. L. Kinsey, J. Chem. Phys. **83**, 453 (1985).
[195] R. L. Sundberg, E. Abramson, J. L. Kinsey, and R. W. Field, J. Chem. Phys. **83**, 466 (1985).
[196] R. N. Zare, *Angular Momentum* (Wiley, New York, 1988), p. 85.
[197] F. L. Tobin and J. M. Bowman, Chem. Phys. **47**, 151 (1980).
[198] K. M. Christoffel and J. M. Bowman, Chem. Phys. Lett. **85**, 220 (1982).
[199] In the $(J^P,\ell)=(1^{\pm},1)$ cases, the natural modals for the radial modes were determined from 465 interacting states lying less than 0.065 a.u. above the lowest VSCF energy of 3465.2 cm^{-1}. The average density matrix was constructed over 150 roots appearing below an excitation energy cutoff of 0.046 a.u.
[200] For $(J^P,\ell)=(1^{\pm},1)$ states, a cutoff 0.065 a.u. above $E_{zp}^{SCF}=3465.2$ cm^{-1} was used. The matrix dimension was 1914, involving 105, 19, and 8 single-mode functions for $\mathfrak{R}$, τ, and r, respectively.
[201] See T. A. Brody, J. Flores, J. B. French, P. A. Mello, A. Pandey, and S. S. M. Wong, Rev. Mod. Phys. **53**, 385 (1981), and references therein.